SEA
GRANT
PROJECT
OFFICE

AN ANALYSIS OF THE SMALL-SCALE

STRENGTH TESTING OF ICE

by

Kenneth R. Maser

Massachusetts Institute of Technology

Cambridge, Massachusetts 02139

AN ANALYSIS OF THE SMALL-SCALE
STRENGTH TESTING OF ICE

by

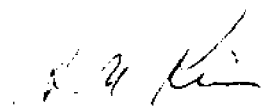Kenneth R. Maser

1.

SEA GRANT PROJECT OFFICE

ADMINISTRATIVE STATEMENT

The study resulting in this report, "An Analysis of the Small-Scale Strength Testing of Ice," was carried out in partial fulfillment of the author's Doctoral Thesis requirement.

The information in this report is of particularly timely interest in view of the expanding development of offshore oil in northern ocean areas subject to sheet ice formation. This new approach to the analysis of ice strength can provide more accurate understanding of the mechanical properties of sheet ice and thereby permit structural designs to better withstand the ice forces applied. This work has attracted wide attention and has been the basis of papers presented by the author to the Third Offshore Technology Conference, at Houston in April 1971, and to the International Conference on Port and Ocean Engineering Under Arctic Conditions, at the Technical University of Norway, in August 1971. The interest evidenced in these papers has motivated the publications of the complete thesis report.

The printing and distribution of this special edition of the report was organized by the M.I.T. Sea Grant Project Office under the project established to expedite dissemination of important studies and/or research findings developed at M.I.T. under other than Sea Grant support.

Alfred A. H. Keil
Director

January 25, 1972

ABSTRACT

AN ANALYSIS OF THE SMALL-SCALE STRENGTH TESTING OF ICE

by

KENNETH R. MASER

The inadequacy of small-scale strength test
results for the prediction of ice sheet strength
is recognized. Certain patterns appear in these
test results which suggest that the plasticity
of the individual crystal is a controlling factor.
It is found from previous investigations that ice
crystal plasticity is dominated by basal glide,
and that the stress-strain-time properties have
the characteristics of strain softening. A stress-
strain-time relation is proposed which best matches
the reported results. This relation is used in
analytical models which treat the small-scale sam-
ple as an assembly of grains. A modeling by springs
and dashpots shows how failure stress in uniaxial
tension increases with increasing strain rate in
a given range. A finite element model for a poly-
crystalline sample gives quantitative support for
this result, and the resulting curve is very simi-
lar to that obtained by previous experiments. The
model also reveals the character of the nonuniform
stress field associated with the coarse grained
sample. Several directions for future research
are discussed.

3

Acknowledgements

The author would like to thank Professor Jerome Connor for his assistance and patience as thesis advisor, and Dr. Andrew Assur and Mr. Don Nevel of CRREL for helping to stimulate the ideas of this thesis. Particular thanks to Mrs. Jessica Malinofsky, who enthusiastically undertook the typing chore, and took much of the pain out of preparing this thesis. The author would also like to acknowledge the National Science Foundation for providing fellowship support for four years of graduate study. Finally, the author would like to thank Mr. Mark Horenstein for assisting in the preparation of the figures.

4

Table of Contents

List of Symbols

A'	relaxation constant
A_i	cross sectional area of grain i
b	Burger's vector
B	constant; element strain function
C	constant
d	depth
D	constant; rigidity matrix
E	elastic modulus
E_1	constant
E_2	constant
F_i	force on grain i
F_i^*	failure load of grain i
F^*	failure load of sample
G	shear modulus
G_i	spring constant associated with grain i
i	grain index
k	flow modulus
k'	constant
k_i	dashpot constant for grain i
k_e	effective flow modulus
K	concentration factor for ring tensile test
K_1	constant
K_2	constant

List of Symbols (continued)

$$K_{BB}$$
$$K_{IB}$$
$$K_{BI}$$
$$K_{II}$$

partitions of the grain stiffness matrix

K_{BB}^{c} condensed grain stiffness matrix

K_{E} element stiffness matrix

ℓ specimen length

m   strain exponent

M   bending moment; initial slope of single crystal stress-strain curve

M_{o} constant

M_{1} constant

n   stress exponent

N   number of grains; element displacement function

p   brine volume exponent; no. of active dislocations; element load distribution

P   specimen load

P_{B} grain boundary nodal load vector

P_{p} element plastic load vector

P_{Bp} grain load vector due to plasticity - boundary nodes

P_{Uo} Grain load vector due to plasticity - interior nodes

P_{Bp} condensed grain load vector due to plasticity

List of Symbols Continued

q	creep curve time exponent
Q	constant
r	stress exponent
r_c	rate exponent for compression
r_t	rate exponent for tension
r_i	inside radius of ring tensile specimen
r_o	outside radius
R	universal gas constant
S	section modulus
t	thickness; time
t_i	incubation time
t_s	time where constant slope in creep curve begins
T	temperature
u	element displacement field
U_B	grain boundary displacement vector
U_I	interior displacement vector
$U_{E,n}$	element nodal displacement vector
v	strain rate
v_s	screw dislocation velocity
α	dislocations per unit strain
γ	resolved shear strain
γ_p	resolved plastic shear strain
γ_{pm}	measured resolved plastic shear strain

List of Symbols Continued

γ_T	total measured resolved shear strain
γ_o	initial resolved shear strain
γ_s	slope of constant rate portion of creep curve
δ	crosshead displacement
δ_i	initial displacement for grain i
ε	element strain vector
ε_p	element plastic strain vector
θ_i	angle between basal plane and plane perpendicular to specimen axis, for grain i
ν	brine volume per unit volume
π	3.14159
σ	element stress vector
σ_{br}	Brazil test strength
σ_c	uniaxial compressive strength
$\sigma_{f\ell}$	flexural strength
σ_{isc}	in-situ cantilever strength
σ_{rt}	ring tensile strength
σ_t	uniaxial tensile strength
σ_f	failure stress
τ_o	failure stress at t = 0
τ	resolved shear stress
τ_y	yield stress
$(\dot{})$	time derivative of ( )

Chapter I

INTRODUCTION

Interest in the mechanical properties of ice has focused around two major areas—the study of the flow of glaciers and the study of the strength of floating ice. The motivation for this thesis arose from an attempt by the author to use an analytical approach to predict the strength of floating ice sheets. Since the results of this thesis have this particular problem in mind, a brief discussion will first be presented.

A. The Strength of Floating Ice Sheets

The numerous engineering problems associated with the strength of floating ice sheets can be categorized as either problems associated with a supporting structure or problems associated with a design force. The problems of support of building facilities, over ice transportation, and aircraft landing are all concerned with the adequacy of an ice sheet as a supporting structure. On the other hand, problems of ice forces on harbor facilities, dams, offshore structures, and icebreakers all deal with the ice sheet as a design force, and hence are concerned with the ability to destroy it.

Ice sheets in nature take on the convenient structural form of a plate. The modeling of ice sheet problems as plate problems will be briefly discussed.

Problems of bearing capacity can be represented as the bending of a plate on an elastic foundation, the bouyant force of the water being represented as a uniformly distributed linearly elastic spring with a spring constant equal to the weight density of the water. The problem of vertical forces due to ice adhering to structural legs and subject to tidal variations can also be modeled this way if the ice sheet rather than the ice-structure contact is expected to fail.

Horizontal forces on structures can be modeled as an ice sheet in plane stress, subject to the forces of the structure plus the forces due to current drag or thermal expansion and contraction. Inclined structural elements and icebreakers apply both horizontal and vertical loads, and hence imply a combination of both plane stress and bending.

The time scale associated with loads on an ice sheet varies considerably. The load duration of a building facility can be measured in months or days. The loadings associated with tidal and thermal fluctuation are measured in hours, the duration of vehicular traffic in minutes, and the load history of an ice floe impact or aircraft landing in seconds.

Some knowledge of the type of failure expected is useful in determining the type of analysis to use. Some information on this subject is already available. Frankenstein[1] conducted bearing capacity tests on relatively thin ice (6 to 18 in. thick) and made the following observations. Failure was always preceded by the formation of cracks on the under side of the ice extending radially outward from the center of the load. Following this event one of two events took place. When the load

was reasonably distributed (i.e., load diameter > 10 x thickness) circumferential cracks formed on the top surface of the ice prior to failure. The failure hole was between 17' and 18' in diameter for a distributed load 15' in diameter. When the load was concentrated (2' in diameter) the number of circumferential cracks was fewer and less visible, and the ultimate failure hole was approximately equal to the diameter of the load. These configurations are shown in figure 1.1.

For lateral loads on structural elements two types of failure have been observed.[2] The first is the formation of radial cracks due to the plane stress or combined plane stress and bending stress fields. This is then followed by either a local crushing of the weakened ice, by the breaking up of pie-shaped pieces due to bending, or, in the case of an ice floe, by cleavage of the floe. Alternatively, no noticeable cracking takes place and the ice is simply crushed by the structure, leaving a clean slot flanked by a berm of crushed ice. These situations are depicted in figures 1.2 and 1.3. Which kind of failure occurs is dictated by the amount of ice which participates in the loading, which in turn seems to depend on the rate of loading, the shape of the ice-structure contact, and the integrity of the ice. The slot type failure has been witnessed in the Cook Inlet, Alaska, where ice floes move at speeds of the order of six knots.[2] Radial cracks have been frequently observed at lower load rates. In either case, force time records for structural members subjected to lateral ice loads have revealed a periodic character, which seems to be a property of the ice rather than one of the structure.[3] A typical force-time record is shown in figure 1.4.
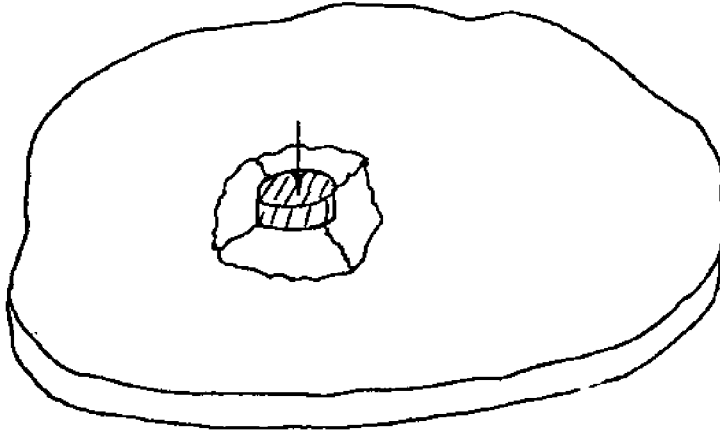
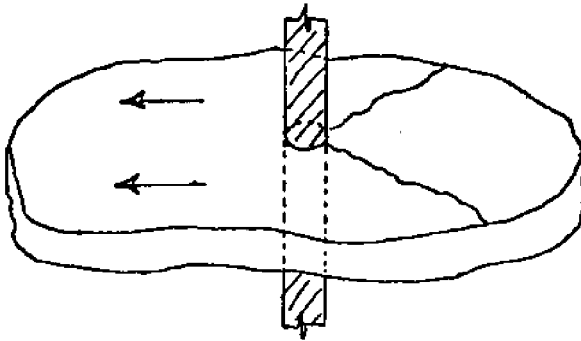Figure 1.1 Bearing Failure Patterns

Figure 1.2 Plane Tensile Failure of an Ice Floe
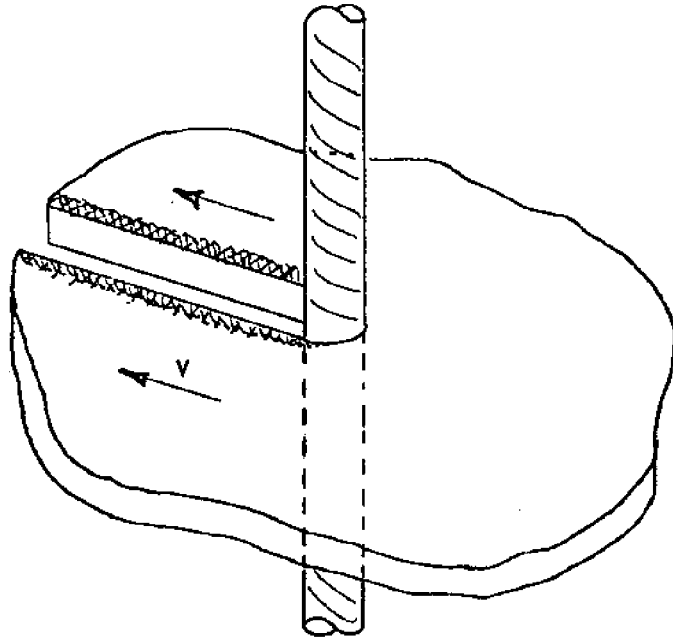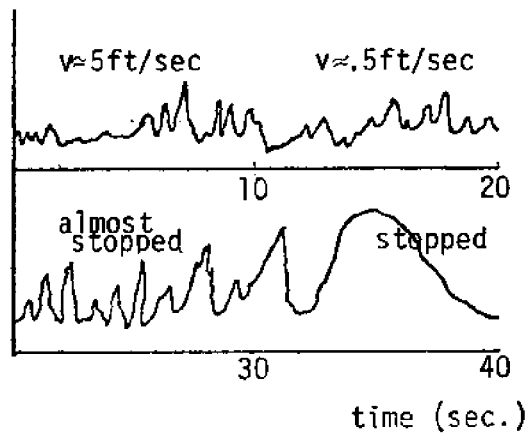(arrows indicate current direction)

Figure 1.3 Slot Failure at Rapid Loads[2]

Figure 1.4 Load-Time History[2]

For problems of plane stress, bending, and combinations thereof, a knowledge of the geometry, the loading, and the expected failure mode invites a variety of solutions. Meyerhoff[4] has treated ice as a rigid-plastic material and has determined the bearing capacity of an ice sheet via limit analysis. The yield lines in his analysis coincide with the radial and circumferential crack patterns which have been observed in ice sheets. Nevel[5] has analyzed an ice sheet as a viscoelastic plate on an elastic foundation. Frankenstein[1] has fit his experimental values of deflection into Nevel's solution in order to obtain the material parameters E (Young's modulus) and η (viscosity). The resulting values show a wide scatter. Nevel[6] has also treated the problem of an infinite wedge on an elastic foundation, observing that ultimate failure in many cases occurs due to failure of pie-shaped pieces.

The major difficulty encountered in applying such analyses is the limited knowledge of the material properties of ice—in particular, the stress-strain behavior and the required failure criterion. This situation is further complicated by the fact that a reasonably thick ice sheet, as normally found in the Arctic, is not uniform through the thickness. While the top surface of the sheet is approximately equal to the ambient temperature (say, -30° C), the bottom surface is always at the freezing temperature of the water (0° C). For any material in the neighborhood of its melting point, this is a critical temperature range, and a considerable variation of properties with temperature, and hence depth, can be expected.

B. Ice as an Engineering Material

Ice does not exhibit many of the niceties which are characteristic of other engineering materials. It is formed in nature under a variety of natural conditions. It exhibits a complex internal structure, much of which is visible to the eye, and in this respect is very similar to concrete. Ice is difficult to work with because the temperatures at which it exists are not normally compatible to most human beings. In addition, ice sheets are not smooth ideal plates, as may have been implied by the previous section. Although lake and lagoon ice is fairly smooth, arctic pack ice has a highly irregular surface, with irregularities (e.g., hummocks and pressure ridges) several feet high.

As indicated in the previous section, the properties of ice as an engineering material are virtually unknown. A few properties have been generally acknowledged. First, ice is weaker in tension than in compression. Hence, when ice is subjected to a general state of stress, maximum tension has been assumed to govern the failure. Second, ice is presumed to exhibit some form of time dependent plastic flow. This was first apparent from observations of the flow of glaciers, which travel down the sides of mountains at sometimes incredible speeds (100 to 200 feet per day has been reported).[7] Hence glaciologists have treated ice as a viscous fluid. The engineer concerned with ice sheets is confronted with a broad range of time scales, and as yet it is not clear when and to what extent such plastic flow is significant. Third, the mechanical properties of ice depend on various parameters. The strength of an

ice sheet depends on its thickness. The strength of ice in general depends on how fast it is loaded, its temperature, and, in the case of sea ice, its salinity. It is important to understand how the mechanical properties depend on these parameters in order to make sensible predictions of ice sheet strength.

Owing to the great thickness attained by Arctic ice sheets (e.g., 3 to 6 ft.), and to the great forces required, to fail such ice sheets, full-scale testing is prohibitively expensive. In addition, the number of variable parameters limits the amount of information which could be derived from such tests. Consequently, the major emphasis has been placed on small-scale testing. The results of great numbers of small-scale tests have been reported in the literature, but as yet there have been few realistic suggestions as to how to apply these results to ice sheet strength problems.

C. Scope

The purpose of this research is to examine the available small-scale strength data with the intention of obtaining some sort of unified view as to their meaning. Since there are so many factors affecting ice strength, attention will be given to tests on a particular type of ice structure which is the dominant form found in ice sheets, i.e., columnar grained ice (to be defined). The test results will be studied in terms of two particular effects, i.e., the effects of grain size and plasticity.

Before studying the results of small tests it is necessary to review the internal structural properties of ice, since they exert a large in-

fluence on the observed strength. This is done in Chapter II. Chapter III presents a review of small-scale test results and some interpretations in terms of grain size and plasticity. Chapter IV reviews the plasticity of single crystals of ice, and presents a flow law which is employed in the polycrystalline models of Chapter V. Chapter VI presents the conclusions of the study and Chapter VII suggests applications to full-scale ice sheets and directions for future research.

Chapter II

THE INTERNAL STRUCTURE OF ICE

A. Introduction

The results which have been obtained in small-scale tests can be directly related to the internal structural properties of ice. Before proceeding with a discussion of small-scale test results, therefore, it will be useful to review the characteristics of the internal structure of ice and to suggest how they manifest themselves mechanically. A thorough review of this subject is presented by Weeks and Assur,[14] and much of the foregoing has been condensed from their report.

B. Ice as a Polycrystal

Although eight known crystalline modifications of solid H_2O have been isolated and identified, only one is known to exist at the normal temperatures and pressures experienced on the earth.[8] This form is known as Ice I (henceforth abbreviated as "ice"), and it is the most widely distributed solid found on the earth's surface. Ice generally exists in the form of a polycrystal, whose grain size and structure are highly dependent upon the conditions of growth. Saturated snow ice, for example, has a grain size of less than one millimeter, while crystals several feet in diameter have been found in glaciers and on the bottom surface of Arctic ice sheets.

Single crystals of ice exhibit a molecular structure in which the

oxygen atoms occupy positions in a puckered hexagonal lattice. The plane of the hexagon is referred to as the "basal plane" and the axis perpendicular to the basal plane is referred to as the "c-axis." The molecules are so arranged that for a given unit cell containing four oxygen atoms, cleavage along the basal plane requires the destruction of two bonds, while cleavage along a plane perpendicular to the basal plane requires the destruction of four bonds.

C. Characteristics of an Ice Cover

Ice crystals initially form on the surface of the water in the form of small discs, whose plane coincides with the basal plane of the crystal. Because of close packing in the hexagonal plane, the discs tend to grow most rapidly in their own plane, until they intersect one another to form a continuous skim of ice over the water surface. Disturbances in the water surface cause many of the discs to be frozen at some inclination to the surface. After the skim forms, the ice must begin to grow vertically, and hence the inclined crystals have the primary growth freedom. The crystals which are closest to being vertical will have the greatest growth freedom, and as the ice sheet thickens, these crystals will begin to predominate. The distance over which this "geometric selection" takes place is referred to as the "transition layer," and it varies with initial conditions of ice growth, with typical values for sea ice between 5 and 10 cm. from the ice-air interface. Below this layer the grains will be columnar shaped with c-axes

oriented randomly in the horizontal plane (figure 2.1). The grain diameter tends to increase with increasing depth, with typical values ranging between .5 and 2.0 cm.

Lake Ice

The ice cover which forms on lakes in northern United States is generally reported to have two distinct layers—a layer of snow ice covering a layer of clear ice.[9,10,11,12] The clear ice is formed from the lake water as described in the previous section. Snow ice is formed from the freezing of lake water that has infiltrated the snow cover.[10] Snow ice in general consists of small size crystals which have neither a preferred orientation of crystal axis nor a preferred geometric shape. Such crystals are referred to as equigranular. The crystals of the clear ice have been found to exhibit both c-axis horizontal and c-axis vertical orientations, although the former occurrence is most favored. This tends to depend on the conditions of growth and the thickness of the sheet.

Sea Ice

The most significant occurrence in the freezing of sea ice is the rejection of salt from the solid phase. At the microstructural level the solid component of sea ice is fresh water ice. This suggests that the entire ice cover should be fresh ice covering a layer of very salty water due to the rejection of brine. The fact that this is not the case, i.e., that pieces of sea ice contain a considerable amount of salt, is explained by the instability of the planar interface between
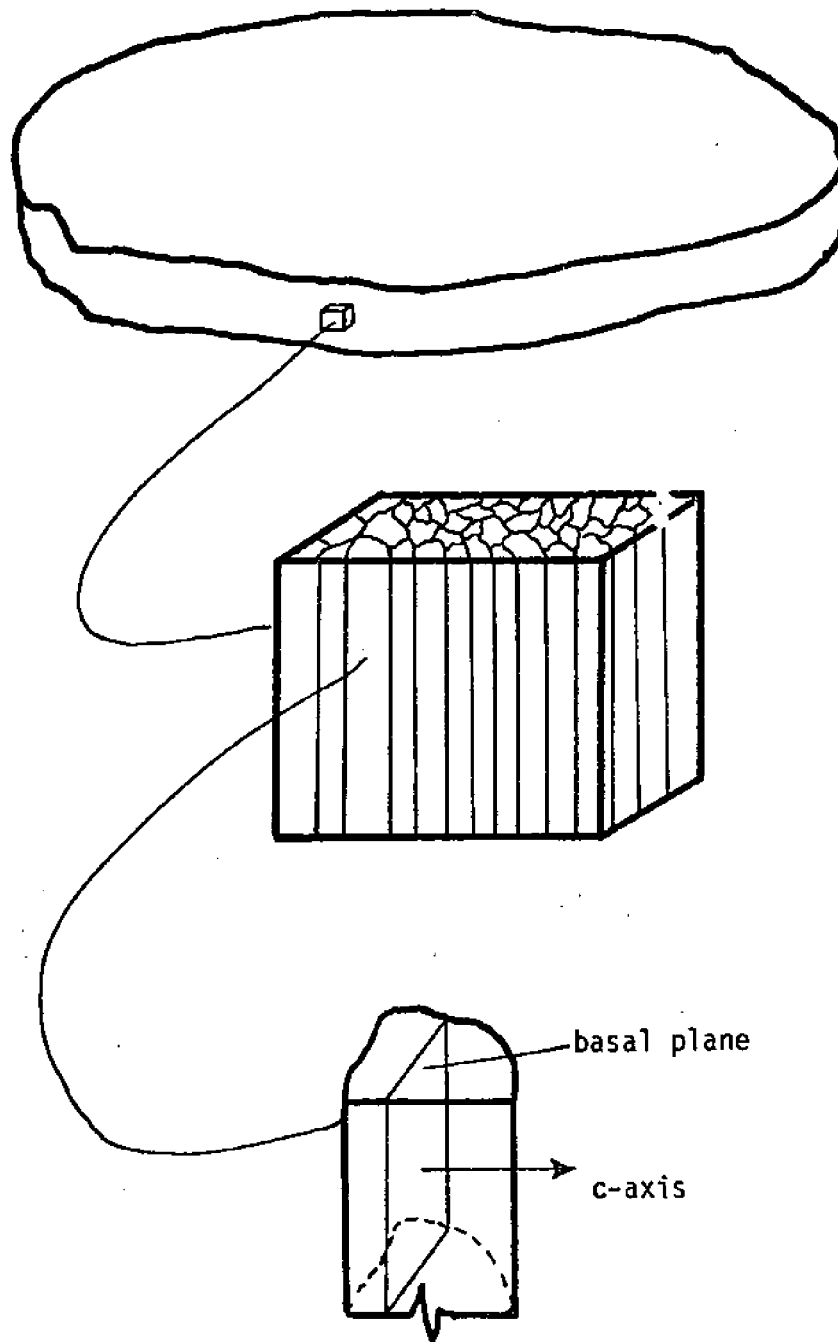
Figure 2.1   Grain Structure in an Ice Sheet

the bottom surface of the ice and the water.[13] This comes about as a result of the changed freezing temperature profile due to the concentration gradient produced by the rejected salts. The result is that ice crystals protruding vertically into the water tend to increase in size, rather than waiting for the rest of the ice to catch up. These vertical crystal plates eventually bridge together and entrap vertical columns of highly concentrated salt water. These entrapped brine pockets are responsible for the salt content of sea ice. They are also responsible for the fact that sea ice is opaque, while lake ice is generally transparent. The geometry of this situation is shown in figure 2.2. A typical grain of sea ice can be thought of as a long bundle of plates, with cylindrical brine pockets sandwiched between the plates.

D. Ice as a Solid Continuum

It is of interest here to deal with ice sheets and ice samples using concepts of stress analysis, and therefore it is necessary to define the continua over which such analyses shall apply. This may seem like a formality, but in the light of the frequent discussions in the literature of "stress concentrators" and their effect on small sample strength,[14] and in the light of the coarse internal structure of ice, it is a necessary step.

The basic continuum for ice is that for which the dimensions of any problem of interest are much greater than the intermolecular dimensions in the ice crystal lattice. A "point" in such a continuum must
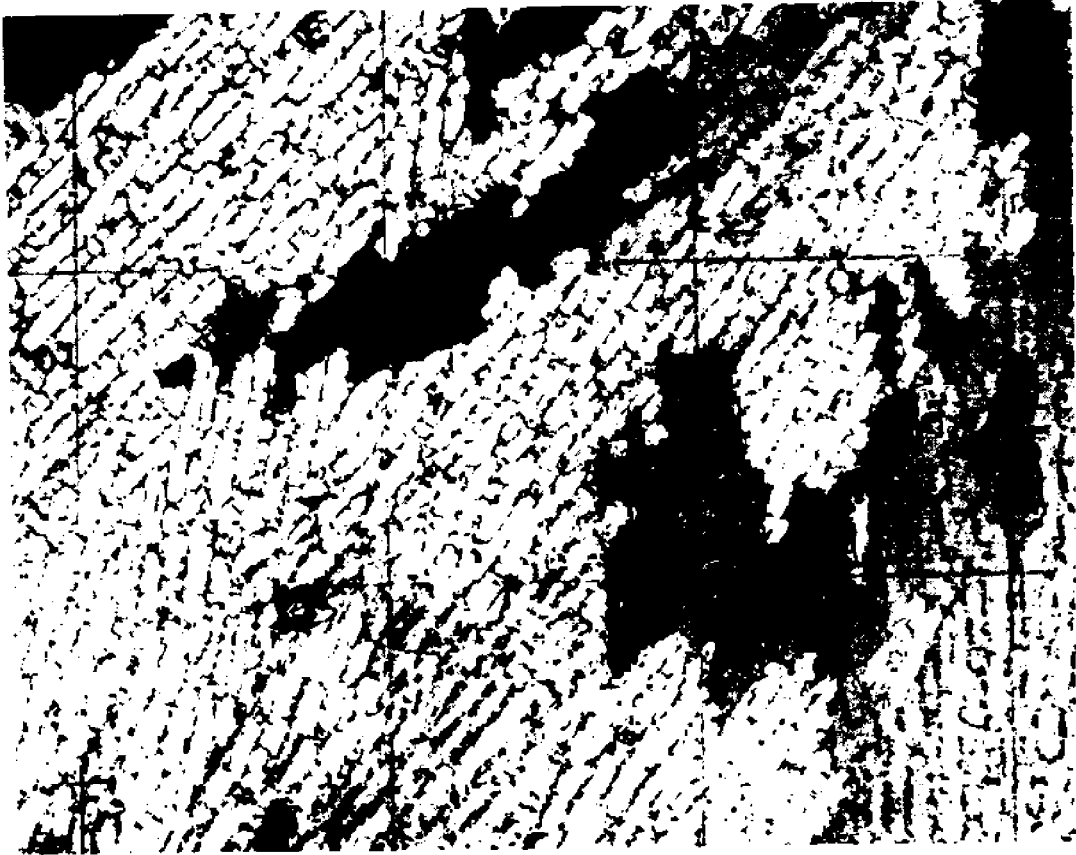
(a) Grain geometry in the horizontal plane. Brine
    pockets are sandwiched between parallel layers.
    The grid length is 1 cm.
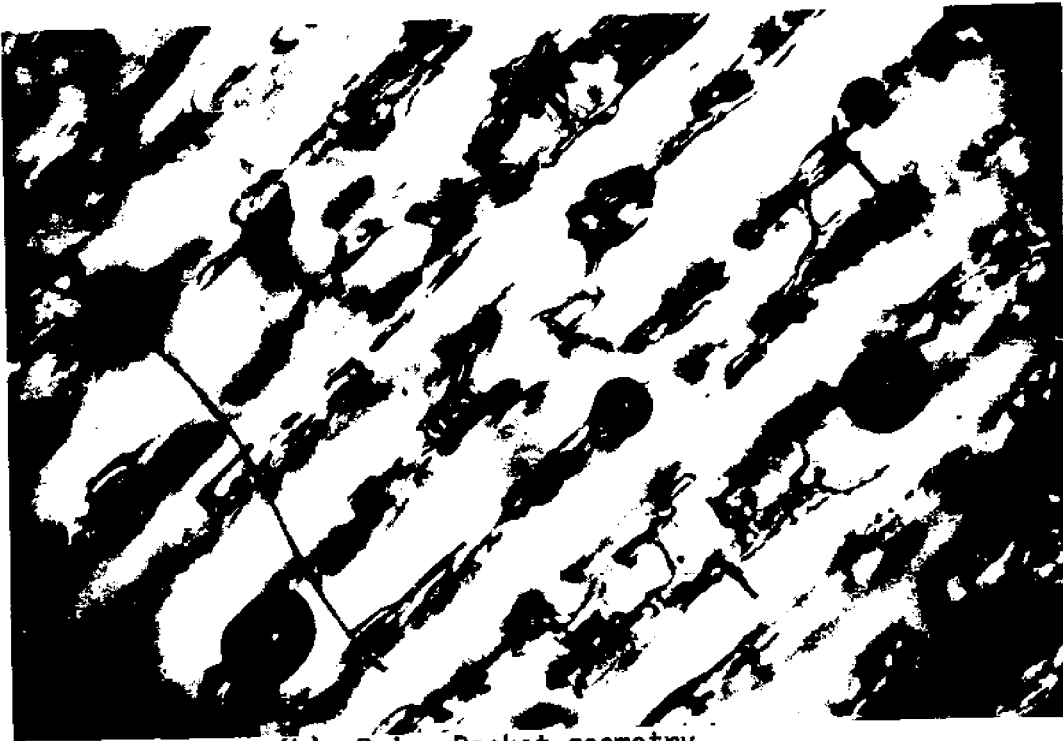
(b) Brine Pocket geometry

Figure 2.2 Internal Structure of Sea Ice (Weeks and Assur)[14]

contain a sufficient number of molecules such that any average continuum property reaches a stable limit as the averaging region approaches the size of a point. This continuum will be referred to as continuum I. It is appropriate, for example, to deal with ice as continuum I for problems involving the concentration of stress about brine pockets or air bubbles, which have typical dimensions between .1 and .5 mm.

A second continuum appropriate for sea ice would be one for which the dimensions of interest are much greater than the typical dimensions associated with the geometry of brine pockets. A "point" in this continuum, referred to as continuum II, must contain seve~al brine pockets. It would be reasonable to say that an individual grain of sea ice, of dimensions of the order of 1 cm., is filled with material of continuum II.

Continuum III is one for which dimensions of interest are much greater than grain sizes. This is the continuum of relevance in determining the strength of ice sheets, and the one for which we would ultimately like to know the full spectrum of mechanical properties. A problem arises from the fact that typical small-scale test dimensions are such that the small sample is about the size of a "point" in continuum III. In addition, the small samples are loaded in such a way that they do not experience the equivalent of "stresses," nor do they exhibit failures characteristic of continuum III. These considerations will be dealt with later in the discussion of small-scale test results and in the development of interpretive models.

E. A Strength Model for Sea Ice

Before proceeding to the results of small-scale tests, it is neces-
sary to mention the most important theoretical development in the study
of the strength of sea ice. The theory, proposed by Anderson and
Weeks[15] and refined by Assur,[16] relates the strength of sea ice to the
volume fraction of entrapped brine, ν. A geometric model is proposed
for the regular arrangement of brine cylinders in sea ice (figure 2.3).
On the basis of this model, the variation of the failure stress, σ_f, is
computed in terms of the reduction in load carrying area due to changing
dimensions of the brine cylinders. The relationship between failure
stress σ_f and brine volume ν takes on the general form

$$\sigma_f = \sigma_0 \, (1 - A\nu^p) \tag{2.1}$$

where σ_0 is the "basic strength" of ice with no brine, A is a constant,
and p takes on the values of 1/2, 2/3, and 1, depending on the type of
geometric similarity maintained with changing brine volume and on the
cross-sectional shape of the brine cylinders. The brine volume, ν, is
computed from temperature and salinity using the phase relations for
sea ice,[16] and is found to increase with increasing temperature and
salinity.

The results of small-scale tests have confirmed the prediction of
Eq. (2.1). Most investigators have found that a value of p = 1/2 offers
the best data fit. Although Eq. (2.1) strictly applies to stress de-
fined in continuum II, the uniformity of temperature and salinity in a
region embracing a sufficient number of grains should make it applica-
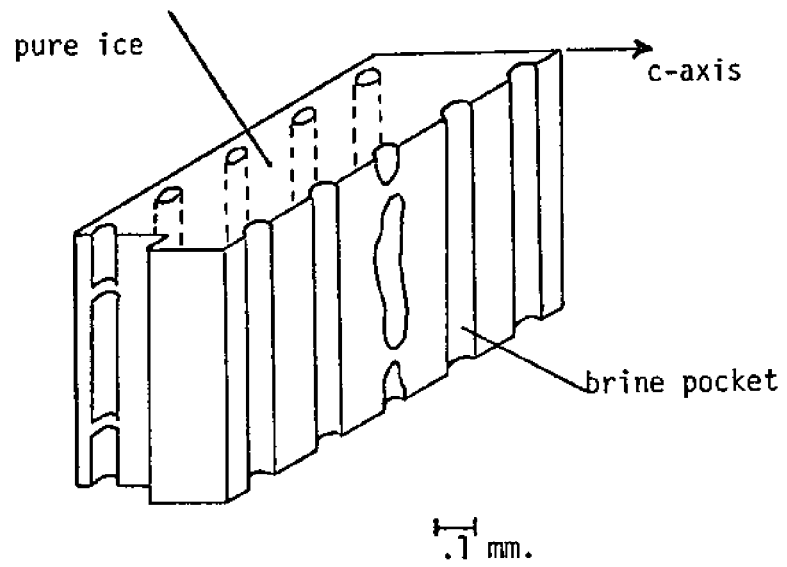ble to continuum III stresses.

pure ice

c-axis

brine pocket

.1 mm.

Figure 2.3 Geometric Model of Brine Pockets[15,16]

Chapter III

A REVIEW OF SMALL-SCALE STRENGTH TESTING

A. Introduction

During the past several years some rather extensive investigations into the small-scale strength properties of ice have taken place. These efforts have been motivated primarily by a desire to obtain a rational basis for the prediction of the strength of ice sheets. Because of the wide scatter associated with small-scale strength results, each investigator has had to perform a great many tests in order to obtain meaningful relationships between strength values and the various parameters involved. In general, each plotted data point represents the average of some 10 to 20 tests.

Tests have been performed both in the field and in the lab. The field tests have the advantage of closeness to the natural environment. These tests simulate the most desirable engineering situation, i.e., the ability to obtain on-site information about the strength of an ice sheet in a particular environment. The environment, on the other hand, generally limits the kind of equipment which can be used and the capability of the human beings performing the experiment. This, therefore, presents restrictions on the kinds of tests which can be performed and on the care with which quantities can be measured and controlled. Laboratory testing permits a more careful study of the dependence of strength on the various parameters which affect it. Lack of environmental constraint permits a greater range of parameters which can be

considered, and greater consistency in test procedures. Their purpose, in general, is to serve as a guide for future field testing.

Some investigators, in an attempt to combine the advantages of both types of tests, have had field samples shipped to a laboratory for testing. This procedure, however, introduces new unknowns due to the effects of storage.

B. Factors Affecting Test Results

In order to perform, analyze, and compare the results of any series of tests, attention must be given to the variability in the internal structure of ice, to the environmental parameters associated with the sample, and to the alternative test and measuring procedures. Some of the significant factors, as described by various investigators, are listed below.

load rate

As shown in figure 1.4, the force exerted on a structure by an ice floe depends on the rate of load application. This effect has also been observed in small-scale tests. Load rate is generally expressed as stress per unit time, and is represented here by $\dot{\sigma}$. The experimenter, however, usually controls the displacement rate of the load-applying device. Hence, the presentation of results in terms of load rate can be misleading. Load rate is usually measured by dividing the computed maximum stress by the time to failure, or by making some kind of linear fit to the load-time curve.

temperature

Temperature is generally expected to have an effect on the mechanical properties of a material. Typical ice temperatures range from 0° to -40° C.

grain structure

As indicated in chapter II, different types of ice have different grain geometries. Some are columnar with random shape in a plane (columnar-grained), while others exhibit a random shape in space (equi-granular). The orientation of crystallographic axes within grains also varies. Some structures have a random c-axis orientation, others have a preferred c-axis orientation. It is important to know the orientation of applied stress with respect to any preferred grain geometries and c-axis orientations.

depth in ice sheet

Ice properties vary with depth in an ice sheet. This property variation is frequently dealt with in terms of variations in temperature, salinity, and grain size.

stress history

The processes of extracting and machining test samples induces initial stresses and strains, not to mention the fact that natural ice sheets are subjected to considerable stresses and deformation before test samples are removed.

sample size

The question of scale effect becomes important when testing the behavior of a structure using a small-scale model. The largeness of the internal structure of ice also indicates that strength might vary with the sample size.

The following factors are peculiar to sea ice:

salinity

As discussed in the previous chapter, the effects of salinity are generally handled in terms of brine volume, and compared against the strength-brine volume theory.

brine drainage

Samples stored for any length of time experience a certain amount of gravitational brine drainage, while samples turned on a lathe will experience centrifugal brine drainage. In addition, the brine volume of any given point in an ice sheet varies with time, with a general tendency to decrease. In these cases, the internal structure which came about as the result of brine entrapment still remains. If strength is to be related to internal structure via brine volume, then these losses must be taken into account.

solid salt reinforcement

The various salts present in sea water crystallize within the brine pockets at various temperatures in accordance with the phase relations for sea water. It has been observed[16] that at -23° C, where

$NaCl \cdot 2H_2O$ precipitates, sea ice takes on noticeably different visual and m chanical characteristics. This observation has led to the belief that these salts precipitai in such a way as to reinforce the walls of existing brine cylinders. Consequently, it has been suggested that discontinuities in strength relationships should be expected to take place at these temperatures, particularly at $-8.2°$ C (precipitation of $Na_2SO_4 \cdot 10 H_2O$) and at $-23°$ C.

age of ice

Differences in properties between annual ice and ice of greater age are expected. One such property is the loss of brine.

geometric hysteresis

Weeks[17] has suggested that a test specimen subject to temperature fluctuations, particularly a warming cycle, might retain the internal structure of the warmest temperature attained, although this is not the test temperature. He found this hypothesis to be significant in affecting strengths below $-23°$ C. This is a problem which may be encountered in the storage of test samples.

It is evident that to discuss the existing data in terms of all of these factors would seriously limit the possibility of drawing any conclusions. They have been brought up now so that their subsequent mention in connection with any of the results mentioned herein will be facilitated.

For the ensuing discussion, attention will be directed towards presenting regular patterns which have been observed between ice sample

strength and temperature, rate of loading, and brine volume.

C. Description of Tests

The most typical types of strength tests employed on ice samples are shown in figure 3.1, and are described briefly below.

uniaxial compression test

These have been generally performed on cylinders or rectangular prisms of width 2 to 8 cm. having a height-to-width ratio from 2 to 3. Russian investigators have frequently used cubes.[18] Compressive strength will be designated as σ_c.

uniaxial tensile tensile test

These have usually been confined to the laboratory because of the problems associated with gripping the ends of the specimen. Devices for accomplishing this have included a braided wire gripping device,[10] freezing the ends to metal fixtures,[20,21] clamping tapered ends between fitted metal grips,[22] and applying the load through a bolt passed through a wide portion of the specimen.[23] Samples are generally 2 to 5 cm. in width or diameter.

Given that there were no problems associated with the load application, the uniaxial tensile test is the best of the tests for tensile strength, since the load is applied uniformly and the stress is computed directly from the applied load. The fact that it is difficult to conduct has caused investigators to seek alternative means for determin-
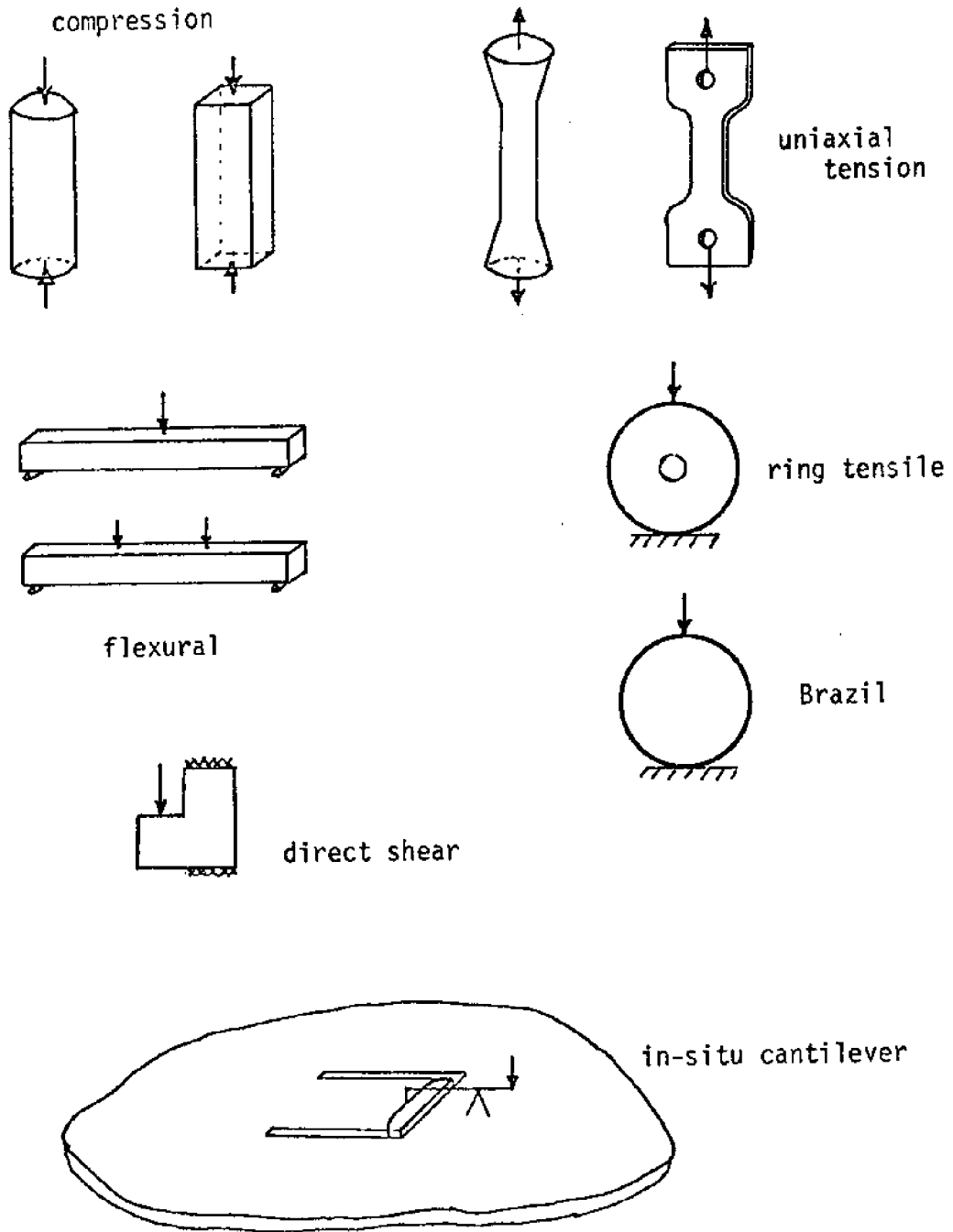
compression

uniaxial
tension

flexural

ring tensile

Brazil

direct shear

in-situ cantilever

Figure 3.1   Geometry of Tests

ing tensile strength. Uniaxial tensile strength values will be designated by σ_t.

flexural test

The use of the flexural test exploits the fact that ice is much weaker in tension than in compression. These tests have employed both center-point and third-point loadings. Beam depths range from 2 to 6 cm. In all cases the stress has been computed via the elastic beam formula, $\sigma_{f\ell} = M/S$, where M is the maximum bending moment, S is the section modulus of the beam, and $\sigma_{f\ell}$ is the computed stress at failure. Due to the nature of the stress distribution from elastic theory, only a very small portion of the cross section is subject to stresses near the computed maximum.

ring tensile test

Due to the simplicity of obtaining and testing samples, this has been by far the most popular of the small-scale strength tests. It originally was used in connection with rock mechanics. Preparation of samples involves cutting a cylindrical core out of the ice sheet, slicing it into discs, and drilling a coaxial hole in each disc. A compressive load is applied perpendicular to the cylinder axis, producing tension at the inside hole under the load. This is where the failure takes place. The tensile stress causing this failure is computed from an elasticity solution to the problem presented by Ripperger and Davids[39] which yields

$$\sigma_{rt} = \frac{PK}{\pi t \, r_0} \qquad\qquad (3.1)$$

where P is the applied load, r_0 is the outside radius of the cylinder, σ_{rt} is the "ring tensile strength," and K is a concentration factor depending on the ratio r_i/r_0, where r_i is the inside hole radius. The dimensions of the ring tensile specimen have been standardized due to available equipment and for the sake of consistency. A 3 in. diameter coring auger extracts the sample (r_0 = 1.5 in.)and a $\frac{1}{2}$ in. diameter coaxial hole is drilled (r_i = .25 in.). For these values, K = 7.09.[16] These dimensions apply to all the results discussed herein, unless otherwise indicated.

The difficulty with the ring tensile test is similar to that of the flexural test. The maximum stress must be computed using elastic theory, and, so computed, is localized in a very small region of the sample. This problem is exaggerated in the ring tensile test because of the high stress gradient at the inside hole.

Brazil test

The Brazil test is a ring tensile test without the hole. The theory of elasticity solution for this configuration predicts a uniform tensile circumferential stress under the load, indicating that failure should be characterized by the cylinder splitting in half. This type of failure has been observed in the testing of rocks. The magnitude of the failure stress is expressed as

$$\sigma_{br} = \frac{P}{\pi t \, r_0} \qquad\qquad (3.2)$$

and is equivalent to the ring tensile solution with K = 1. There has been some confusion over the interpretation of Brazil test results, due to the fact that for the ring tensile stress field,

$$\lim_{r_i \to 0} K = 6.0 \tag{3.3}$$

while Eq. (3.2) implies that K = 1. This is a mathematical discontinuity. In an effort to force Brazil test results to match ring tensile test results, investigators have suggested that the existence of small brine holes and/or air bubbles implies that K = 6 should be used.[16] Considering the discussion of chapter II, it is not appropriate to speak of concentrations due to a .1 to .5 mm. diameter hole and due to 1/2 in. diameter hole in terms of the same stress field. Mellor and Hawkes[24] have also suggested that the large compressive stresses in the Brazil test specimen (3 times the tensile stress at the center) should be considered in the failure criterion. Due to these problems of interpretation, and due to the great amount of scatter reported to be associated with Brazil test results, this test has not been used extensively.

shear test

No standard shear test has been developed for ice. Torsional shear tests by Butkovich[10] resulted in spiral shaped failure surfaces, indicating failure due to tension. "Direct shear" tests are designed to force the specimen to fail in shear on one or two particular planes.

This has been accomplished by several different methods, and the limited results which are available seem to depend on the method used.

in-situ cantilever

Although this is not a small-scale test, available results are sufficiently numerous and of sufficient interest that they merit attention in the context of small-scale tests. The cantilever is carved out of an ice sheet by cutting three sides with a saw and allowing the fixed end to remain connected to the ice sheet. The load is applied, up or down (tension in bottom or top) via some sort of lever arrangement. Ice thicknesses tested have ranged from 15 to 95 cm. The computation of the moment at the fixed end has generally neglected the change in bouyancy due to deflection, and the maximum stress, denoted as σ_{isc}, is computed from the moment using elastic beam theory.

D. A Review of Test Results

The presentation of test results in this section will be limited to those results to which the analyses of the ensuing chapters are applicable. In particular, attention is given to results for columnar-grained ice, with c-axis perpendicular to the long axis of the column and randomly oriented in the horizontal plane of the ice sheet. Those loadings will be considered for which the applied stress is perpendicular to the long axis of the column and in the plane of the c-axis. Although this is a rather specialized situation, it is the most frequently encountered geometry and stress state associated with the bend-

ing and/or plane stress states in an ice sheet. This type of loading
and grain geometry is illustrated in figure 3.2, and shall be assumed
unless otherwise stated. Other types of grain geometries and loadings
will occasionally be mentioned for the sake of comparison. A compre-
hensive review of small-scale strength test results is presented by
Weeks and Assur.[14]

compression test—fresh water ice

Compression tests are generally characterized by the formation of
small internal cracks at loads far below the failure load.[18,25] When
enough of these cracks have formed, failure takes place either along
a plane of maximum shear or along fault zones, the latter occurring at
higher load rates than the former.[25] Some of the strength results are
summarized below.

1) geometric effects

Butkovich[9] found that compressive strength decreased with increas-
ing ratio of length to diameter, and with increasing cross-sectional
area. He also found that larger grained ice yielded higher strength
values.

2) rate of loading

Gold[25] found that the compressive strength of ice increases with
increasing crosshead speed as shown in figure 3.3. At the low load
rates the specimen yields, while at the high load rates, failure is
abrupt, as can be seen from the typical stress-strain curves shown in
figure 3.4. Weeks and Assur[14] report results of Butiagin, which show
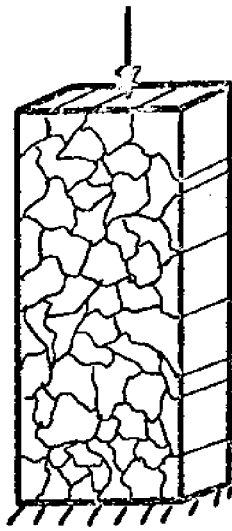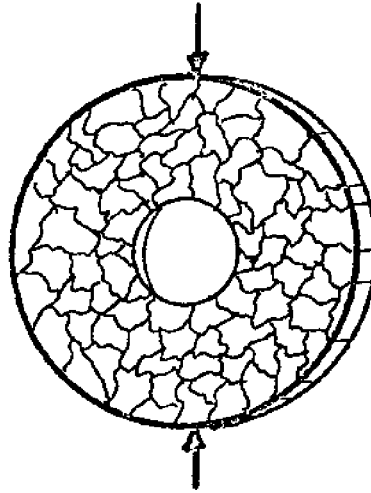
uniaxial   ring tensile
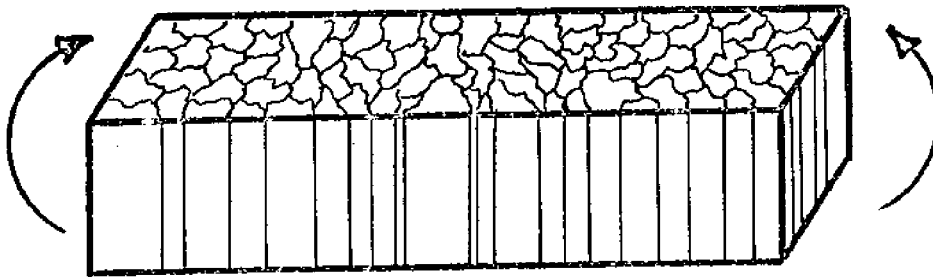
flexural

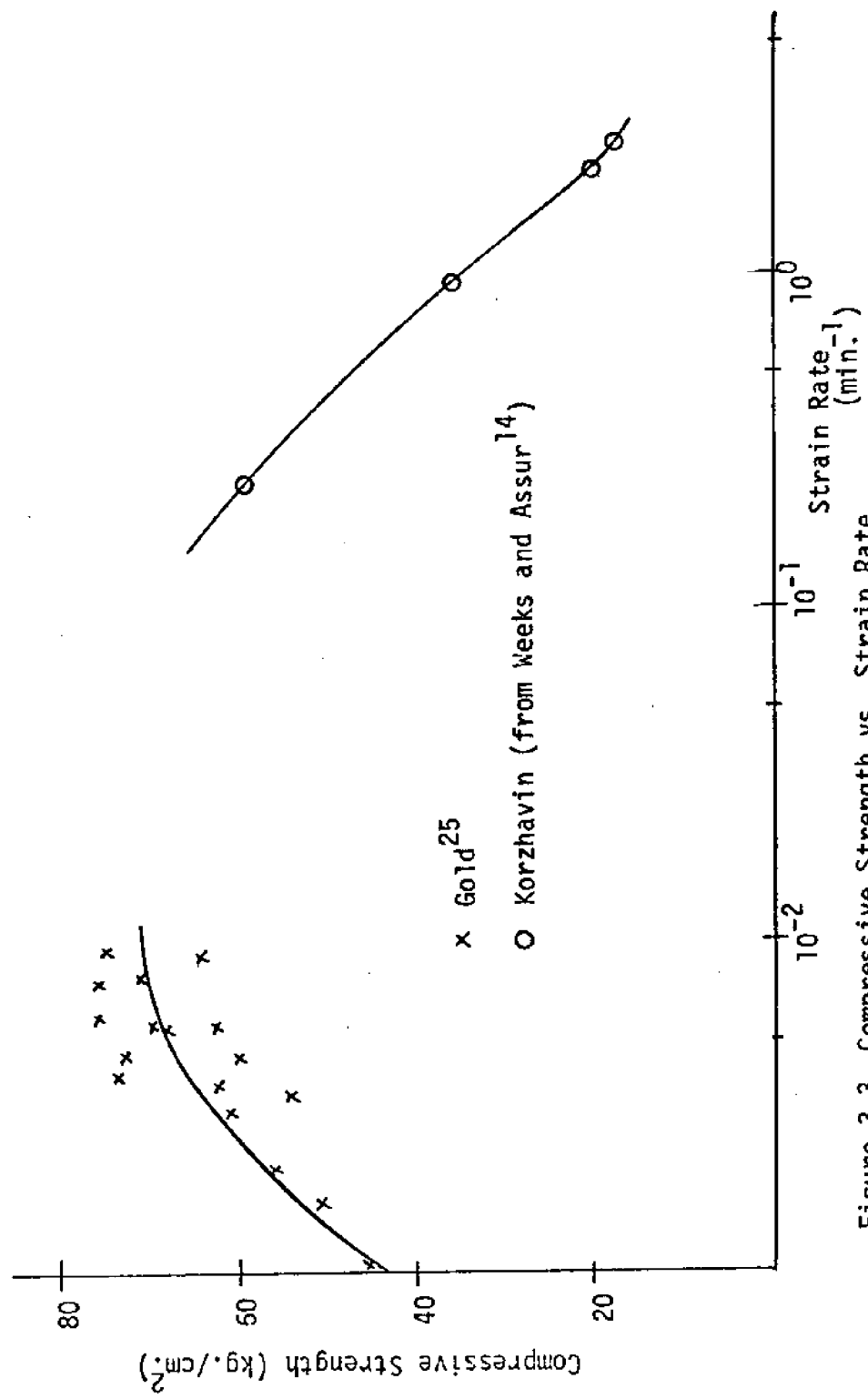Figure 3.2 Orientation of Grains with respect to Specimens

Figure 3.3 Compressive Strength vs. Strain Rate
(fresh ice between -9° and -11°C)

a decrease of strength with increasing rate. These are also shown in figure 3.3.

3) temperature

In general, fresh ice compressive strength has been found to increase with decreasing temperature.[10,23] The results of Butkovich[10] are shown in figure 3.5, and are typical of those of other investigations. For infiltrated snow ice, Butkovich found a much weaker temperature dependence.

compression test—sea ice

Compressive strength studies on sea ice have been carried out by Butkovich[27,28] and Peyton.[20] Specimens tested were both parallel and perpendicular to the plane of the ice sheet. For both it was found that failure was either by rapid deformation at the maximum load (ductile) or by "bursting with a loud report into hundreds of small fragments."[27] He also reports strengths of vertical cores to be two to three times greater than horizontal cores. The following results apply to horizontal cores.

1) rate of loading

Peyton has studied the load rate effect extensively. He expresses the effect of load rate on strength as

$$\sigma_c \propto (\dot{\sigma})^{r_c} \tag{3.4}$$

where $\dot{\sigma}$ is the stress rate in psi/min. The rate exponent in compression, r_c, is expressed via a regression analysis, as

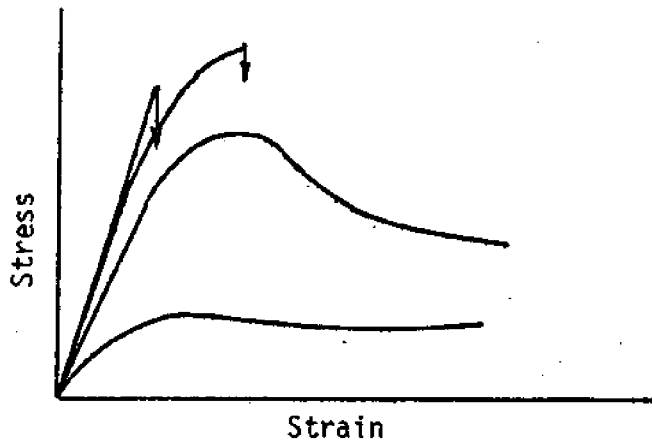$$r_c = .166 \ d^{.138} \ T^{.09} \tag{3.5}$$

Figure 3.4   Stress-Strain Curves in Compression - Fresh Ice[25]
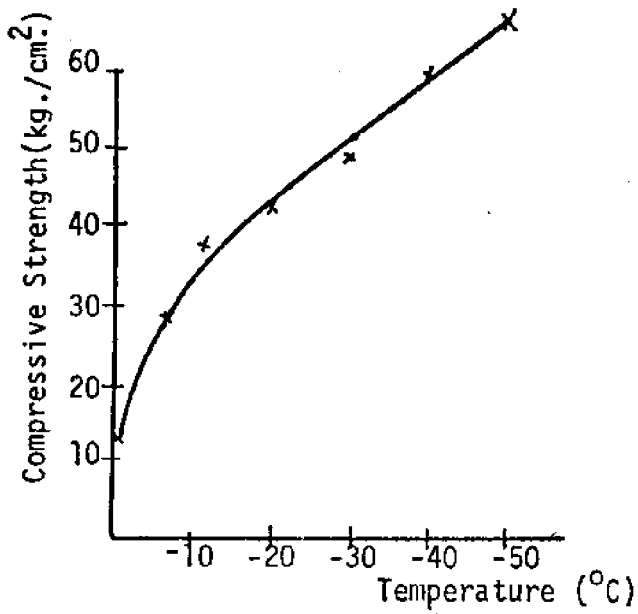

Figure 3.5   Compressive Strength vs. Temperature-Fresh Ice[10]

where d is the depth of the ice sheet in inches and T is minus °C.
This relation was derived from load rates up to 3000 psi/min. The im-
plied strength—load rate relationship for a given depth and tempera-
ture, passing through an arbitrary data point, is shown in figure 3.6.
Later results in a higher load rate regime show the opposite effect,
i.e., decrease of strength with increasing load rate. These are also
shown in the figure.

2) <u>brine volume</u>

Butkovich presents limited data which indicates decreasing strength
with increasing brine volume. Peyton analyzed his results in terms of
the brine pocket model discussed in chapter II, and found that the
strength variation with brine volume could be represented by a linear
variation with $\sqrt{v}$. His data also suggest that the slope of this rela-
tion changes discontinuously at -8.2°C, implying a reinforcing effect
due to the precipitation of $Na_2SO_4 \cdot 10H_2O$. Peyton's analysis indicates
that the effect of temperature, other than through brine volume and
solid salt precipitation, although more significant with increasing load
rates, is not so significant as in fresh water ice.

uniaxial tensile test—fresh water ice

The uniaxial tensile strength of ice is about 1/4 of its uniaxial
compressive strength. Unlike compressive failure, uniaxial tensile
failure occurs suddenly and without the noticeable formation of inter-
nal cracks.[18] Uniaxial tensile results have been presented by Butkov-
ich,[10] Jellinek,[21] and by the South Manchuria Railway Co.[23] Butkovich
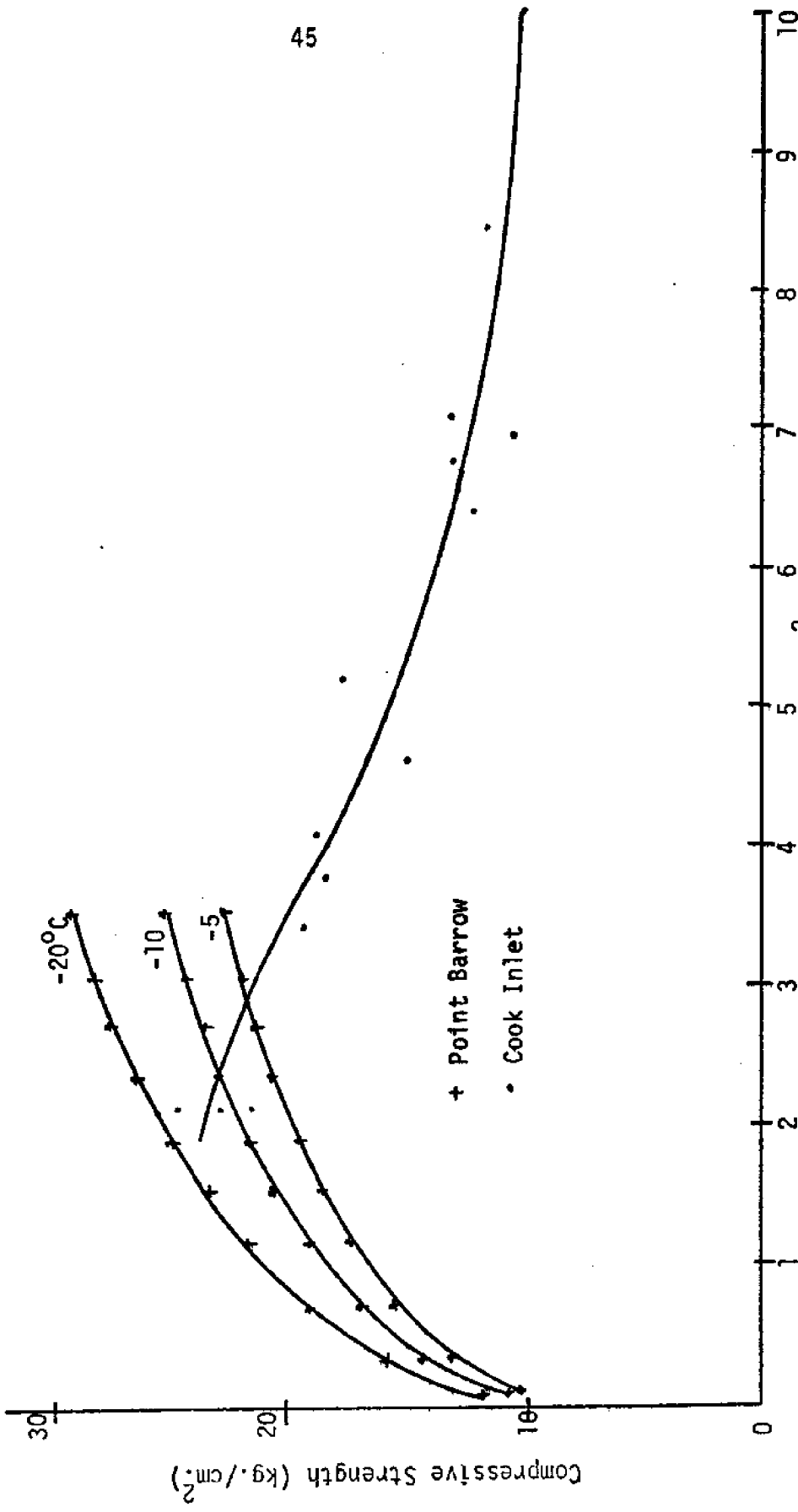
Figure 3.6 Compressive Strength vs. Load Rate (Peyton[20])

used commercial ice with loading normal to the columnar grains. Tests reported in reference 23 loaded specimens parallel to the ice sheet. Although the crystal orientation of the latter is not made clear in the reference, these two test series will be considered comparable. Jellinek used fine grained equigranular snow ice prepared in the lab.

1) load rate

Figure 3.7 shows the dependency of strength on load rate as presented in references 21 and 23. The magnitudes should not be compared because of the difference of ice types, but the trends are interesting to note.

2) temperature

References 10 and 23 show σ_t increasing with decreasing temperature. Their results have been plotted together in figure 3.8.

uniaxial tensile test—sea ice

Uniaxial tensile tests on sea ice have been performed by Dykins[22] and Peyton.[20] The tests by Dykins were performed on sea water frozen in the lab under conditions which simulated sheet ice growth. Peyton used samples obtained in the field.

1) geometric effects

Dykins found no variation of strength with depth, for a fixed temperature and salinity range. Since grain diameter increases with depth, he uses this to conclude that there is no variation of strength with grain size. Dykins also found tensile strengths perpendicular to the ice sheet to be two to three times greater than horizontal tensile strength.

Tensile Strength (kg./cm²)

Jellinek[21]

Reference 23

15

10

5

0.2   0.4   0.6   0.8   1.0

Load Rate (kg./cm²/sec.)
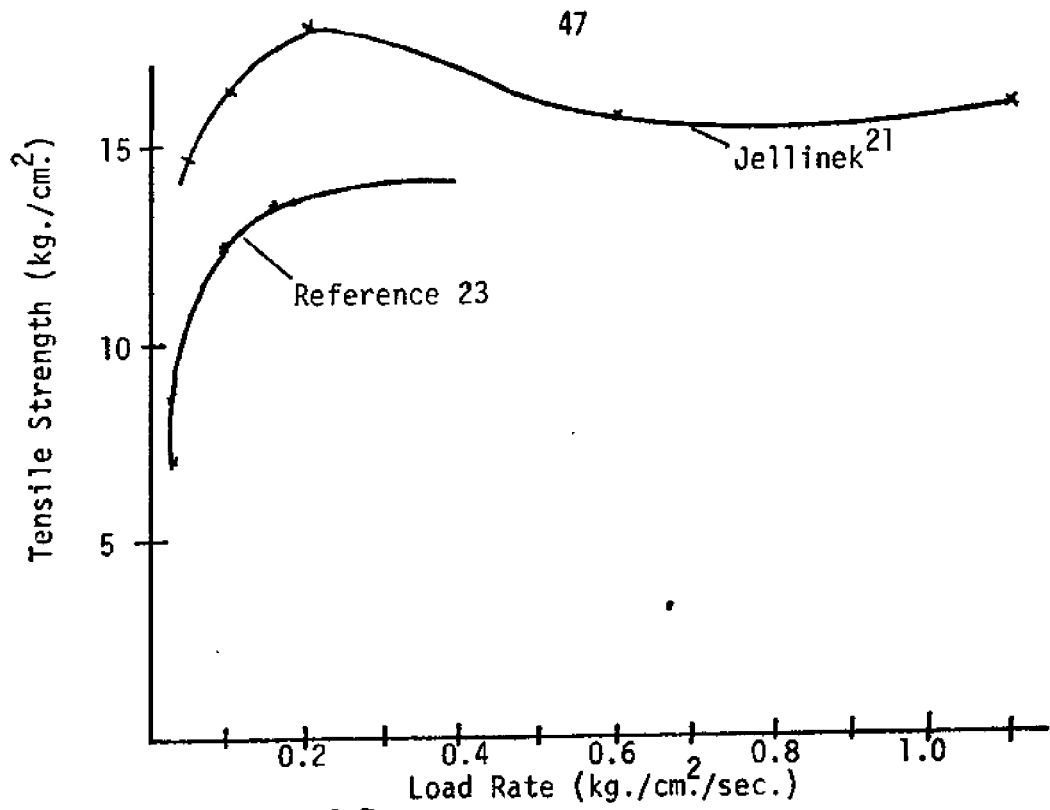
Figure 3.7
Tensile Strength vs. Load Rate-Fresh Ice

Tensile Strength (kg./cm²)

20

Butkovich[10]

15

Reference 23

10

5

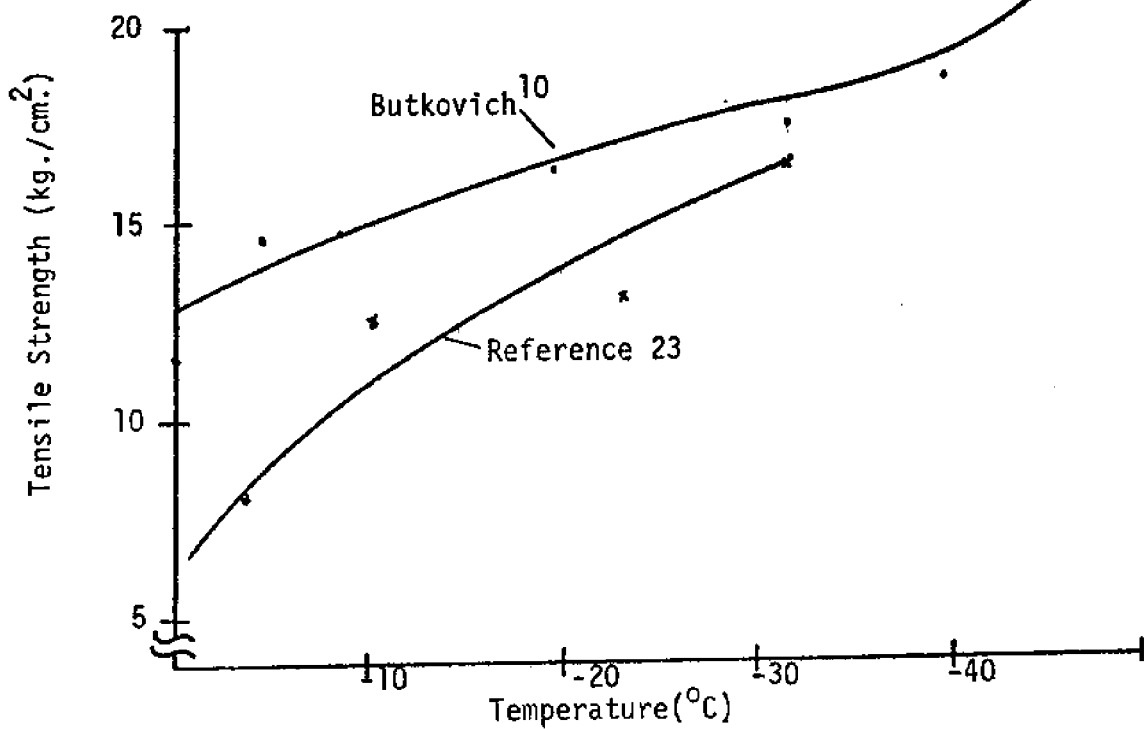-10   -20   -30   -40

Temperature(°C)

Figure 3.8   Tensile Strength vs. Temperature-Fresh Ice

2) **load rate**

Peyton's analysis of his data follows the format of Eq. (3.4), where r_c is now replaced by r_t, the rate exponent in tension. A regression analysis of his data leads to the following relationship for r_t:

$$r_t = .082(d)^{-.295}(T)^{-.065}$$

(3.6)

This relation indicates a much lower strength sensitivity to rate than was found in compression for the tensile load rates used. The rate sensitivity to temperature is almost unnoticeable. It is interesting to note that the rate dependence on depth is opposite to that found for compression. Dykins found strength to decrease with increasing load rate in a higher load rate regime. The results of these two studies are plotted together in figure 3.9.

3) **brine volume**

Both investigators found an approximately linear dependence of strength on $\sqrt{v}$. Dykin's results are shown in figure 3.10.

flexural tests—fresh water ice

Test results presented in reference 23 show that the flexural strength of small beams decreases with increasing beam depth and with increasing temperature. The results for temperature are shown in figure 3.11.

flexural tests—sea ice

1) **load rate**

Dykins[29] and Tabata[30] have studied the flexural strength of ꞏ all
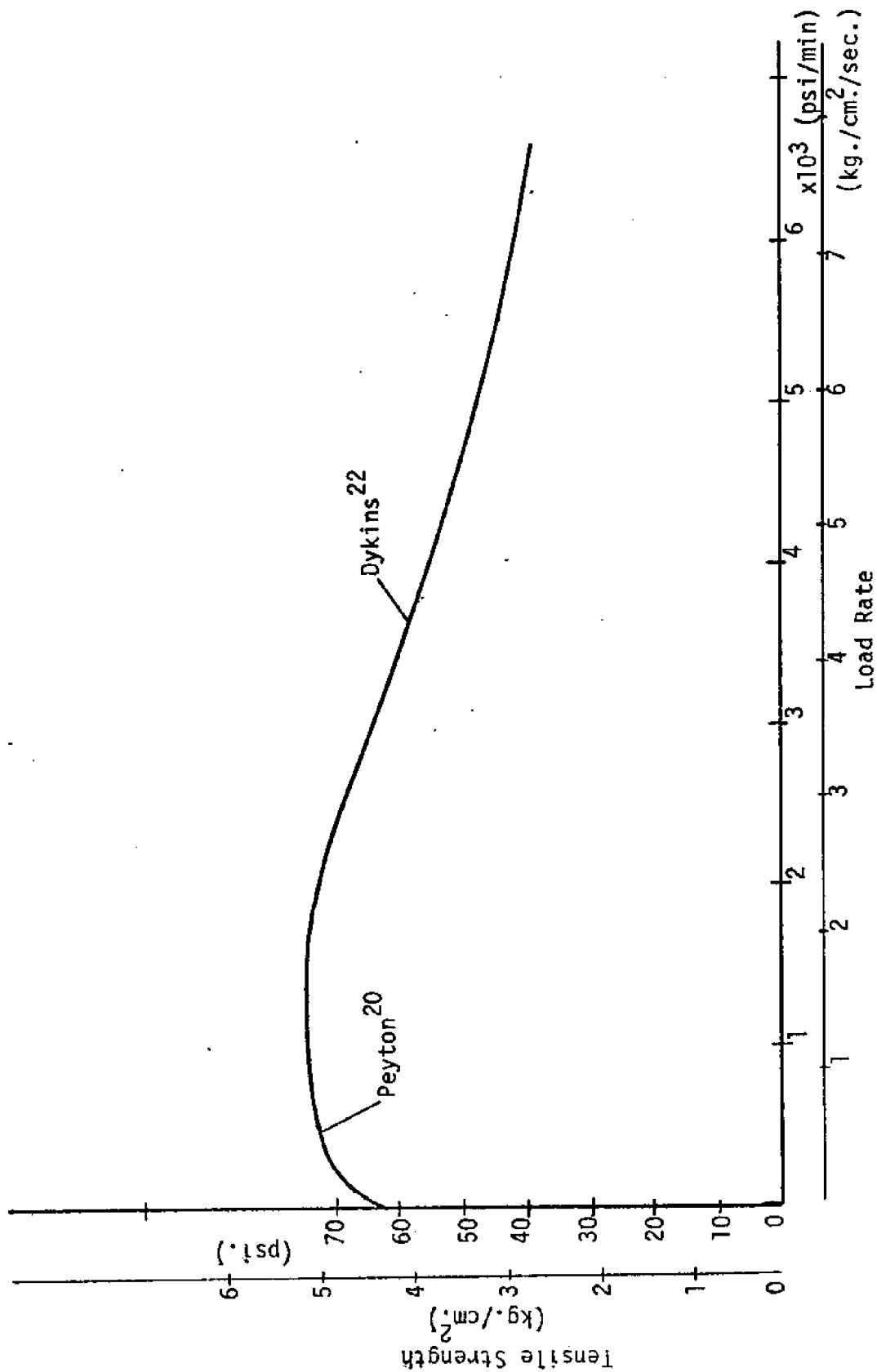
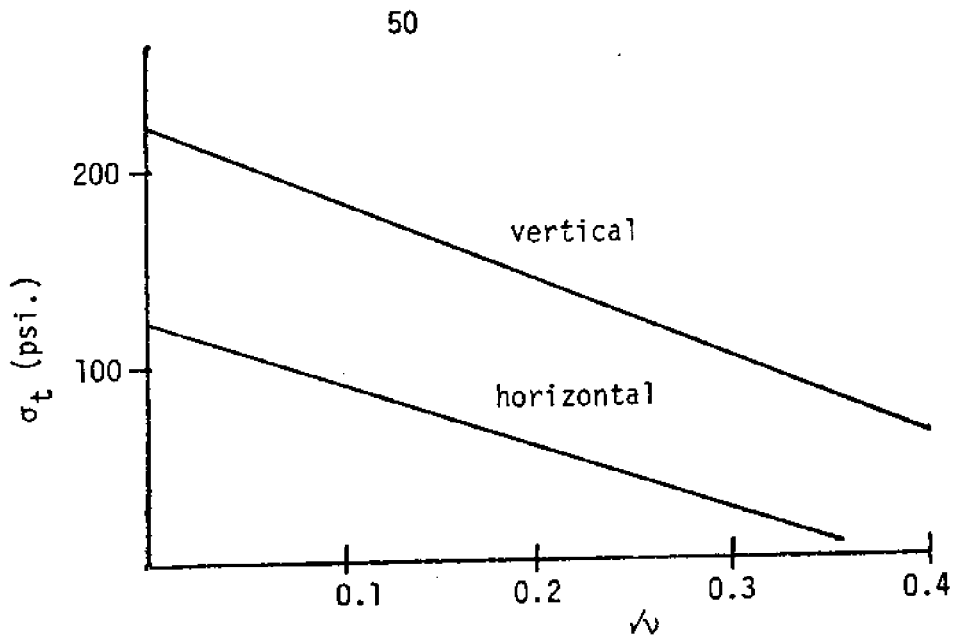Figure 3.9 Tensile Strength vs. Load Rate-Sea Ice (arbitrary reference point)
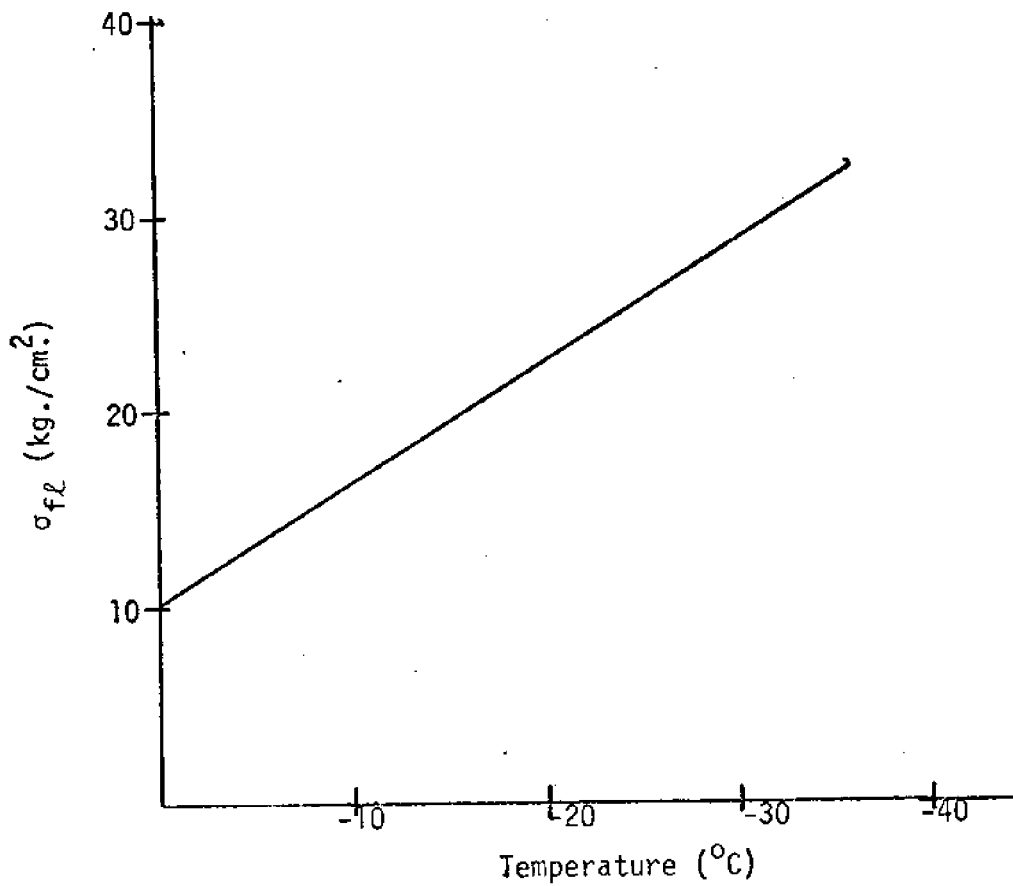
Figure 3.10 Tensile Strength vs. Brine Volume[22]

Figure 3.11 Flexural Strength vs. Temperature-Fresh Ice[23]

sea ice beams. Tabata has studied the effect of load rate and has found an increasing strength with increasing load rate, with the exception of very low rates. His results are shown in figure 3.12.

2) brine volume

The temperature-salinity results are similar to those found in uniaxial tension. Dykins uses brine volume as the relevant variable and finds a linear relation between strength and $\sqrt{v}$. Tabata shows increasing strength with decreasing temperature at a fixed salinity, which coincides with decreasing brine volume. These results are shown vs. brine volume in figure 3.13.

ring tensile test—fresh water ice

The limited number of ring tensile results available for fresh water ice indicate an increase in strength with decreasing temperature, down to about -10° C, followed by a region of relative insensitivity to temperature between -10° C and -35° C.[17,31]

ring tensile test—sea ice

1) load rate

Paige and Kennedy[32] have studied the effect of load rate by testing samples at various crosshead speeds. A typical curve of their results is shown in figure 3.14. As the crosshead speed is increased, the computed strengths approach values comparable to those obtained in uniaxial tensile tests. The speeds required to bring this about, however, far exceed those normally used for other ring tensile results.
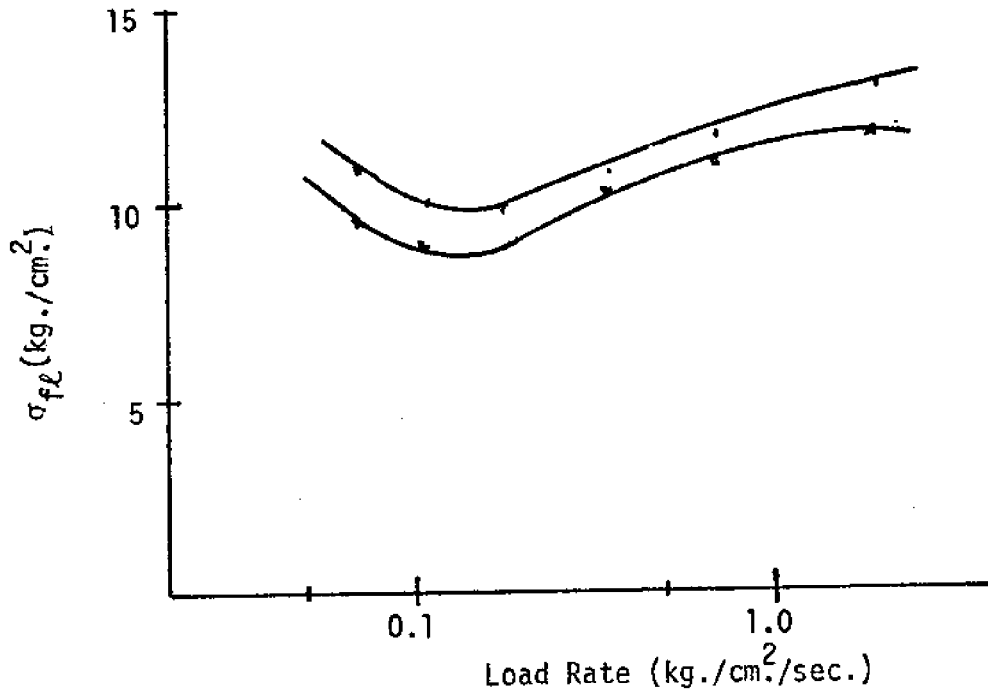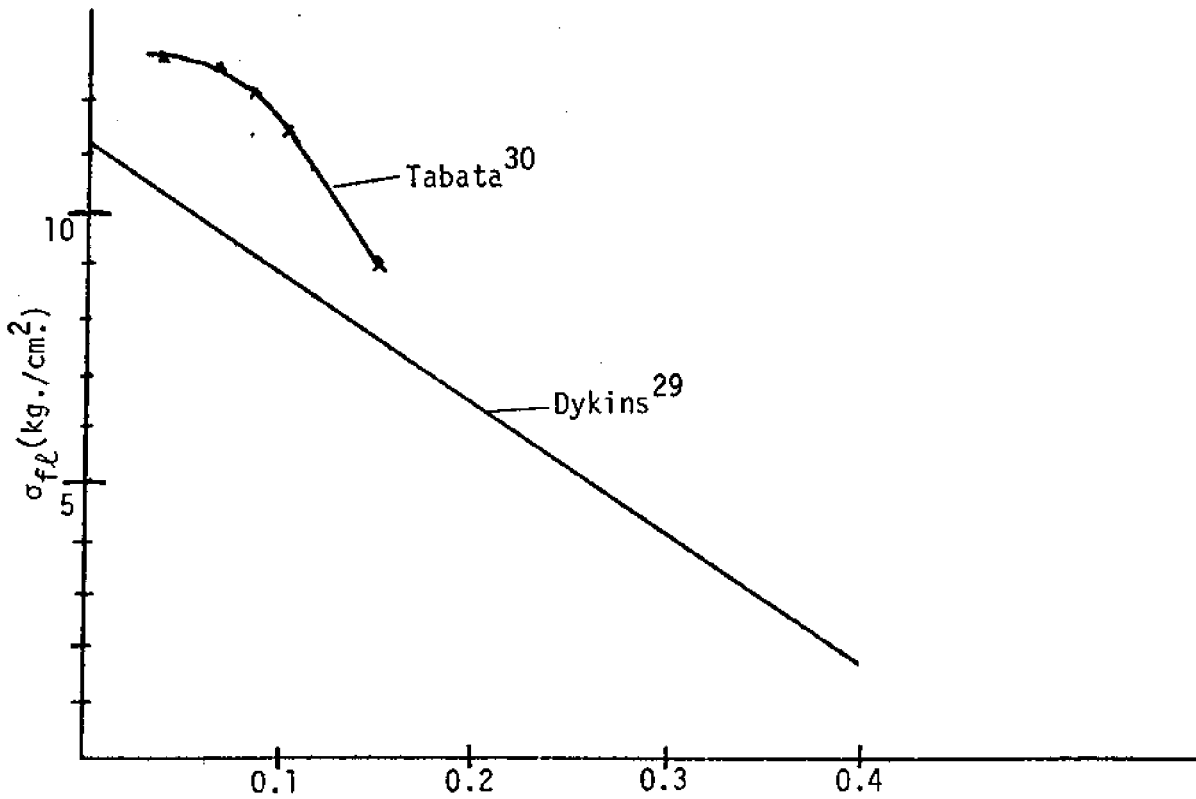
Figure 3.12 Flexural Strength vs. Load Rate-Sea Ice[30]

Figure 3.13 Flexural Strength vs. Brine Volume
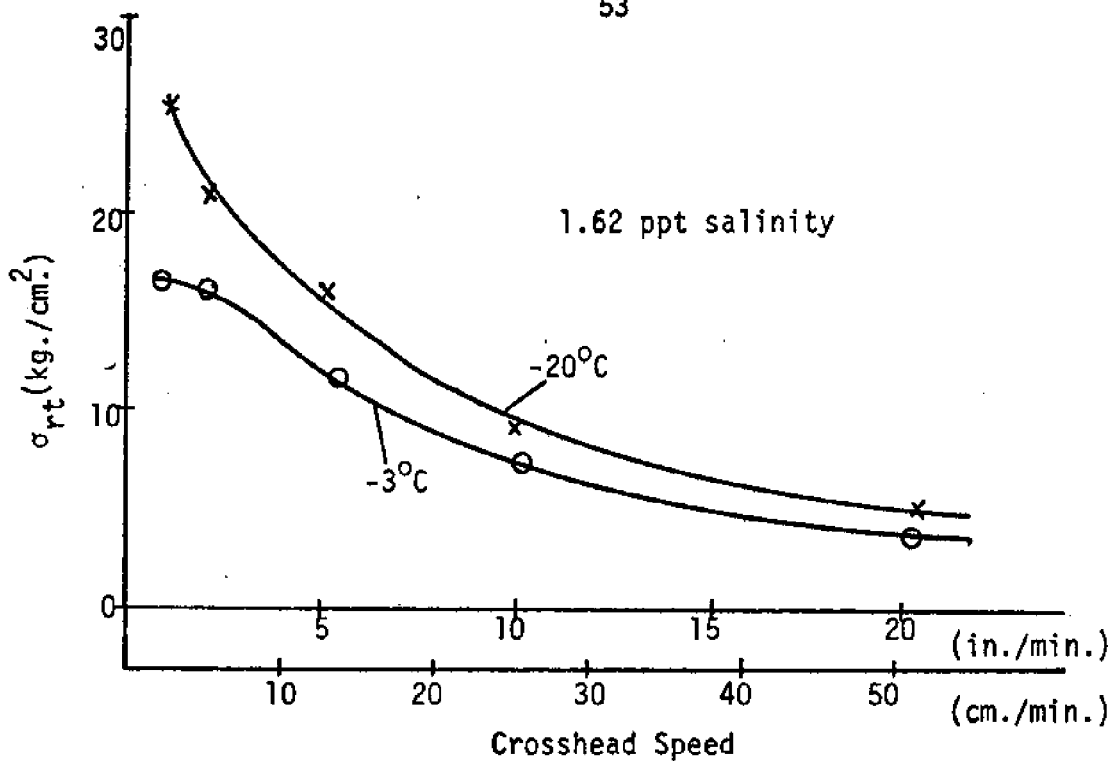
Figure 3.14 Ring Tensile Strength vs. Crosshead Speed[32]
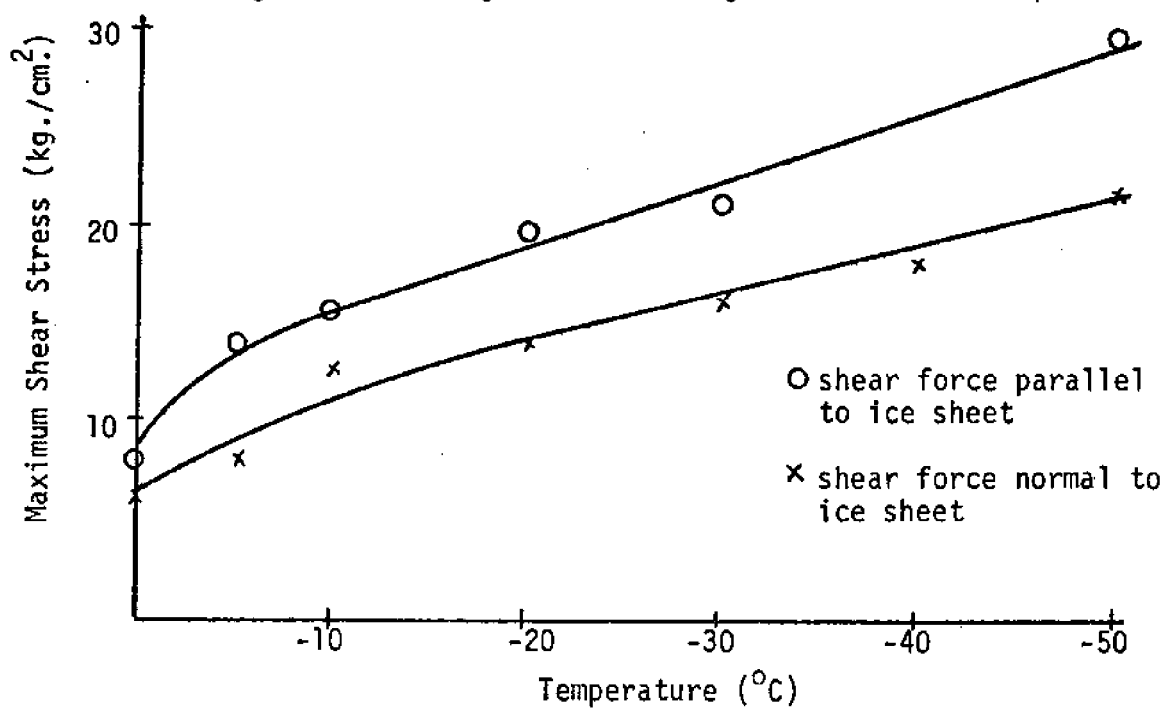
Figure 3.15 Torsional Shear Strength vs. Temperature - Fresh Ice[10]

2) brine volume

Ring tensile testing has been used extensively to study the relationship between strength and brine volume, and represents the most consistent study of any ice strength property. Table 3.1 shows the strength-brine volume relationships which have been obtained by the authors indicated. Strength is in kg./cm^2 and brine volume is measured as the volume fraction.

Weeks[17] has studied the effect of the precipitation of $NaCl \cdot 2H_2O$ by conducting tests on laboratory ice formed from a solution of NaCl and water. He found that below the precipitation temperature, σ_{rt} was independent of the amount of precipitate present and comparable to that for fresh water ice. The results of Greystone and Langleben[33] indicate no effect on strength with the precipitation of $Na_2SO_4 \cdot 10H_2O$.

3) geometry

Tests by Paige and Kennedy have indicated that ring tensile strengths are not affected by increasing the diameter of the inner hole. Early results of Butkovich,[27,28] however, using a one-inch diameter hole, exhibit strengths lower than those which seem to be typical for standard ring tensile tests. Langleben[35] has found a consistent increase of strength with depth, regardless of brine volume. From this he implies an increase of strength with grain size, the other depth dependent variable. Horizontal cores have yielded lower strengths than vertical ones.[36]

Table 3.1 Strength vs. Brine Volume Relations for Ring
Tensile Tests

$$\sigma_{rt} = a - b\sqrt{\nu} \quad (kg./cm.^2)$$

Investigator	a	b	Remarks
Greystone and Langleben[33]	29.0	53.3	results adjusted to a common temperature of -10°C using results from fresh water compression tests[10]
Weeks [17]	24.7	51.5	tests on laboratory grown NaCl ice (not actual seawater) $0<T<21.2^\circ$C
Frankenstein[31]	28.2	58.1	$\sqrt{\nu} < .4$
	6.7	0	$\sqrt{\nu} > .4$
Vinieratos and Dykins[34]	22.2	36.8	high load rate (20 in./min.)
Dykins[75]	30.4	3.95	(K=6) solid cylinder (Brazil test)

Brazil test

Very few results are available for the Brazil test. Those which are available have been interpreted using K = 6, and as such show values slightly higher for those of equivalent ice tested by the ring tensile test.[31] Frankenstein[31] tests the K = 6 assumption by comparing Brazil test results to companion ring tensile results and finds that using K = 5.2 would make them similar. The brine volume dependence as reported by Dykins is shown in Table 3.1 along with the ring tensile results.

shear tests

The results of shear tests vary with the type of test. Figure 3.15 shows the effect of maximum shear in torsion on temperature, as reported by Butkovich.[10] Direct shear between two blocks was used in reference 23 to produce the results shown in figure 3.16. Voitkovsky mentions results which show that the shear strength increases with increasing compression on the shear plane. Butkovich[27] used a double shear method on sea ice, by putting the specimen in a three-sectioned box with the load applied to a movable middle section. Failures in the section between the two shear planes always occurred before the final shear failure, and the resulting shear failure stresses were considerably higher than those from other investigations.

in-situ cantilever—fresh water ice

Frankenstein[11,12,37] has tested in-situ cantilever beams of lake ice with thicknesses ranging from 11 to 75 cm. His samples consisted

of clear ice, snow ice, and combinations. His values for strength

ranged between 2 and 8 kg/cm^2 for load rates between 0.1 and 2.0 kg/

cm^2/sec. For clear ice, the data shows greater strengths when the

bottom was in tension, and showed no significant effect of temperature

on strength. Small-scale beam tests on the same ice gave values two

to three times higher than those for the in-situ beams. Voitkovsky[18]

reports strength results for in-situ cantilevers (referred to in

Russian as "piano keys of ice") which are similar to those of Franken-

stein.

Brown[38] suggests that there is a stress concentration at the corner

of the fixed end, and that the actual stress is increased by a factor

of 2.8, a value obtained from photoelastic analysis. Frankenstein[12]

has tested simply supported beams in place, and has found strengths to

be slightly higher than those for companion cantilevers, but not suf-

ficiently to justify the 2.8 factor.

in-situ cantilever—sea ice

In-situ cantilever tests on sea ice beams have shown no noticeable

difference between push down and pull up results.[15,40] Weeks and

Assur[14] have presented the in-situ cantilever results of references 27,

15, and 40 in terms of $\sqrt{v}$ as shown in figure 3.17. Tabata et al.[40]

has found the strength to increase with increasing load rate for ice

sheets less than 30 cm. thick at temperatures close to 0° C, i.e., ice

sheets less with fairly uniform temperature through the thickness. These
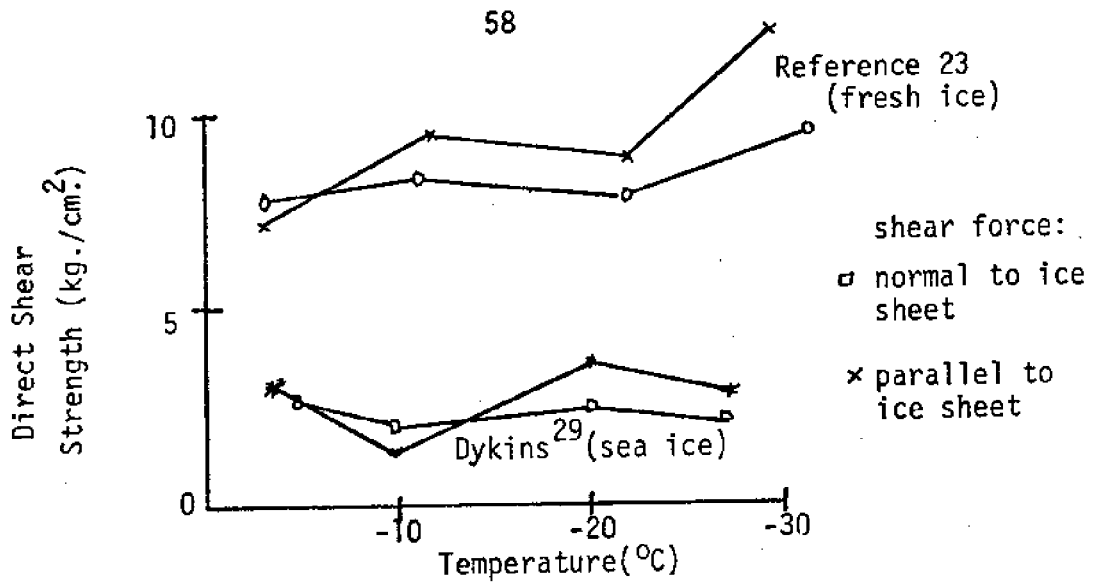
Figure 3.16 Shear Strength vs. Temperature

The vertical axis is labeled Direct Shear Strength (kg./cm^2.) with values 0, 5, 10. The horizontal axis is Temperature(^{o}C) with values -10, -20, -30.

Labels on the graph: Reference 23 (fresh ice); shear force: σ normal to ice sheet, $\times$ parallel to ice sheet; Dykins[29] (sea ice)
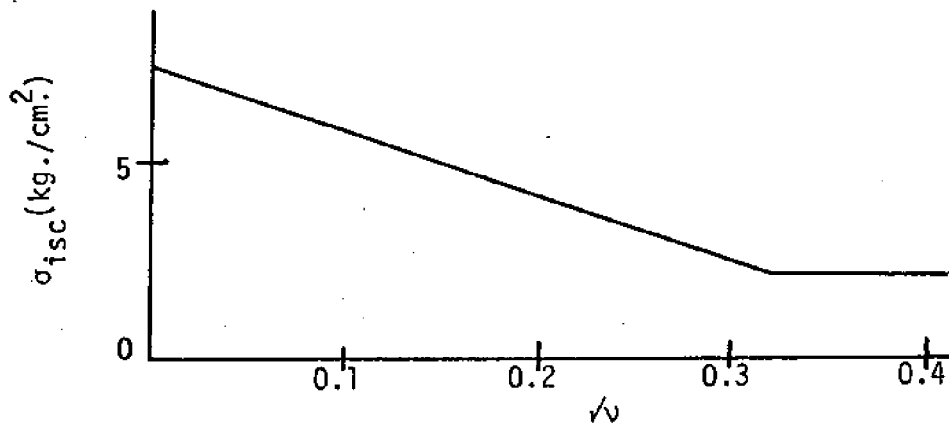
Figure 3.17 In-situ Cantilever Strength vs. Brine Volume

The vertical axis is labeled σ_{isc}(kg./cm^2.) with values 0, 5. The horizontal axis is $\sqrt{\upsilon}$ with values 0.1, 0.2, 0.3, 0.4.
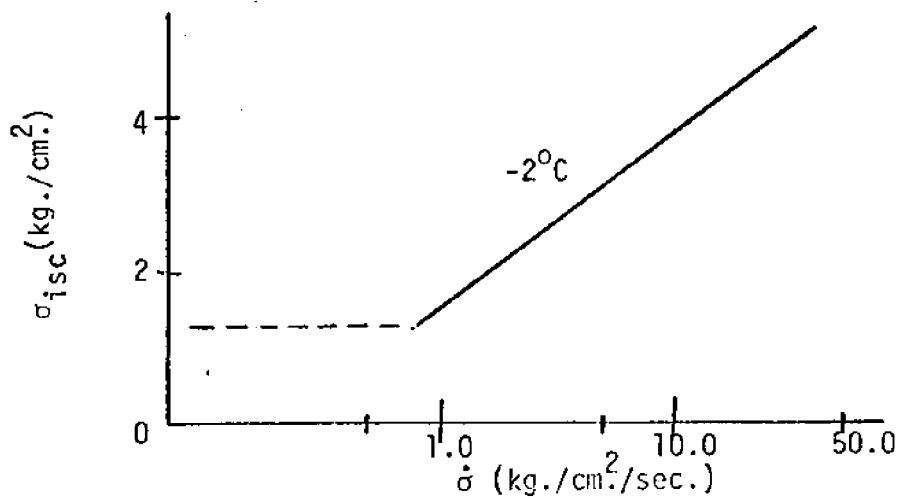
Figure 3.18 In-situ Cantilever Strength vs. Load Rate (Sea Ice)

The vertical axis is labeled σ_{isc}(kg./cm^2.) with values 0, 2, 4. The horizontal axis is $\dot{\sigma}$ (kg./cm^2./sec.) with values 1.0, 10.0, 50.0. Label on the graph: -2°C

results are shown in figure 3.18. It can be seen that strength values from in-situ cantilever tests are lower than those for any of the small-scale tests.

E. Interpretation of Test Results

Scope

The basic purpose of a small-scale test is to obtain some information about the failure of ice, which can then be applied to a full-scale ice sheet problem. The first problem in doing this is that the stress state experienced by the small-scale sample, and the type of failure produced by this stress state, are both distinctly different from what is experienced in the full-scale ice sheet. The second problem is that the interpretation of a small-scale test result relies on a knowledge of the stress state in the sample. The complex internal structure of ice, and the lack of understanding of the small-scale properties of ice, make this knowledge difficult to obtain. It should be emphasized that the problem of interpretation is distinct from the problem of application; i.e., having satisfactorily interpreted the results of a series of small-scale tests does not imply that they are directly usable for the prediction of the strength of an ice sheet.

The basic attempt here is to interpret the small-scale test result; i.e., what information does the test yield? This attempt will be founded upon the idea that there are some fundamental properties of ice which manifest themselves in the small-scale test. The results of ex-

tensive experimental studies are available. It is desired to utilize these results to see if they suggest any intrinsic properties which have heretofore been ignored in the analysis of the data. The identification of these properties and their quantification via some sort of physical-mathematical model will allow for a reassessment of test results and will shed further light on the results that have been obtained. This has been done in the case of brine volume (see chapter II). This approach shall be pursued here. One would like to know, for example, if the variation of strength on a particular parameter is a function of the type of test conducted or of the material being tested. If the former is true, then one can guess just what intrinsic properties manifest themselves in that type of test but not in others. If the latter is true, then something has been learned about the material, and it can be assumed that that property will somehow exhibit itself in other test situations and in full-scale behavior.

Summary of Test Results

In the light of the test results just presented, the following generalities can be made.

1. compressive strength

As expected, the strength of ice in unconfined compression far exceeds that found in any other type of test. The failure process, which is accompanied by a high degree of internal cracking, suggest further investigation.

2. tensile strength

Of the four predominant methods of tensile strength testing, the following inequality seems to be the rule:

$$\sigma_{rt} > \sigma_{f\ell} > \sigma_t > \sigma_{isc} \tag{3.7}$$

Typically for sea ice, ring tensile strength values lie between 15 and 30 kg/cm^2, flexural strength values between 7 and 15 kg/cm^2, uniaxial tensile strength values between 2.5 and 8 kg/cm^2, and in-situ cantilever strength values between 1.5 and 6.0 kg/cm^2.

3. shear strength

Very little information has been obtained from shear strength tests due to the limited results available, the variety of testing techniques, and the fact that specimens do not generally fail in shear unless forced to do so.

4. strength—temperature

With the exception of ring tensile results between -10° and -35° C, all small-scale test results on fresh ice exhibit a marked increase of strength with decreasing temperature, usually most prominent in the range between 0° and -10° C (figures 3.5, 3.8, 3.11, 3.15). Independent of its effect via brine volume, temperature seems to have no effect on sea ice strength.

5. strength—brine volume

It is difficult to conclude anything other than the linear dependence of strength on $\sqrt{\upsilon}$, since almost all results have been fit in this

manner (Table 3.1). The most convincing results have been those obtained via ring tensile tests, and it is possible to have deduced the $\sqrt{v}$ relationships from these results. The results of other tests are not so convincing.

6. strength—load rate

As suggested in chapter I, the strength variable which takes on the greatest range of values is the load rate. It is evident from the results which have been presented that the effect of load rate has not been clarified. Strength seems to increase with increasing load rate in the low load rate regimes, while the opposite effect is observed in the higher regimes. With the exception of the results of Jellinek (figure 3.7), each test series has exhibited either one trend or the other (see figures 3.3, 3.6, 3.7, 3.9, 3.12, 3.14, 3.18). The transition point (if one really exists) varies considerably depending on which tests are considered.

7. strength—grain size

Although this effect has not been investigated extensively, there are indications that grain size plays an important role. Butkovich (compression), Jellinek (uniaxial tension), and Reference 23 (flexural) all found decreasing strength with increasing sample size. The extremely low strength results for in-situ cantilevers also coincide with this trend. Butkovich (compression), and Langleben (ring tensile) found increasing strength for larger grained ice. Dykins' results (uniaxial

tension) show no such effect, while Peyton's results (compression and uniaxial tension) go both ways, if depth in both of these cases is considered to be a measure of increasing grain size. In any event, these results suggest a possible dependency of strength on the number of grains per sample. This seems to be a reasonable variable for these small-scale tests, where specimen size is not much greater than grain size.

8. small scale vs. full scale

The results of in-situ cantilevers are difficult to interpret because of lack of understanding of the variation of properties through the thickness. One thing that is apparent is the similarity in magnitude between in-situ cantilever results and uniaxial tensile results. This suggests that the uniaxial tensile test yields a strength value which is applicable to full-scale ice sheets. The dependency on rate of loading, however, does not seem to agree for these two tests.

These observations invite a multitude of explanations which can go back and forth indefinitely. The remainder of this research is concerned with the influence of two specific factors—time-dependent plasticity and the existence of grains, and an attempt will be made to see how these two factors can reconcile some of the existing results.

Effects of Plasticity and Grains

Time-dependent plasticity and the existence of grains are effects which have generally been ignored in the interpretation of small-scale

strength data, but which have been occasionally mentioned in the context of explaining anomalous behavior. The exceedingly high ring tensile results give a first indication that such effects are significant. These results were originally explained by the "critical flaw" argument—that the smallness of the region of maximum stress in the ring tensile test yields a lower probability of finding the critical failure-producing flaw than in the larger area of, say, the uniaxial tensile test.[28] This is a Griffith-type argument based on a uniform distribution of flaws in an otherwise homogeneous material. This argument, however, does not seem to be relevant for a material as inhomogeneous as small sample ice. A more relevant argument seems to be the fact that in the ring tensile test, the maximum stresses are experienced by individual grains (points A and B , figure 3.19) rather than by the polycrystalline aggregate as a whole. Failure then depends on the way in which these individual grains carry the load, and the way in which the grains along section AB distribute the load.

The results of Paige and Kennedy (figure 3.14) suggest that the time-dependent plasticity of individual grains governs the computed failure load. The apparent load-rate effect is very likely due to the miscalculation of the maximum stress as a result of plastic stress relief in the highly stressed regions, as suggested by Nevel[41] and depicted in figure 3.20. Lower load rates allow for greater stress relaxation and redistribution, and hence result in a greater error associated with the elastic stress computation. As load rates increase, the response becomes more elastic and the computed stress approaches a value near to that of the
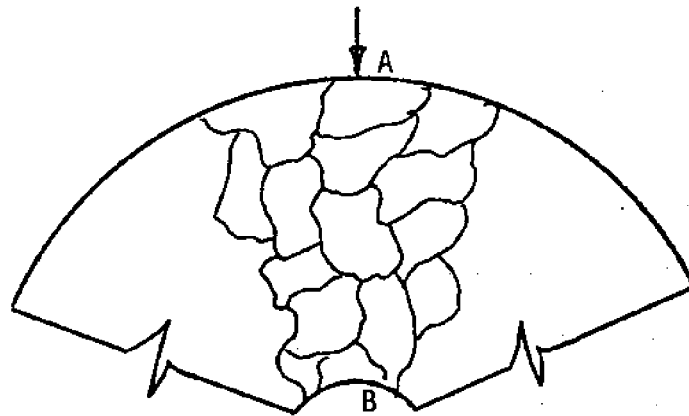
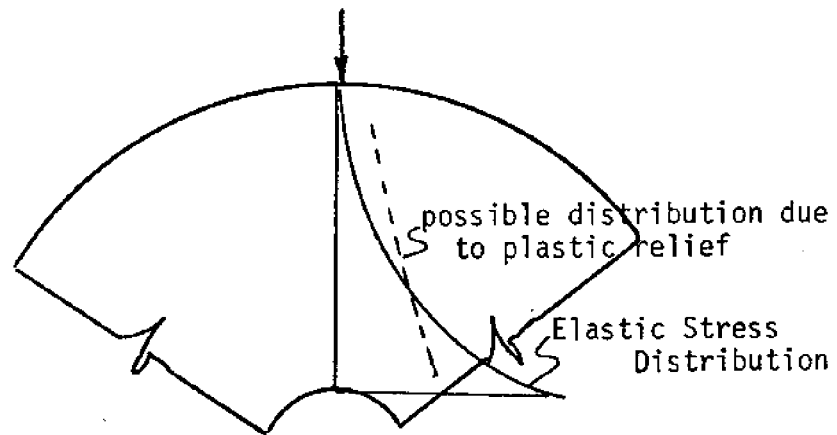Figure 3.19 Grain Structure Under Ring Tensile Load

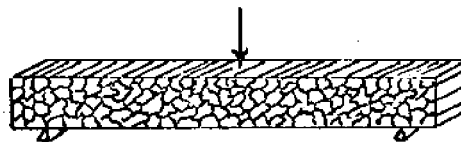Figure 3.20 Tensile Stress Distribution in a Ring Tensile Test

Figure 3.21 Alternative Flexural Test

uniaxial tensile strength.

The place of $\sigma_{f\ell}$ in the sequence of Eq. (3.7) is more difficult to explain in this context. The first temptation is to explain this effect as an overcomputation due to the neglect of plasticity, as was just done for the ring tensile test. The only results available for $\sigma_{f\ell}$ vs. load rate (figure 3.12), however, show a mild increase of strength with load rate, similar to that found in uniaxial tension in the same range (figure 3.9). This contradicts the plasticity argument. A characteristic of the flexural test which makes it different from the uniaxial and ring tensile tests is that the stress gradient lies along the long axis of the columnar grain (see figure 3.2). Consequently, only a small portion of each grain is subjected to the maximum tensile stress, with the opposite end of the grain subjected to compression. This could very likely inhibit the sample from failing at the uniaxial tensile strength.

Reference 23 mentions the results of flexural tests performed on small beams of similar structure as those described herein, but with the loading perpendicular to the column axes (figure 3.21). The results are reported to be similar to those loaded parallel to the column axes. This coincidence suggests that these alternate test results fit properly into the Eq. (3.7) sequence according to stress relief arguments. It is suggested that future small beam tests be cut horizontally from the ice sheet (as is currently done), but loaded in the horizontal plane. A study of the effect of load rate for these types of tests

should exhibit the strength-load rate characteristics of the ring tensile test.

It should be pointed out that the fact that the plasticity arguments ascribed to ring tensile tests are not valid for flexural tests is not contradictory. The former concentrates stresses on one grain, while the latter distributes stresses across several. At the moment, there is no reason to assume that the plastic behavior of the single crystal and the polycrystal is similar. This observation, accompanied by the influence of single crystal plasticity on ring tensile results implied above, suggests that further study of the plasticity of ice single crystals would shed some light on the observed behavior of small samples. A knowledge of single crystal properties would also allow for the treatment of the small sample as the coarse aggregate of grains which it really is.

A review of the plasticity of single crystals of ice is presented in the next chapter.

Chapter IV

THE PLASTIC FLOW OF SINGLE CRYSTALS OF ICE

A. Introduction

Since single crystals are going to be treated as distinct entities in the analysis of polycrystalline samples, it is first necessary to establish a general flow law; i.e., a relationship between stress, strain, and time which is valid for all possible stress and strain histories. The effect of load rate will be implied by such a relationship, while the effects of temperature and salinity will affect the material parameters. It will be kept in mind that such a law need only span a regime which incorporates the stresses, strains, strain rates, and temperatures experienced by single crystals in an ice sheet. For the problem outlined at the end of the last chapter, this regime is further limited to that range of variables applicable to a small-scale strength test. In view of the fact that a good deal of the research to be discussed has been oriented towards explaining the flow of glaciers, this point is important to keep in mind.

The elastic properties of single crystals have been fairly well defined. The hexagonal symmetry of the crystal lattice implies the existence of five independent elastic constants. These values have been reported by Jona and Scherrer.[66]

B. Qualitative Aspects of Single Crystal Flow

Description of Tests

The most significant research concerning the flow of single crystals

of ice has taken place in the past 16 years. During this time, the two basic types of ice which have been studied are natural single crystals found in glaciers and artificial single crystals grown in the laboratory. Both of these single crystal types are different from the single crystals found in an ice sheet in both the method of growth and in the impurity content. Natural single crystals of glacier ice are desirable because of their purity and because of the reproducibility of the results obtained from them.[42] Artificial single crystals, on the other hand, approximate more closely the type of growth experienced by single crystals in a natural ice sheet. In spite of these differences, however, it will be assumed that the basic characteristics of the flow of ice single crystals can be deduced from these types of samples. The similarities between the results obtained from glacier and artificial single crystals supports this view.[43] To this author's knowledge, there has been no reported research concerning the flow of single crystals of salt water ice.

The types of tests which have been performed consist of uniaxial, beam bending, and shear tests. The uniaxial tests include both tension and compression of cylinders and thin plates. The beam tests are performed on simply supported beams with a concentrated load at midspan. The shear tests are performed on blocks sheared on two opposite faces.

Geometry of Deformation

It has been known since the late 19th century that the most significant aspect of ice creep is slip along the basal plane of the crystal.

tensile test

(a)

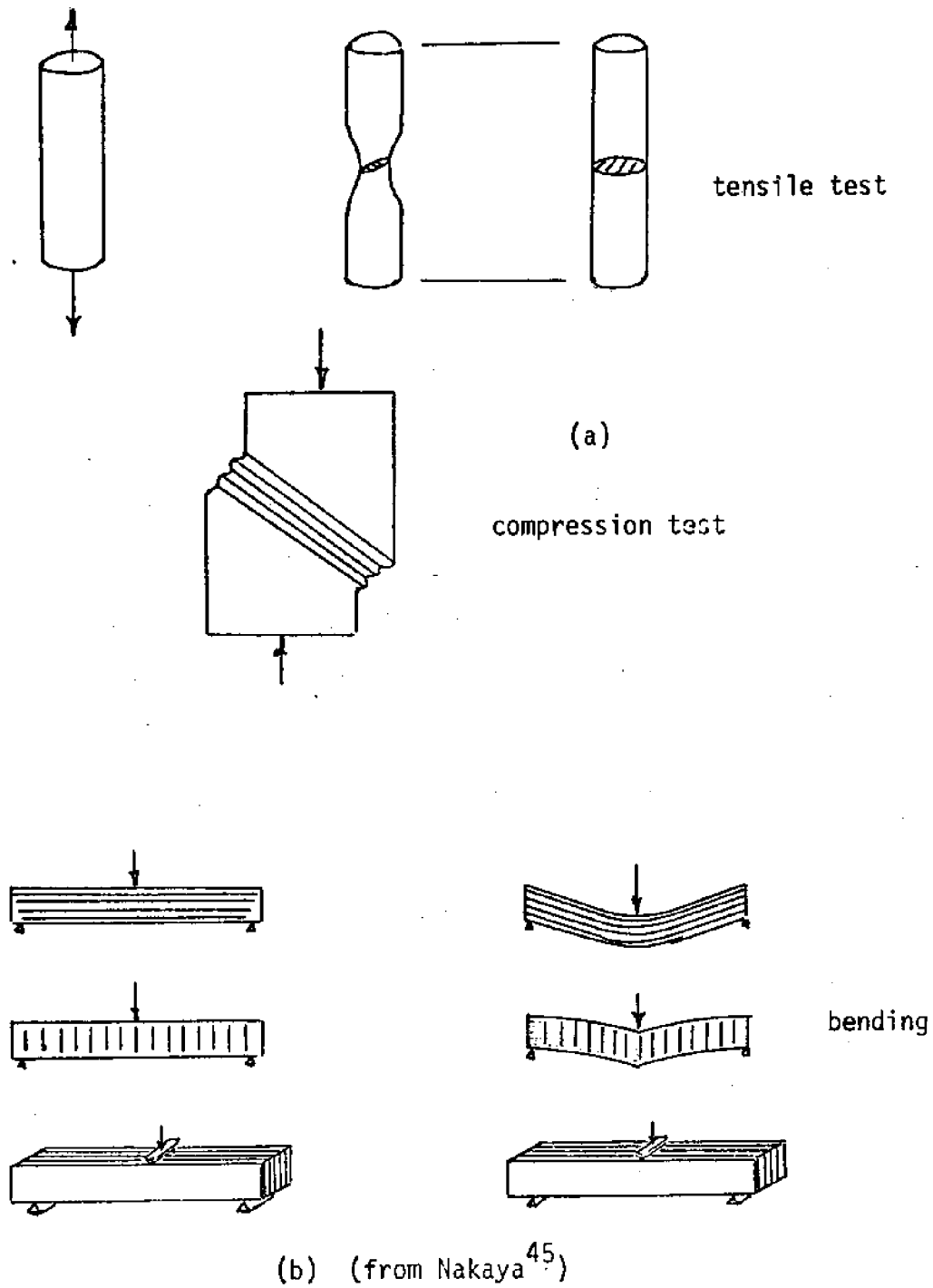compression test

bending

(b) (from Nakaya[45])

Figure 4.1 Geometry of Single Crystal Deformation

This type of deformation is visible to the naked eye, for largely deformed samples, as cylinders necking into tapes, or compressed into segments sliding over one another[43,44] (figure 4.1a). Tests of small single crystal beams by Nakaya[45] have shown that single crystals deform like a deck of cards, with the deformation concentrated in discrete layers (figure 4.1b).

Attempts were made by most of the early creep investigators to establish a preferred slip direction in the basal plane, similar to the slip directions found in most metals. From the viewpoint of atomic structure, a likely slip direction would be one of the three <$11\bar{2}0$> directions, due to the fact that these directions exhibit the highest density of oxygen atoms.[46] Experimental studies have shown, however, that the direction of slip always seems to be in the direction of the maximum resolved shear stress in the basal plane, regardless of the orientation of the a-axes. Figure 4.2 shows the crystallographic notation which is being used here.

Creep Curve Characteristics

Almost all investigators who have investigated the transient creep behavior for ice single crystals have found that whenever a component of shear stress exists on the basal plane, the resulting creep curve is concave upward. Figure 4.3 shows a typical creep curve. This result was originally thought to be due to the geometric effects associated with tertiary creep[53] but subsequent investigations showed that this
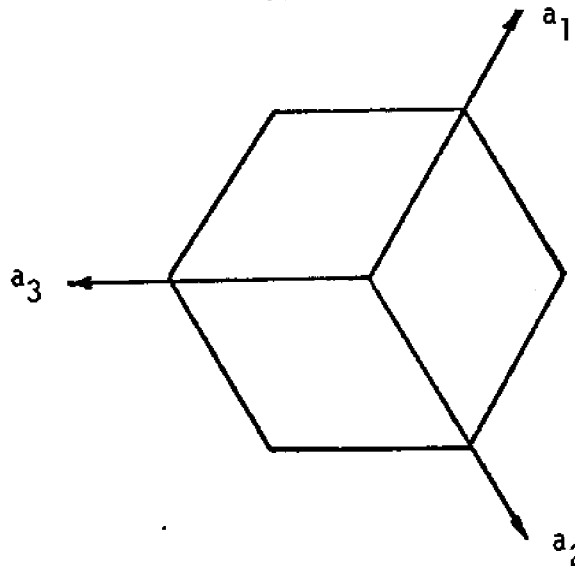
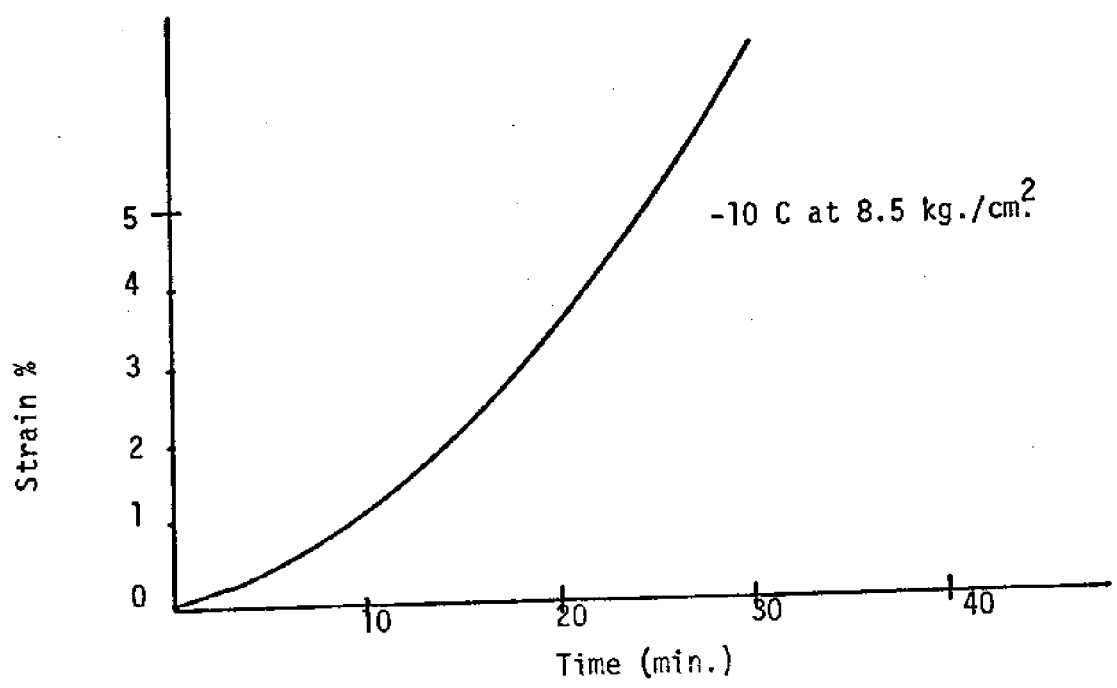Figure 4.2 Crystallographic Notation (basal plane)

Figure 4.3 Typical Creep Curve[43]

was observed at strains well below those associated with geometric nonlinearity. This creep curve is unusual when compared to the creep of metals.

Steinemann[46] tested single crystals in shear and found that the creep curve had two distinct regions— a "hard" region for strains less than 10% to 20% and a "soft" region for strains greater than 10% to 20%, the transition being characterized by an abrupt change in slope. He described this phenomenon as "work softening." The second stage was found to terminate in a linear region of constant strain rate. Compression creep tests by Griggs and Coles[43] yield curves similar to those of Steinemann in their upward concavity but without the transition and the terminal linear stage. Tensile creep tests by Jellinek and Brill[48] have also revealed the accelerating creep rate. In references 43 and 48 the authors claim to have had difficulty in reproducing their creep curves. Subsequent creep investigations by Butkovich and Landauer,[49] Higashi et al.[50] and Jones and Glen[51,52] have all confirmed the idea that a resolved shear stress on the basal plane produces an accelerating creep curve. Higashi et al. have found curves which terminate with constant slope. In general, terminal portions of creep curves are due to the combined effect of large deformations and the type of testing procedure.

For cases where there is no resolved shear stress component on the basal plane, Butkovich and Landauer,[49] Jellinek and Brill[48] and Glen and Perutz[53] have found initially decelerating creep typical of most metals,

with average strain rates on the order of one hundredth of those found for specimens oriented favorably for basal glide. Glen and Perutz have explained this as due to a slight misorientation of the basal plane in the testing machine, while Butkovich and Landauer suggest that the creep is due to mechanisms other than basal glide.

Stress-Strain Curves at Constant Strain Rate

Readey and Kingery,[54] Higashi et al.,[50] Jones and Glen[51] and Wakahama[55] have conducted stress-strain experiments at constant machine crosshead speed. All of their resulting stress-strain curves showed an initial linear portion leading to a maximum followed by a gradual decrease in stress, as shown in figure 4.4. In general, the maximum stress is a function of temperature and strain rate. The most interesting aspect of this curve is the "yield drop" which leads to a "strain softening." This is opposite to the results for low temperature metals, which generally exhibit a strain hardening.

Higashi et al. report that the slope of the initial linear portion of the curve depends on the strain rate, a result which contradicts the idea that the initial linear portion is due to rate independent elasticity. This dependency has not been found by the other investigators. Wakahama finds that only his curves for high strain rates exhibit the yield drop, while the others retain the maximum stress with continued straining. His samples are thin plates 1 mm. thick, while the other investigators used cylinders about 1 to 2 cm. in diameter. Muguruma[37] has shown that the existence of surface layer imperfections has a ten-
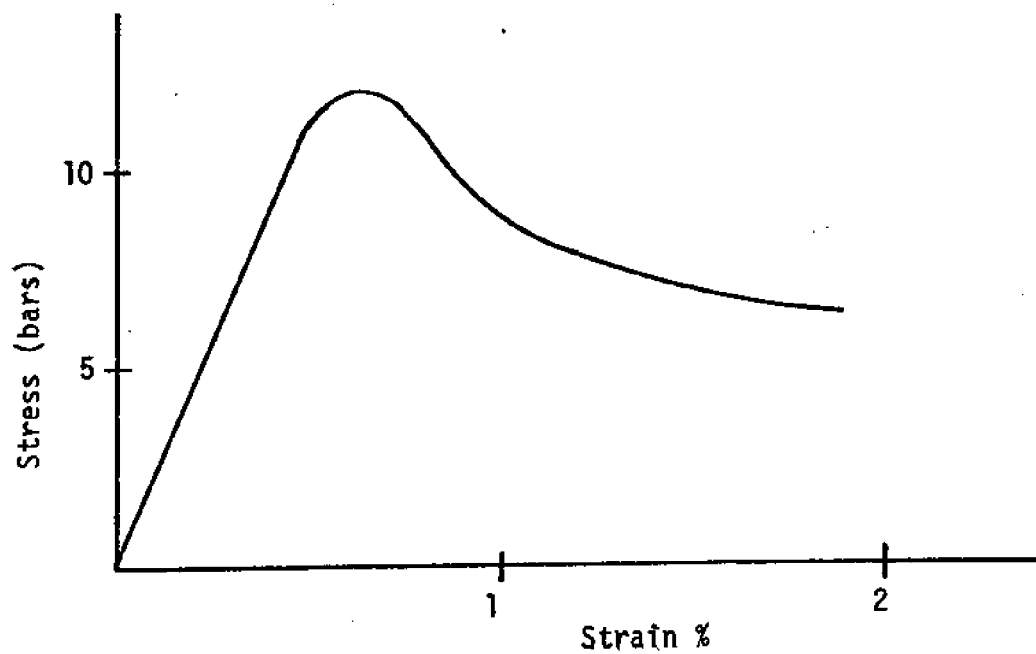
Figure 4.4 Stress-Strain Curve at Constant Crosshead Speed[51]
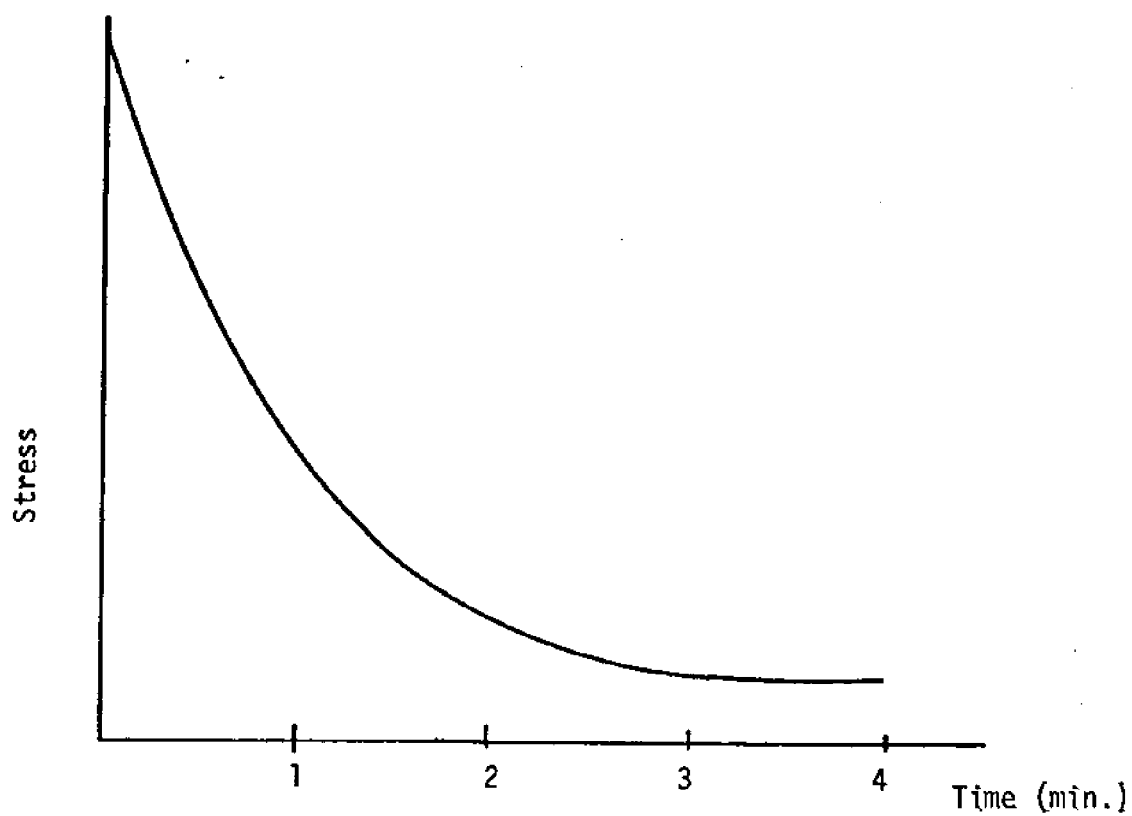

Figure 4.5 Relaxation Curve[54]

dency to lower the yield points and flatten curves. Wakahama's results suggest that such imperfections might exert a greater influence on smaller samples. Wakahama's results also imply that there is a transition from yield drop to constant yield stress with decreasing strain rate.

Stress Relaxation at Constant Strain

Little attention has been given to the stress relaxation characteristics of ice single crystals since these characteristics represent a strain history least likely to be experienced by a natural ice crystal. The consideration of relaxation here, however, will give a more complete picture of the general flow properties. Such test results have been reported by Wakahama[55] and Readey and Kingery.[54] A typical stress-relaxation curve is shown in figure 4.5.

Dislocation Models

Several attempts have been made to explain the observed plastic deformation of ice crystals in terms of the theory of dislocations. The most common dislocation model suggests that plastic deformation is due to the motion of dislocations along the basal plane. Kamb[47] has explained the apparent lack of preferred slip direction by hypothesizing that dislocation motion takes place simultaneously along the a_1, a_2, and a_3 axes according to a power law stress-strain rate relationship similar to that proposed by previous investigators (see next section). He has shown that for values of the exponent n up to and including 4, the maximum angular deviation between the maximum resolved

shear stress and the maximum resolved shear strain is 2.9°, compared to a value of 24° for a tetragonal crystal. One would not expect such a small deviation to be observable in a typical creep experiment, and hence the flow appears to follow the maximum shear stress.

A dislocation theory which has been frequently referenced is that proposed by Johnston.[56] The theory was developed to explain the observed creep and stress-strain results for LiF. Since these results bear a resemblance to those found for ice crystals, it has been suggested that the flow of ice may also be explained according to Johnston's theory.

Johnston begins by expressing the plastic shear strain rate $\dot{\gamma}_p$ in terms of the Burgers vector, b, the number of active dislocations, p, and the velocity of screw dislocations, v_s as

$$\dot{\gamma}_p = 2bpv_s \qquad (4.1)$$

It is assumed that p is a function of the total amount of plastic strain, γ_p, and v_s is a function of the resolved shear stress τ. Observation of etch pits on the surface of crystals of LiF reveal the suggested relationships to take the following form

$$p = \alpha\gamma_p \qquad (4.2)$$

$$v_s = (\tau/D)^n \qquad (4.3)$$

where α, D, and n are constants for LiF. Substituting Eqs. (4.2) and (4.3) into Eq. (4.1), Johnston obtains the following flow relationship:

$$\dot{\gamma}_p = 2b\alpha\gamma_p (\tau/D)^n \qquad (4.4)$$

The solution of Eq. (4.4) implies the existence of an initial strain γ_0, associated with an initial density of mobile dislocations. Since no suitable etchant has been found for revealing basal dislocations in ice, equations (4.2) and (4.3) can not be directly established.[51] Nevertheless, the quantitative results presented in the next section suggest that Johnston's theory is applicable to ice crystals.

Wakahama[55] has sought to model his observed stress-strain behavior by successive activation of Frank-Read sources on different planes with different threshold stresses. This model reproduces only his stress-strain curves with no yield drop, and not those typically observed by other investigators. His theory, with some additional considerations, might be able to incorporate the yield drop phenomenon.

Recently some investigators have begun to study the problem of non-basal slip. Readings and Bartlett[57] have observed short slip line segments perpendicular to the basal plane. They explain these as manifestations of the cross-slip of screw dislocations on the basal plane. Higashi[58,59] has explained the higher yield stress and work hardening found in non-basal slip in terms of intersections of non-basal dislocations. Dislocations on the (10$\bar{1}$0) plane can easily intersect dislocations on other prism planes, an occurrence which tends to impede the motion of these dislocations.

C. Mathematical Descriptions of Single Crystal Flow

This section presents some of the relations which have been observed between stress, strain, and time for the creep, constant strain rate,

and relaxation results presented in the previous section. The ultimate purpose is to obtain a flow law which most accurately reproduces all of the results, and which is applicable to the study of polycrystalline ice.

Creep

Early investigators attempted to develop relationships between stress and strain rate for the stationary portion of the creep curve. This portion, referred to as secondary creep, is where the strain rate is minimum and constant. The resulting creep curves produced some confusion since in most cases there was no well-defined region of secondary creep. Nevertheless, the data was interpreted according to the following law:

$$\dot{\gamma} = k\tau^n \qquad (4.5)$$

where k was observed to be a function of temperature. $\dot{\gamma}$ was taken as either the minimum strain rate (tangent at zero time), the slope of some straight line passed through the points, or the maximum strain rate associated with some linear terminal stage. Table 4.1 summarizes some of the results obtained.

Other investigators, realizing that there was no observable steady state creep, attempted to express the strain as a function of time for a given stress. All of the proposed expressions take on the form

$$\gamma = C\,t^q \qquad (4.6)$$

where C is a constant depending on stress and temperature, t is time, and q is a constant. Table 4.2 summarizes the results of these investigations.

Table 4.1 Summary of Steady State Creep Results ($\dot\gamma = k\tau^n$)

Investigator	Temp. (range) $^{\circ}C$	Stress (range) $kg./cm^2$	k	n
Butkovich and Landauer[49]	-4 to -6.5	(shear) .5 to 3.0	134×10^{-8}	2.49
Glen and Perutz[53]	-6	1.45 to 2.9 (tension)		
Higashi, Koinuma and Mae[60]	-4.8 to -40	12 to 60 (bending)	$K \exp(-Q/RT)$	1.58
Lavrov[61]	-3 to -23	(shear)	1.7 to 4×10^{-8}	1.0
Steinemann[46]	-2.3	.45 to 2.2 (shear)		"hard" 2.3 to 4 "soft" 1.3 to 1.8

Table 4.2 Summary of Transient Creep Results ($\gamma = Ct^q$)

Investigator	Temp. (range) $^{\circ}C$	stress (range) $(kg./cm^2)$	q
Glen and Jones[62]	-50	(tension) 3.5 to 6.5	1.5
Butkovich and Landauer[49]	-5	(shear) .5 to 2.0	1.7
Griggs and Coles[43]	-1 to -18	2 to 14 (compressive)	2.0
Jellinek and Brill[48]	-5	(tension) .5	2.0

Constant Strain Rate

Readey and Kingery,[54] Higashi et al.,[50] and Jones and Glen[51] made quantitative observations of the stress-strain relations for single crystals at constant strain rate. Readey and Kingery begin with the general relation:

$$\dot{\gamma}_p = k \, \gamma_p^m \, \tau^n \tag{4.7}$$

For the case of constant total strain rate, and for n = 2.0, an analytical solution is derived, which can be approximated by the following relation for stress vs. total strain:

$$\tau \cong \left(\frac{\dot{\gamma}}{k}\right)^{1/n} \gamma^{-m/n} \tag{4.8}$$

for the region of the stress-strain curve past the maximum. Using this relation and experimental data, it is concluded that n varies from 2.5 to 1.5 with increasing strain, and that m is approximately 1.

Jones and Glen[51] have analyzed their data according to Eq. (4.4), derived from Johnston's dislocation model. They have worked under the assumption that by adjusting the various parameters in (4.4), some agreement could be reached between the observed stress-strain curves for ice and those predicted by Johnston's theory. Considering a uniaxial specimen of length ℓ_o, cross-sectional area A, Young's modulus E and crosshead speed v the relationship between shear stress and total shear strain takes on the form:

$$\frac{d\tau}{d\gamma} = C - B(\tau/D)^n \, (C \, \dot{\gamma} - \tau) \tag{4.9}$$

where C = E/2A and B = 2bα/$\dot{\gamma}$. The solution curves for Eq. (4.9) show a shape which is rather insensitive to changes in α and D, but sensitive

to changes in n and γ_o, the initial strain. By matching the theoreti-
cal curves with their experimental curves, and using the same value of
α as that used by Johnston for LiF, they found n = 3.0, D = 1035 kg/cm^2,
and γ_o = 5 x 10^{-4}. All of their tests were conducted at the same strain
rate (2.7 x 10^{-7}/sec.) and at temperatures between -20° and -70° C.

Higashi, Koinuma, and Mae[50] have studied the constant rate test in
terms of the initial slope and the maximum stress. They found the ini-
tial slope M and the maximum slope τ_n to follow the relations:

$$M = (M_o + M_1\dot{\gamma}) \exp (E_1/RT) \tag{4.10}$$

$$\tau_{max} = C_1\dot{\gamma}^{1/n} \exp (E_2/RT) \tag{4.11}$$

where E_1 = 8.4 Kcal/mole, E_2 = 10.4 Kcal/mole, n = 1.53, T is absolute
temperature and M_o, M_1, and C_1 are constants. These tests were conduc-
ted at temperatures between -15° and -40° C and at strain rates between
1.3 and 25 x 10^{-7}/sec. The increasing yield point with increasing
strain rate is characteristic of all stress strain results described
herein. The variation of initial slope with strain rate, however, is
difficult to explain.

Relaxation

Both Readey and Kingery[54] and Wakahama[55] have developed quantitative
descriptions of their relaxation curves. Readey and Kingery have ana-
lyzed their data in terms of Eq. (4.7), specializing for the case where
γ = const (the definition of relaxation). They have treated the plastic

strain on the right-hand side as the total strain in order to facili-
tate a solution, and the resulting equation is:

$$\dot{\tau} = -Gk\gamma^m \tau^n \tag{4.12}$$

where G is the elastic modulus in basal shear. The procedure of neglec-
ting the elastic strain on the right-hand side is questionable, since
relaxation involves the mutual interplay of elastic and plastic effects.
This is particularly apparent for the early portions of the curve,
where the deformation is almost totally elastic. Consideration of an
initial strain, however, as presented by Johnston, would increase the
validity of Eq. (4.12).

Wakahama concluded his constant strain rate tests by holding the
strain fixed and allowing the samples to relax. His data fit the follow-
ing relation:

$$1/\tau = 1/\tau_y + A'\,(\tau_y)\,t \tag{4.13}$$

where t is measured from the time the crosshead stopped, τ_y is the
stress at t = 0 (in his case, the yield stress), and A' is a function
of τ_y and temperature. For n = 2, the solution to Eq. (4.12) takes on
a form similar to Eq. (4.13). Since Eq. (4.12) is valid for relatively
large plastic strain, the coincidence supports the validity of Eq. (4.7).

D. General Flow Rule

Using the aforementioned results as a background, and keeping in
mind the ultimate aim of understanding the behavior of small sample

strength tests, a stress-strain time relationship shall be proposed
for single crystal ice. If such a law can reasonably reproduce the
creep, constant strain rate, and relaxation characteristics just de-
scribed, then it will be assumed to be valid for arbitrary stress and
strain histories.

Certain observations should be made with regard to time scale.
First of all, the creep results which have been reported and the ana-
lytical expressions describing them, generally cover time spans of sev-
eral hours. At the moment the most significant portion of the creep
curve is the very beginning, since this represents the time span of a
small-scale test. A second observation is that the strain rates used
in the constant strain rate tests are generally much lower than those
experienced by the polycrystalline test sample. It will be assumed, how-
ever, that the stress-strain characteristics described are still applica-
ble at higher rates. Finally, most of the action in a relaxation test
takes place during the early periods, where the elastic and plastic
strains are comparable, and hence the information supplied by these tests
should be reproducible by the proposed flow law.

We shall begin by first assuming that all inelastic deformation is
due to slip on the basal plane. Although this assumption seems obvious
from experiments on single crystals, it is not so obvious for a single
crystal surrounded by other crystals in a polycrystal. Basal slip is
geometrically inhibited by the constraints of the surrounding grains,
and it has been suggested that in a polycrystal there are other mechan-
isms which control the plastic behavior of each grain.[63] Included in

these mechanisms are grain boundary migration, formation of small-angle boundaries, recrystallization, and crack formation.[64] With the exception of crack formation, these other deformation mechanisms are generally associated with greater time spans than those connected with small-scale testing. Crack formation has been associated with the stress states caused by basal slip,[65] and hence basal slip must be treated before crack formation. This subject will be discussed in the next two chapters.

Since hydrostatic pressure has not been found to affect basal slip, and since the influence of stresses normal to the basal plane on basal slip has not been clarified,[63] it will be assumed that the basal plastic strain will be directly related to the shear stress on the basal plane, independent of the other stress components. The proposed relation has the form

$$\dot{\gamma}_p = k\, \gamma_p^m\, \tau^n \tag{4.14}$$

Although this is the same as Eq. (4.7), a slightly different approach will be used here. The first thing that is apparent from Eq. (4.14) is that if no plastic strain has occurred at any given time, then no plastic strain will occur in the next increment in time, regardless of the stress. Consequently, in order to apply this relation it is necessary to assume the existence of an initial plastic strain, γ_o. This, as Johnston points out, is equivalent to assuming an initial density of mobile dislocations, and is a reasonable assumption to make. This is a fairly obscure quantity to deal with, however, and hence it must be

treated as a free parameter to be adjusted for best data fit, as has been done by Jones and Glen.[51] The plastic strain developed and/or measured in a test, γ_{pm} , must be treated as distinct from the total plastic strain as follows:

$$\gamma_p = \gamma_{pm} + \gamma_o \qquad (4.15)$$

Representing the measured plastic shear strain as

$$\gamma_{pm} = \gamma_T - \tau/G \qquad (4.16)$$

where γ_T is the total applied shear strain and G is the shear modulus, Eq. (4.14) yields

$$(\dot{\gamma}_T - \dot{\tau}/G) = k(\gamma_T + \gamma_o - \tau/G)^m \tau^n \qquad (4.17)$$

Eqs. (4.14) and (4.17) have already been identified with constant strain rate tests.[54,51] This involves replacing γ_T by vt, where v is now a constant equal to the strain rate. Solution curves for Eq. (4.17) for constant strain rate are shown in figure (4.6), along with the various parameter dependencies, for m = 1 and n = 2. It remains to apply Eq. (4.17) to creep and relaxation.

Creep

In a creep experiment, samples are assumed to be loaded instantaneously to a stress τ and immediately respond with a strain τ/G. The stress is then held constant while the specimen deforms plastically. Since the elastic response is constant, the quantity generally considered is the measured plastic strain. Using Eqs. (4.14) and (4.15), this is expressed as:

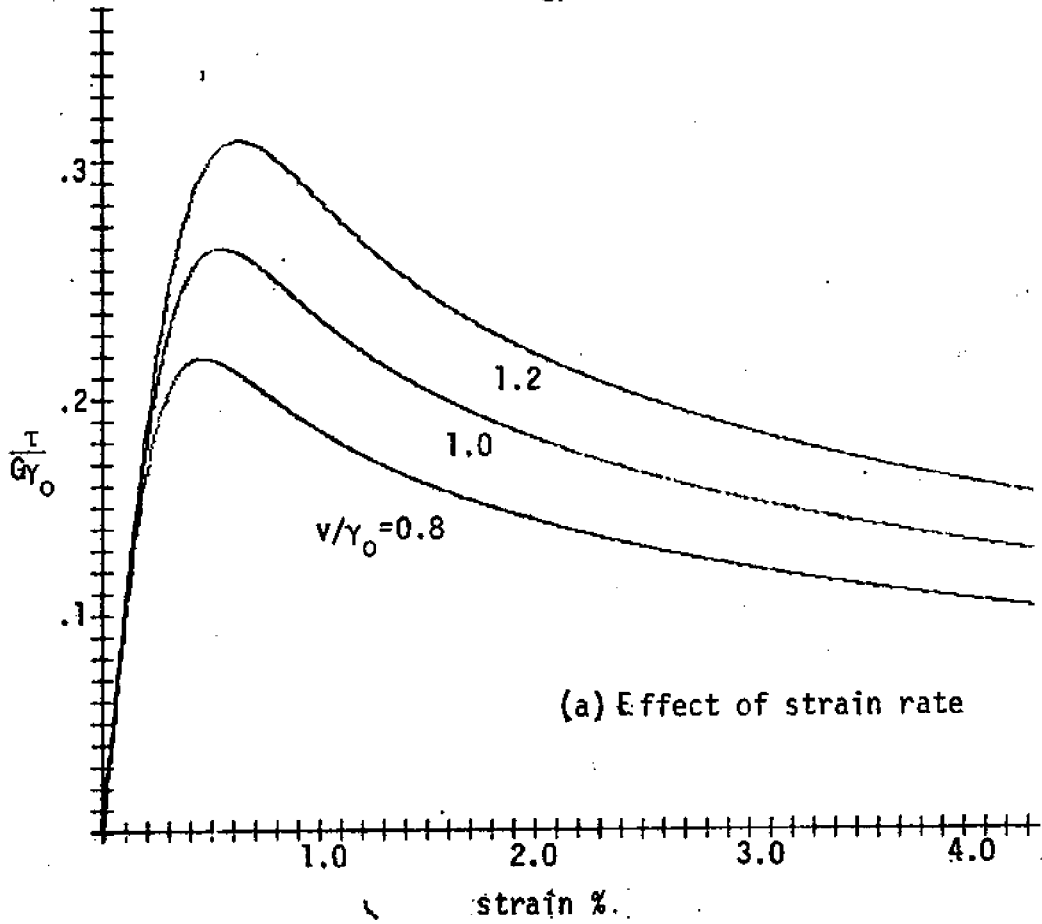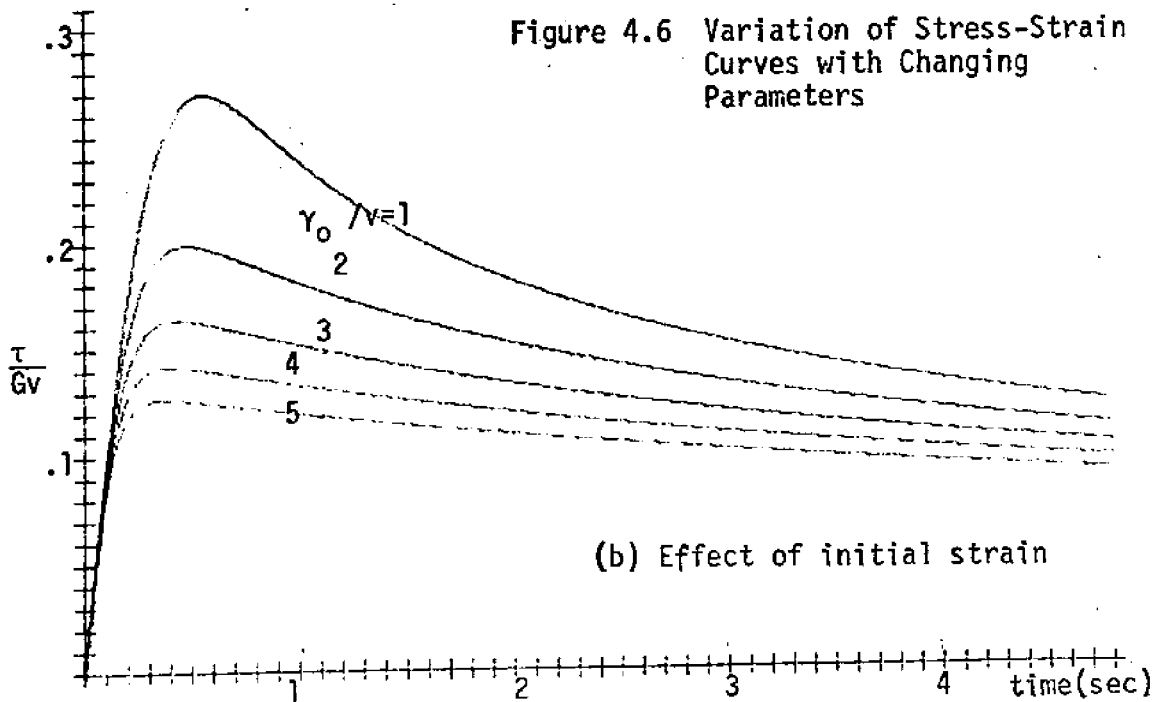$$\dot{\gamma}_{pm} = k(\gamma_{pm} + \gamma_o)^m \tau^n \qquad (4.18)$$

(a) Effect of strain rate

Figure 4.6   Variation of Stress-Strain
Curves with Changing
Parameters

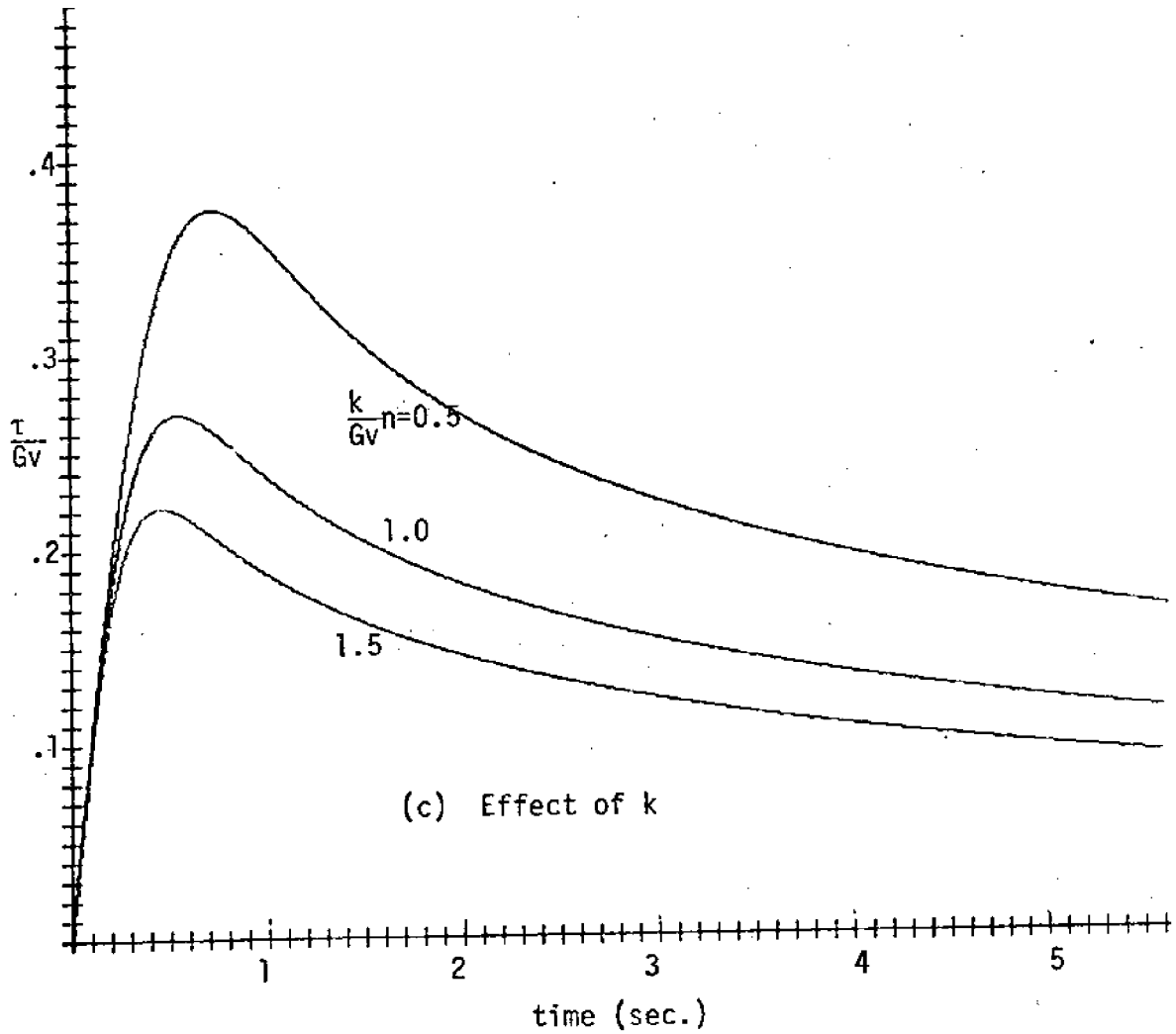(b) Effect of initial strain

(c) Effect of k

Figure 4.6 (continued)

where τ is now a constant. As will be shown, for $0 < m \leq 1$, the resulting creep curves are all concave upward, similar to those found in the previously described investigations. Consequently, the minimum creep rate occurs at $t = 0$, where $\gamma_{pm} = 0$. Steinemann[46] measured the minimum creep rate as a function of stress, and found the relation

$$(\dot{\gamma}_{pm})_{min} \propto \tau^n \qquad (4.19)$$

Eq. (4.18), for $\gamma_{pm} = 0$, yields

$$(\dot{\gamma}_{pm})_{min} = k\gamma_0^m \tau^n \qquad (4.20)$$

which is equivalent to Steinemann's results. Glen and Jones[62] found the strain rate of several tests to be proportional to τ^n at a given strain, a result which also follows from Eq. (4.18). As shown in Appendix A, an analysis of the creep results of Higashi, Koinuma, and Mae[60] shows that the stress dependence associated with their constant slope portions and with their "reciprocal incubation times" is also the same as that of Eq. (4.18). Therefore it is safe to assume that n used in Eq. (4.14) is equivalent to that found by previous creep investigators.

An appropriate interpretation of m is more elusive. Eq. (4.18), solved for the measured plastic strain vs. time, yields:

$$\gamma_{pm} = [(1-m)k\tau^n t + \gamma_0^{1-m}]^{1/1-m} - \gamma_0 \qquad 0 < m < 1 \qquad (4.21)$$

$$\gamma_{pm} = \gamma_0 [\exp(k\tau^n t) - 1] \qquad m = 1 \qquad (4.22)$$

The creep investigations summarized in table 4.2 used an equation of the form

$$\gamma \propto t^q \qquad (4.23)$$

where q took on values between 1.5 and 2.0. Although Eq. (4.23) implies a zero slope at t = 0, most exhibited creep curves do not have this property. It must be assumed, therefore, that the curve fit was intended to cover a broad time range, with no particular attention to t = 0. For the case where m = .5, it should be noted that Eq. (4.21) approaches Eq. (4.23), with q = 2.0, as t increases. Such a statement must be qualified in terms of the magnitudes of k, τ^n, and γ_0 to see if the relevant time scales overlap. The same kind of treatment can be generalized for arbitrary m between 0 and 1.0. Unfortunately, lack of knowledge of γ_0 prevents such an analysis. At the moment, then, there is no preferred choice for m.

Relaxation

Relaxation implies the application of a fixed strain and observing the decrease of stress with time. Eq. (4.17), specialized for relaxation, takes on the form:

$$\dot{\tau} = - Gk \left(\gamma_T + \gamma_0 - \tau/G\right)^m \tau^n \qquad (4.24)$$

where γ_T is now a constant. Since this equation is difficult to integrate, special cases will be noted. For the early portions of the curve, where the applied strain is mostly elastic (i.e., $\gamma_T \approx \tau/G$), Eq. (4.24) yields:

$$\frac{1}{\tau^{n-1}} = (n-1) \, k \, G\gamma_0 t + (G\gamma_T)^{1-n} \qquad (4.25)$$

For the later regions where the applied strain is mostly plastic (discussed earlier), γ_0 is replaced by $\gamma_0 + \gamma_T$ in Eq. (4.25). These two

forms are similar to those observed by Readey and Kingery (Eq. (4.12)) and by Wakahama (Eq.(4.13)). This suggests that Eq. (4.14) suitably describes the relaxation behavior of ice crystals.

Temperature Effects

It has been generally implied that the proportionality constant in the various flow relationships is a function of temperature. Therefore it will be assumed that the flow modulus $k = k(T)$. Readey and Kingery found the relationship to be of the following form:

$$k(T) = k' \exp (-Q/RT) \tag{4.26}$$

where Q = 14.3 Kcal/mole, R is the gas constant and T is absolute temperature. An analysis of the creep results of Higashi et al.[60] in terms of Eq. (4.21), as shown in Appendix A, reveals the same result with Q = 15.8. Eq. (4.26) reveals k to be highly temperature sensitive, as can be seen from the fact that $k(-3° C) = 24 \times k (-33° C)$. This relation suggests a starting point for future analysis of temperature effects on small-scale sample strength.

Salinity

It is suggested that the effect of salinity (or brine volume) can be incorporated into the constant k. This can be done both by correlating the results of polycrystalline models (see next chapter) with stress-strain-time tests on polycrystalline samples, and by a theoretical model. One possible theoretical approach is to use the geometric brine pocket model of Weeks and Anderson[15] and to determine the effective modulus k_e

of the composite material of ice and brine. A similar treatment would

also be applicable to the elastic constants.

Chapter V

MODELS FOR POLYCRYSTALLINE BEHAVIOR

In this chapter the results presented in the last chapter will be used in the formulation of models to describe the behavior of polycrystals, which will be applied to the conditions of small-scale strength tests.

A. Deformation and Failure Mechanisms in Polycrystalline Ice

As was mentioned in the last chapter, of the several proposed single crystal deformation mechanisms in polycrystalline ice, basal slip has been chosen because it is most likely to prevail in the small-scale strength test and because it is most readily quantifiable. The question of the effect of elastic anisotropy should first be mentioned. Goetze[73] suggested that elastic anisotropy causes stress concentration at grain boundaries which induces brittle failure. The values of the elastic constants,[66] however, indicate that elastic anisotropy is not very pronounced, and, in the light of chapter IV, plastic anisotropy is the more prominent directional characteristic.

Detailed investigations of the single crystal deformation and failure mechanisms in polycrystalline ice have been conducted by Gold.[65,67,68] His investigations involved the study of samples deformed in compressive creep at -9 to -10° C, with the load perpendicular to the columnar grains. His experimental observations and conclusions can be summarized as follows:

1) The fact that single crystals slip only on one plane implies that there are only two independent slip systems in a three-dimensional situation and one independent slip system in a two-dimensional situation. Taylor[69] has shown that for an arbitrary change of shape at constant volume (or area), five independent slip systems are required in three dimensions and two are required in two dimensions. This implies that individual ice grains cannot accommodate an arbitrary change of shape in plastic deformation. The tendency to slip, accompanied by the geometric restrictions of the surrounding grains, causes the development of large stress differences from grain to grain, and of high stress concentrations at the grain boundaries.

2) The nonuniform internal stresses which develop as a result of the above behavior are responsible for the occurrence of internal cracks which are observed in compression tests to occur at loads well below the failure load of the sample. In other words, cracking is required to accommodate the required deformation. Figure 5.1 shows internal cracking in compressive samples.

3) This cracking occurs well before the other deformation mechanisms, described earlier, take place.

4) Cracking occurs primarily within the grains, and, at low loads, these cracks form and then do not propagate. The most frequently observed crack orientation is parallel to the basal plane, with cracks perpendicular to the basal plane taking second place. In a study of 407 transcrystalline cracks, 206 were parallel to the
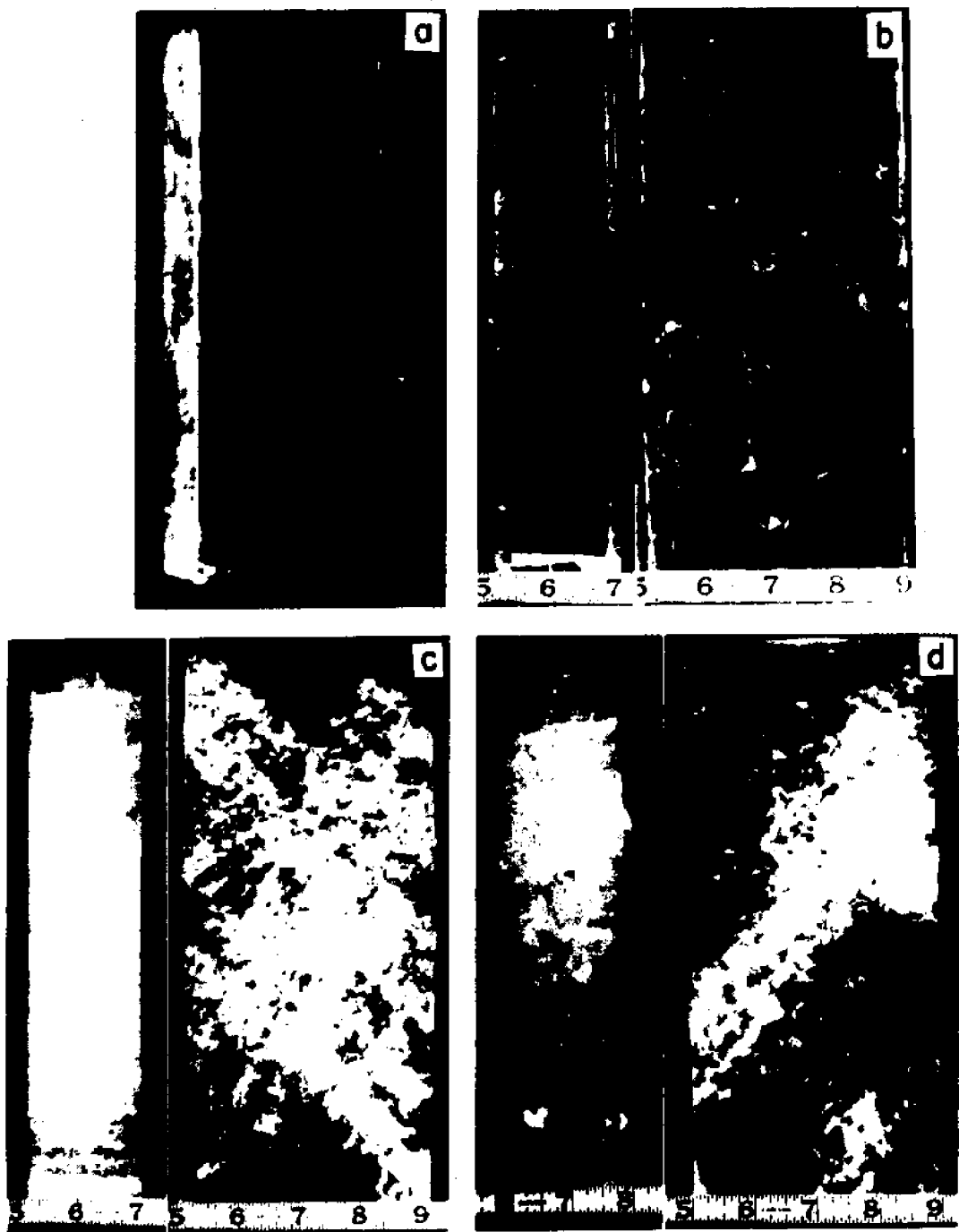
Figure 5.1   Cracking Activity in Compression - Four
Different Stages of Crack Development (Gold[67])

basal plane, 106 were perpendicular to the basal plane, and 14 were either one or the other.[65] In the same study, of 121 grain boundary cracks observed, 85 occurred between grains whose boundaries were either parallel or perpendicular to the basal plane of one or both of the grains making up the boundary. Figure 5.2 shows photographs of plastically deformed grains which have cleaved parallel and perpendicular to the basal plane.

5) Cracks form due to tension across the above-mentioned planes caused by the nonuniform stress field.

6) The formation of cracks causes stress redistribution in the sample. If the load is applied for a sufficient length of time, continuous cracking occurs, causing a continuous redistribution of stress, until it is finally carried by those grains with basal planes parallel to the direction of maximum shear. The accelerating creep on these planes (described in chapter IV) terminates in a plastic failure of the sample. Experiments by Gold show, therefore, that compressive creep samples fail at loads far below those achieved in rapidly conducted strength tests (see also Kingery[26]).

The above observations are very enlightening, and they strongly suggest that the modeling of polycrystalline ice in terms of single crystal properties would be a very fruitful approach. Of particular interest would be to quantify these nonuniform stress states for the purpose of predicting cracking and ultimate failure. Such information, in fact, is what is required for the interpretation of small-scale sample results.
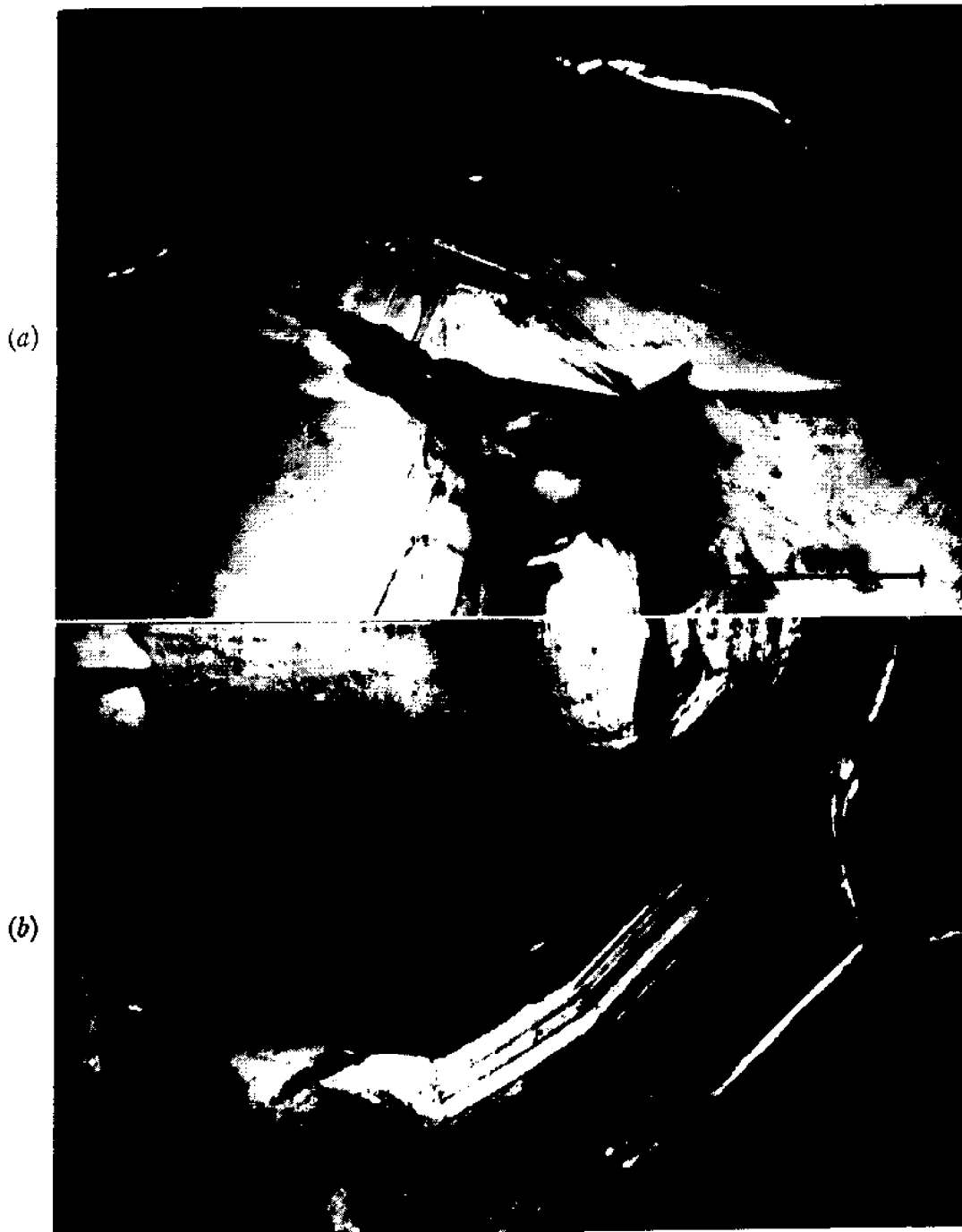
Figure 5.2 Plastic Deformation and Cracking in a Single
Crystal of a Polycrystalline Sample (Gold)[65]
(b) Cleavage parallel to basal plane
(a) Cleavage perpendicular to the basal plane

It should be noted, before continuing, that a good deal of theory has been developed for predicting the behavior of a polycrystal from single crystal properties.[71] This work has been primarily concerned with predicting the stress-strain behavior of the polycrystal from that of the single crystal. The type of single crystal stress-strain behavior implied by these theories (generally applicable to metals) does not embrace that observed for ice. In addition, these theories seek results for a fine grained polycrystal (continuum III, chapter II). At the moment, then, these theories do. not seem applicable to the interpretation of small-scale strength tests, nor, i.. fact, to ice in general.

B. A Two-Grain Model

A first approximation to polycrystalline behavior can be obtained from single crystal properties by considering two grains of different sizes and orientations located in a small sample[72] (figure 5.3). For simplicity, a uniaxial, tensile test, subject to a constant crosshead speed $\dot{\delta}$, will be considered. Due to constraints from the neighboring grains, and the conditions of the test, the two grains are considered to be subject to a constant rate of strain $v = \dot{\delta}/\ell$ in the direction of the applied load, where ℓ is the length of the sample. The purpose here is to show how the total load carried by the two grains can vary with the crosshead speed.

The force-displacement character of each grain is represented by a spring-dashpot system. The lateral interaction between the two grains
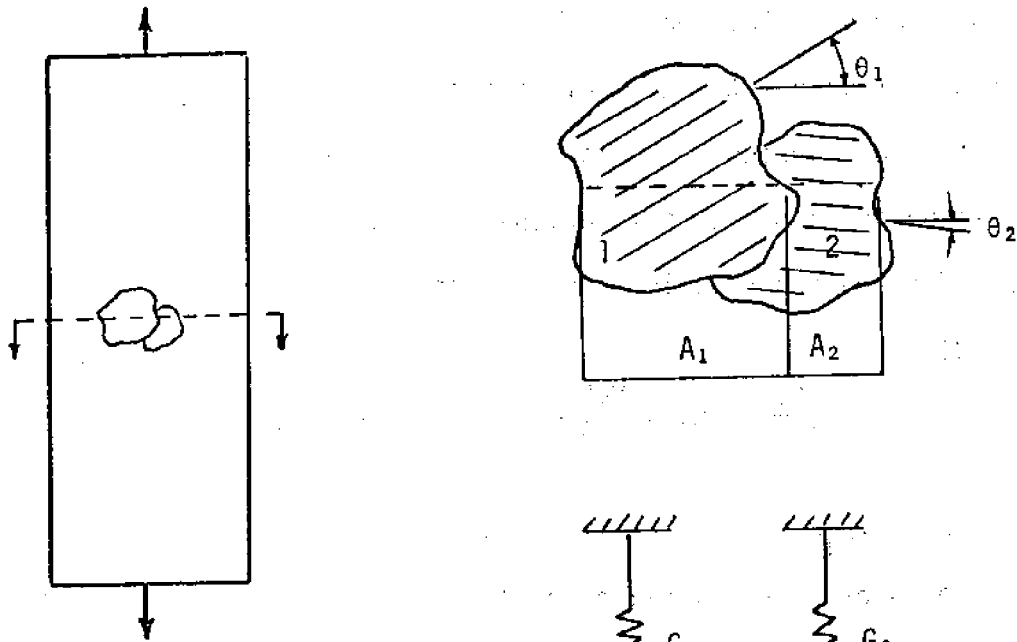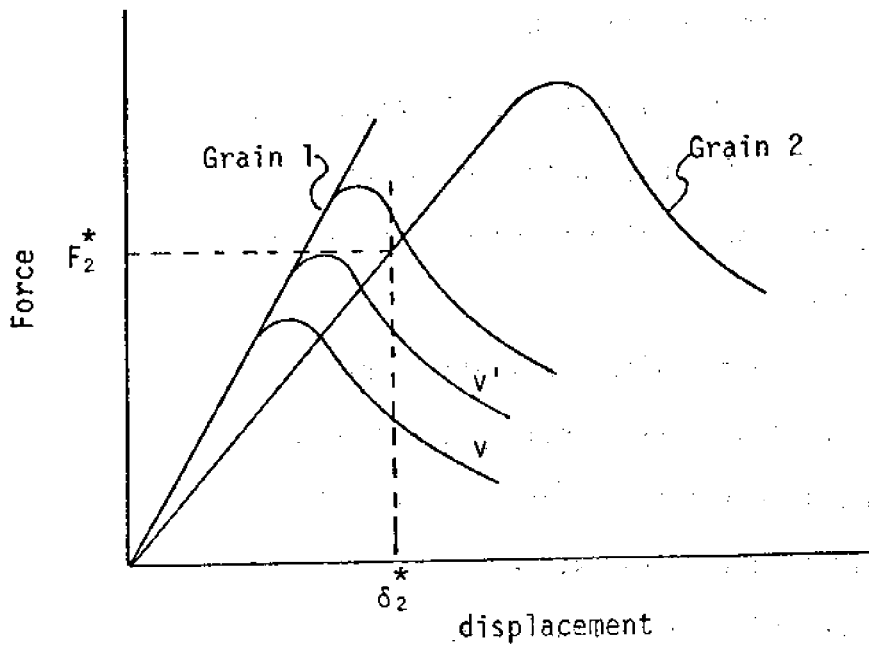
Figure 5.3 A Two-Grain Model

Figure 5.4 Spring-Dashpot Force-Displacement Curves

is not considered in this model. The force, F_i, in each spring-dash-pot system corresponds to the applied strain, which, by assumption, is the same for both grains. The material parameters k, G, and γ_0 are assumed to be the same for both grains. Using Eq. (4.14) with m - 1, the force-deformation relationship for each grain takes the form (see Appendix B)

$$\frac{dF_i}{d\delta} = G_i - \frac{G_i k_i}{v} \left(\delta + \delta_i - \frac{F_i}{G_i} \right) F_i^n \qquad i = 1, 2 \quad (5.1)$$

where

$$G_i = 2A_i G$$

A_i = cross sectional area of grain i

$$k_i = \left(\frac{\sin 2\theta_i}{2A_i} \right)^n k$$

$$\delta_i = \frac{\gamma_0}{\sin 2\theta_i}$$

θ_i = angle between the basal plane and the plane perpendicular to the specimen axis

This equation is the same as Eq. (4.17), with a slightly different definition of variables. With the solution curves of figure 4.6 in mind, proposed force-deformation curves for grains 1 and 2 are shown in figure 5.4.

Due to the particular basal plane orientation, grain 1 is favorably oriented for plastic flow while grain 2 is not. It is expected that in any given sample there will be some distribution between favorably and unfavorably oriented grains. As a result, k_1 is much greater than k_2. This has the effect of giving grain 1 a lower yield point than grain 2 on the force deflection curve (see figure 4.6a). The different A_i also

affect the k_i values, but not as strongly. The different G_i values change the initial slope but do not have much influence on the plastic properties. The different δ_i values have the opposite effect of k_i on the yield point, and tend to flatten the after yield curve for the less favorably oriented grain. Since $n > 1$, the k_i influence on the yield point will predominate.

It is now assumed that failure of the two-grain system occurs when grain 2 fails. This is a reasonable assumption, since it is clear from figure 5.4 that grain 2 will carry the brunt of the stress. Also, it was mentioned earlier that failure due to tensile stress across the basal plane is the most frequently observed grain failure mode. The failure load F_2^* is a function of A_2 and perhaps temperature and salinity. It is assumed that F_2^* does not depend on the load rate. F_2^* corresponds to a displacement δ_2^*, and the total load F^* at failure is the sum of the ordinates of the two curves at δ_2^*.

The effect on F^* of increasing the strain rate v is now examined. At increased strain rate v', F_2^* is still located on the same point of the grain 2 curve, but the value of F_1 at the same displacement has increased; hence it can be seen that the total load carried by the two grains increases with increasing strain rate. When the rate becomes sufficiently high, both grains will be in their linear regions, and subsequent increases in strain rate will not affect the load capacity.

The above phenomenon for two grains is just as likely to occur for the several grains comprising the cross section. If the failure is controlled by one grain (as is likely considering the relatively small

number of grains in the cross section of the average tensile specimen),
the conclusion follows in the same way. If several grain failures are
required for ultimate failure, then one can say that internal cracking
begins at higher loads with higher strain rates. Since internal crack-
ing is required to precipitate failure, it is safe to conclude that
higher strain rates will result in higher failure loads.

The conclusion just arrived at coincides with the experimental re-
sults for uniaxial tensile tests (chapter III, uniaxial tensile test
results) . Exceptions to this seem to occur at load rates higher than
those for which the strength was found to increase with increasing rate.
This suggests that once the load rate reaches the point where all the
grains are in their linear regions at failure, a rate mechanism other
than plasticity controls the failure load.

Another conclusion which can be drawn from this grain analysis con-
cerns the nature of tensile and compressive failures. The failure of
one grain in a tensile specimen causes a sudden increase in the tensile
field supported by the remaining grains. Although their load carrying
capacity increases as a result of the sudden increase in strain rate,
the fact that tension controls failure makes it unlikely that the re-
maining grains will be able to withstand the increased load. Hence ten-
sile failures are abrupt, and there is no time to observe the internal
cracking. Compression failures follow two different patterns. At low load
rates, the tension set up by inhomogeneous deformation is gently re-
lieved by the formation of cracks, and the specimen continues to support
an increasing load. At high load rates, an internal tensile crack can

can precipitate an instability which cannot be relieved by plastic deformation. Hence, a gradual shear failure occurs in the former, while an abrupt bursting occurs in the latter.

C. A Two Dimensional Finite Element Model

The ability to explain an observed strength phenomenon from single crystal properties encourages the development of more refined models which can deal quantitatively with some of the more complex situations associated with small-scale tests. For this purpose, a finite element model was developed.

At first glance, the finite element method is a natural for a polycrystalline analysis, since the grains themselves are "finite elements." The idea of treating one grain as one element, however, was discarded early in this research because the available elements have limitations in their geometric flexibility, and because every internal node in such an analysis would represent the intersection of at least four grains. It was felt that these factors would bias the analysis. Instead of the one-element, one-grain approach, each grain was assembled from several linear square and 45° triangular elements. To facilitate the analysis, the division of the grain into such elements was programmed into the computer analysis. This restricted the choice of grain node points to lie on a grid equal in size to the element width.

The two dimensionality of the program fits in nicely with the treatment of columnar grains. The ring tensile and uniaxial specimens of figure 3.2 are readily modeled as plane stress or plane strain problems,

depending on the sample thickness. For the flexural test, the extreme fiber can be treated to be in plane stress.

Figure 5.5 shows a flow chart of the procedure used, and Appendix C presents the matrix equations upon which the analysis is based. This method is an extension of the basic finite element method for an elastic continuum, which is reviewed by Zienkiewicz.[74]

The elastic constants used in the analysis are those presented by Jona and Scherrer[66] for ice single crystals. From the results presented in chapter IV, a value of n = 2 was chosen, while m=1 was arbitrarily used because it coincides with the plotted curves of figure 4.6.

D. Results of the Finite Element Analysis

The most reasonable problem to deal with is the effect of load rate on tensile strength, since this is the problem analyzed in section B of this chapter. It was desired to see whether or not the conclusions arrived at using the two-grain model could be verified by the finite element approach. This is a necessary verification, since the two-grain model, and the conclusions reached through it, might be altered by the general interaction between grains and by the nonuniformity of stresses in the grains.

Figure 5.6 shows the geometry of the model which was used. This model represents a uniaxial specimen subject to a constant strain rate v. The thickness was taken as 0.1 inch. Figure 5.7 shows the resulting force-deflection curves of this model for different values of v. As ex-

```
┌─────────────────────────────┐
│ Read grain boundary         │
│ coordinates, connectivity   │
│ and material constants      │
└─────────────────────────────┘
              │
              ▼
┌─────────────────────────────┐
│ Divide each grain           │
│ into finite elements        │
└─────────────────────────────┘
              │
              ▼
┌─────────────────────────────┐
│ Compute condensed stiffness │
│ matrix of each grain        │
└─────────────────────────────┘
              │
              ▼
┌─────────────────────────────┐
│ Assemble total              │
│ stiffness matrix            │
└─────────────────────────────┘
              │
              ▼
┌─────────────────────────────┐
│ Read prescribed load        │
│ and/or displacement rate    │
│ for each boundary node.     │
└─────────────────────────────┘
              │
              ▼
┌─────────────────────────────┐
│ Assemble total              │
│ load vector                 │
└─────────────────────────────┘
              │
              ▼
┌─────────────────────────────┐
│ Solve for displacements     │
└─────────────────────────────┘
              │
              ▼
┌─────────────────────────────┐
│ Backsubstitute for element  │
│ stresses and strains        │
└─────────────────────────────┘
              │
              ▼
┌─────────────────────────────┐
│ Compute increment of basal  │
│ plastic strain from         │
│                             │
└─────────────────────────────┘
              │
              ▼
┌─────────────────────────────┐
│ Update previously computed  │
│ plastic strain              │
└─────────────────────────────┘
              │
              ▼
┌─────────────────────────────┐
│ Compute total load vector   │
│ due to plastic deformation  │
└─────────────────────────────┘
```

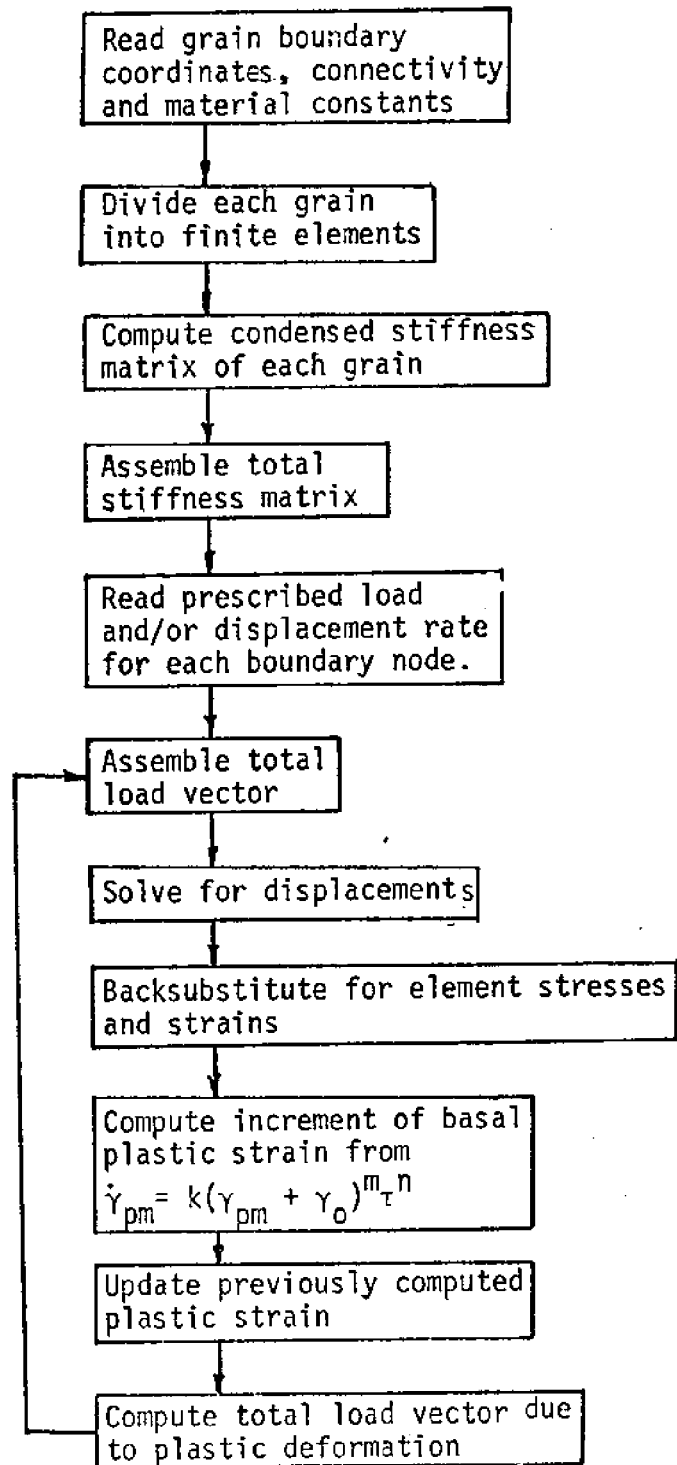$$\dot{\gamma}_{pm} = k(\gamma_{pm} + \gamma_o)^m \tau^n$$

Figure 5.5   Flow Chart of the Finite Element Method
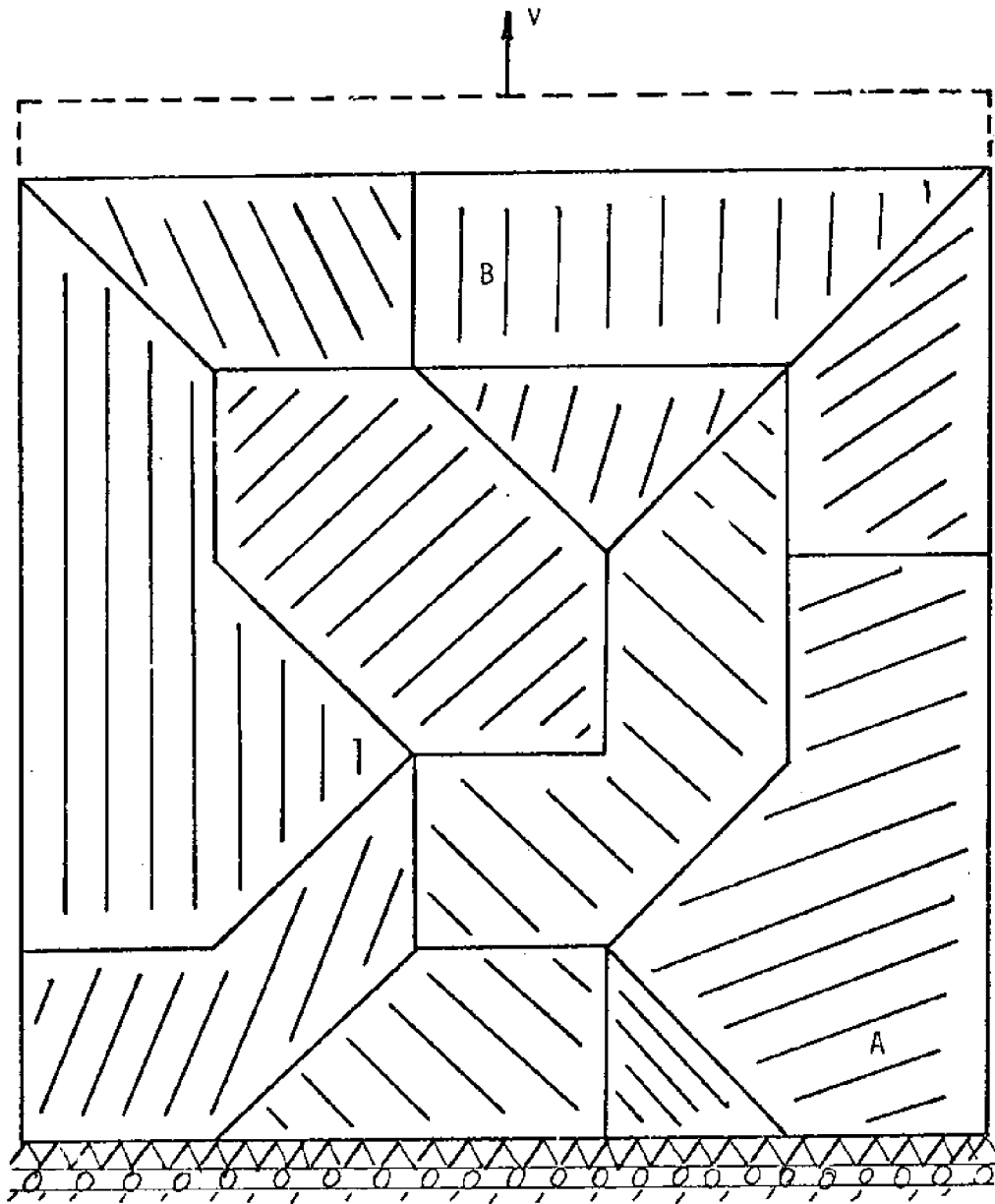Applied to an Elasto-Plastic Polycrystal

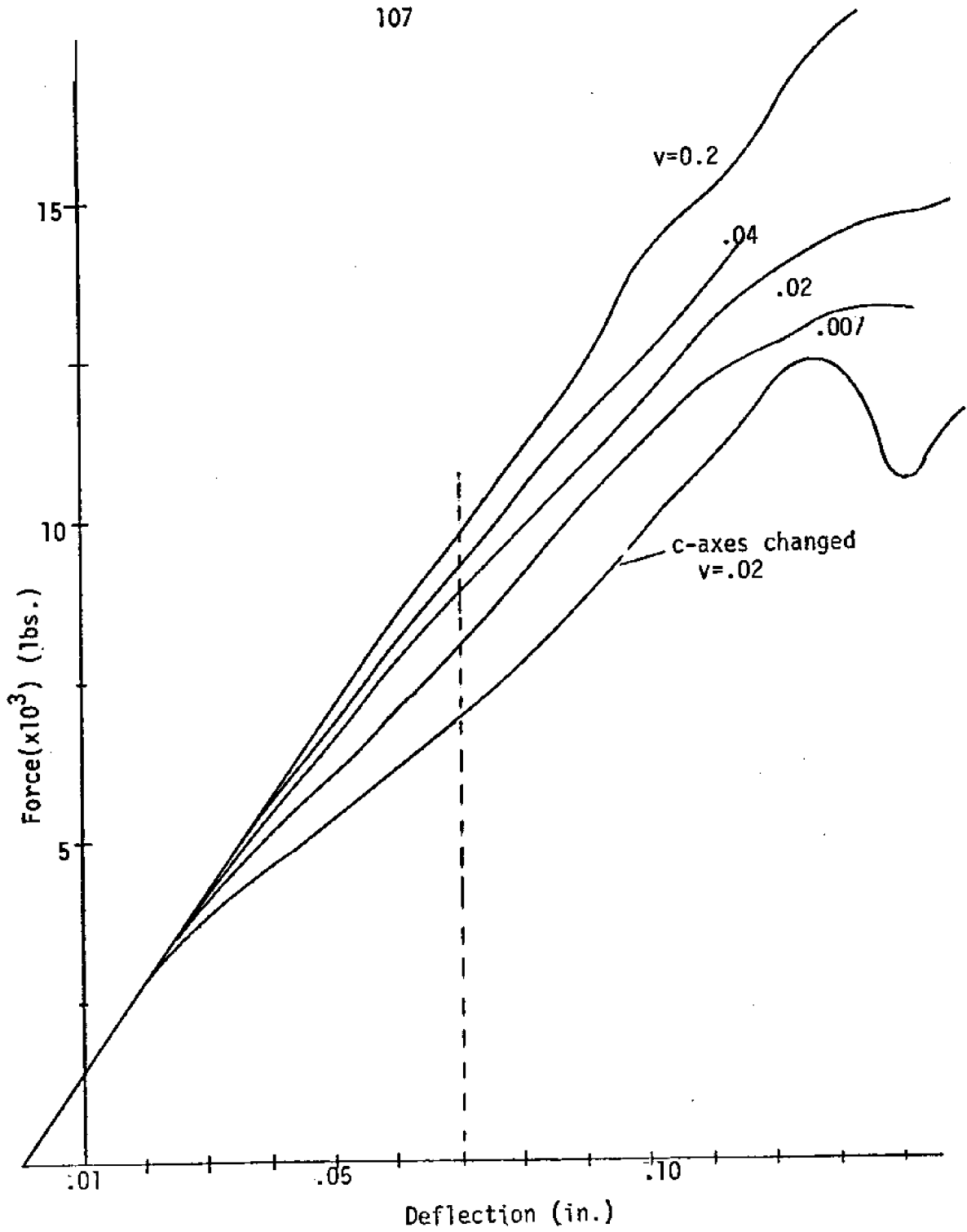Figure 5.6 Finite Element Simulation of a Uniaxial Tensile Test

Figure 5.7 Simulated Force-Deflection Curves for Varying
Strain Rates

pected, the stress-strain curves for higher values of v are more linear than those for the lower v values. The curvature changes in the force-deflection curves are due to the behavior of yielded grains, an example of which is shown for point B in figure 5.8. Typically, the attempt of a point in a grain to yield in the direction of applied displacement is thwarted by the constraints of the surrounding material in the grain, which in turn is constrained by the neighboring grains. Hence it appears that the point can not decide whether or not to yield. This is a basic feature which is revealed by the finite element method, but not by the spring-dashpot model.

For the purpose of predicting the load at failure, it is observed from the program output that point A in figure 5.6 experiences the most severe tensile stress across the basal plane. It is proposed, therefore, that failure initiates when this component reaches a critical value. Figure 5.9 shows the relation between basal tensile stress and crosshead displacement at point A for different strain rates. It is observed that for most of the test, the curves practically coincide. For the purpose of illustration, an arbitrary failure stress for this point is assumed, coinciding with δ = 0.07 in. From figures 5.9 and 5.7, a relationship between failure load and strain rate is obtained, and is plotted in figure 5.10. This compares favorably with the uniaxial tensile results of references 23 and 20, as shown in figures 3.7 and 3.9 respectively. It is difficult to compare the strain rate regime here to the load rate regime in these references because of the uncertainty in the material properties used in this analysis. It is clear, however,
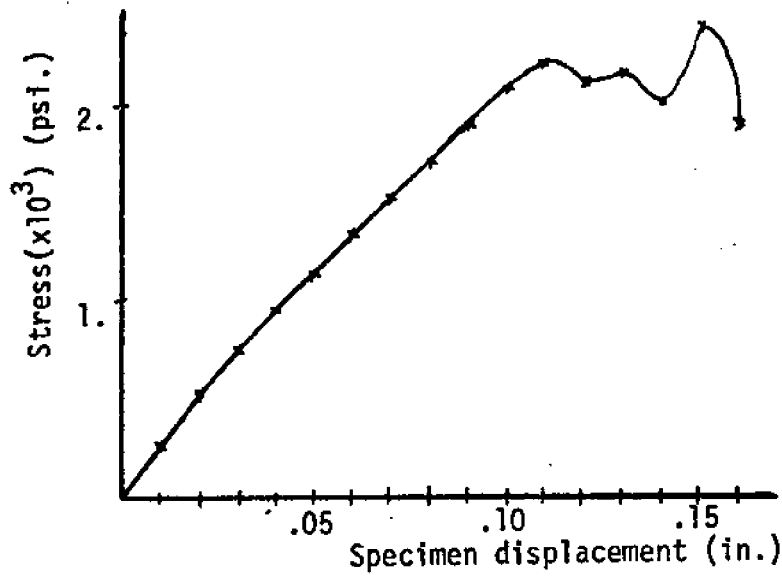
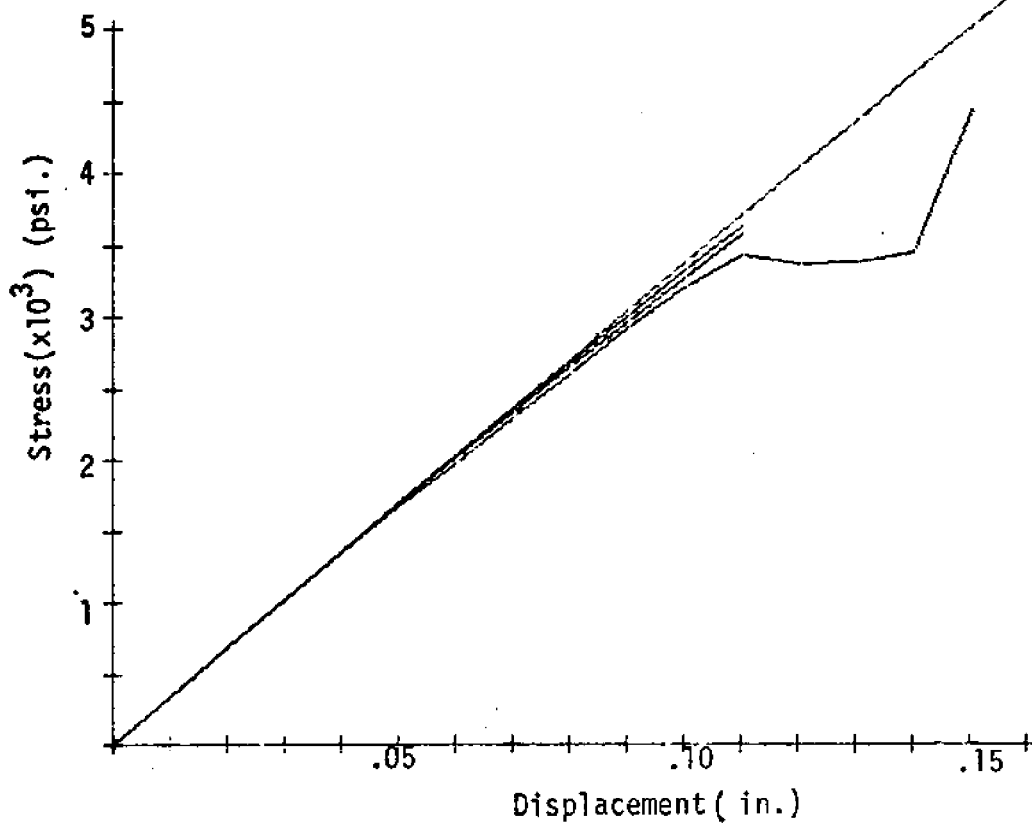Figure 5.8 Tensile Stress in the Direction of the Applied Load vs. Total Displacement (point B)

Figure 5.9 Tensile Stress Across the Basal Plane at Critical Point A for Different Strain Rates
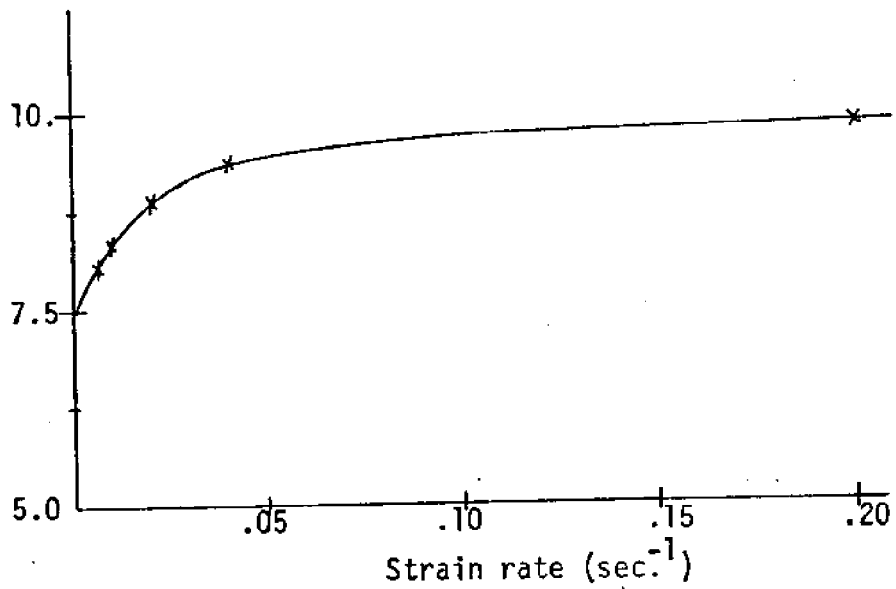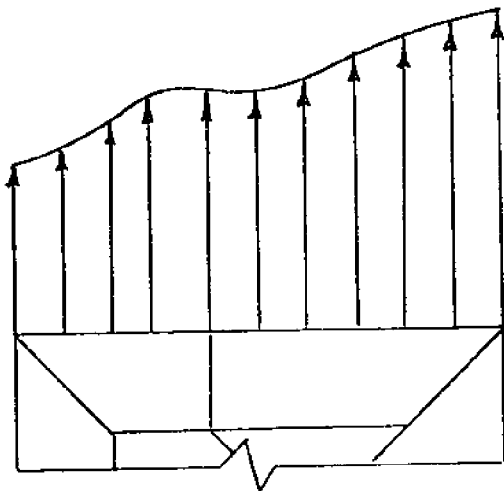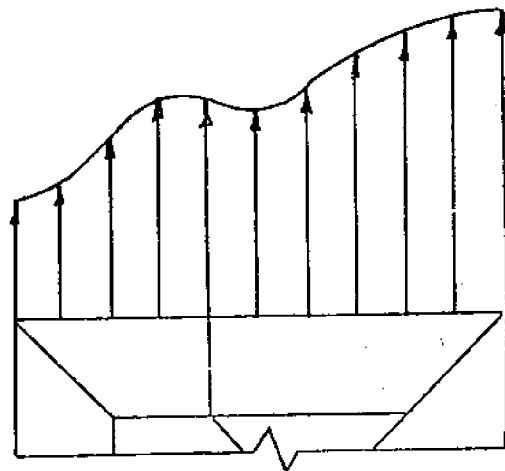
Figure 5.10 Failure Load vs. Str.in Rate

v=.04   v=.0067

Figure 5.11 Stress Distribution Across Simulated Specimen Section

that the behavior shown in figure 5.10 will always occur regardless of the material parameters, because it is a basic property of single crystal plasticity.

The distribution of stress through the section at a fixed displacement for different crosshead speeds is represented in figure 5.11. As suggested by the experimental studies of Gold, which were described in section A of this chapter, the nonuniformity of stresses is a function of plastic flow. Here, the nonuniformity is more pronounced at the lower speed, where plasticity effects are more pronounced.

For variety, the same model with different Lasal plane orientations was simulated at v = .02/sec. The resulting force-deflection curve is shown along with the others in figure 5.7. Although this curve is different from the other curve at v = .02/sec. due to the different grain orientations, the nature of the curve is basically the same. The yield behavior of this sample is interesting to note.

Chapter VI

SUMMARY AND CONCLUSIONS

Summary

1. The determination of the strength of ice sheets requires a better knowledge of the strength of ice and its dependence on environmental parameters and loading rate.

2. The existing small-scale strength test results do not supply a sufficient amount of information to make them useful in the determination of the strength of ice sheets.

3. The smallness of these tests compared with ice sheet dimensions; the unclear nature of the effect of load rate; and the consistent dependence of strength values on the type of test employed suggest alternative means for analyzing the data.

4. The coarse internal structure of ice coupled with the highly directional aspect of single crystal plastic flow imply that the sample material can not be treated as homogeneous.

5. The apparent load rate effect found in ring tensile tests indicates that further investigation into single crystal plasticity would enlighten some of the anomalous results observed in small-scale strength tests.

6. Single crystal plasticity has been found to be dominated by basal

glide. An analysis of the creep, constant strain rate, and relaxation results on single crystals of ice by various authors yields the following relationship between the resolved shear stress and the applied shear strain on the basal plane.

$$(\dot{\gamma}_T - \dot{\tau}/G) = k \, (\gamma_T + \gamma_0 - \tau/G)^m \, \tau^n \qquad (4.17)$$

where

γ_T = total applied shear strain

τ = resolved shear stress

γ_0 = initial strain

G = shear modulus

k = "flow modulus"

$0 < m \leq 1;$ $1.5 < n < 4.0$

7. The results of Readey and Kingery[54] concerning the dependence of k on temperature are confirmed by using Eq. (6.1) to analyze the results of Higashi, Koinuma, and Mae.[60] The relation has the form

$$k = k' \, \exp \, (-Q/RT)$$

where

k' is a constant

Q is approximately 15.0 kcal/mole

T is absolute temperature

R is the universal gas constant

8. Single crystal deformation mechanisms observed in compressive creep tests of columnar polycrystalline ice suggest that an ice

sample should be modeled as an assembly of single crystals with random orientation, each exhibiting the stress-strain-time behavior of Eq. (6.1).

9. The treatment of two grains modeled by springs and dashpots shows how the failure stress of a uniaxial tensile specimen increases with increasing load rate.

10. A finite element model, treating a test sample as an assembly of grains, simulates the character of stress inhomogeneity due to single crystal plasticity. In a uniaxial tensile test simulation, the assumption of sample failure due to basal cleavage of the most critically stressed grain leads to a relationship between failure load and strain rate strikingly similar to those obtained in actual uniaxial tensile tests. The strain rate (load rate) regime in which this relationship is applicable depends on the material constants, which in turn depend on temperature and salinity.

11. The Finite Element Method is a powerful tool for analyzing the behavior of a polycrystal from single crystal properties. Although such an analysis may be considered academic for fine grained polycrystals, it is a very real approach to understanding the results of small-scale strength tests on ice, and, in general, to the study of ice mechanics. Some suggestions as to its possible applications are presented in the next chapter.

Conclusion

It has been shown that the mechanical properties of ice which manifest themselves in a small-scale strength test can be understood by considering the plastic properties of ice single crystals. Two models have been presented which, by considering the sample as an assembly of grains, are able to predict the increase of tensile strength with increasing load rate. The use of such models can be extended to study a wide spectrum of ice mechanical properties.

Chapter VII

PROPOSALS FOR FUTURE RESEARCH

The use of the models presented herein have only scratched the surface of the wide expanse of problems to which they are applicable. In addition, some other possible research areas have come to light in this study. These, plus some proposed analytical model studies, are listed below.

Experimental Studies

It seems that the potential use of the Brazil test is much more promising than has been generally assumed. The problems surrounding its previous use have been created partly because of the desire to match ring tensile results. The ring tensile test, on the other hand, provides a poor index for bulk ice strength, and its continued use for such a purpose is not recommended. It may, however, provide some interesting information concerning single crystal properties.

A study of small beam flexural tests with the load applied in the plane of the ice sheet rather than perpendicular to it should supply some correlation with ring tensile results.

Single Crystal Properties

An analytical treatment of the effect of brine volume on single crystal elasticity and plasticity, similar to that which has been done for strength, is recommended. This should involve the treatment of the single crystal material as a composite of ice and holes. Elasticity

solutions exist[19] for the stress distribution associated with a regular array of holes. Using an energy approach, this can be applied to the determination of the effective elastic moduli. Similar logic might be applicable for the determination of an effective flow modulus.

Spring-Dashpot Model

The qualitative discussion of the spring-dashpot model can be quantified using Eq. (5.1). This can lead to the treatment of N grains, and relationships between strength, rate, and N would be interesting to see, in the light of the size effects which have been reported. Another refinement would involve introducing some kind of lateral connection between spring-dashpot elements to model the lateral interaction of grains.

Finite Element Model

The most interesting potential application of this model is to the treatment of internal cracking. Grains reaching a threshold tensile stress across their basal plane can be programmed to "crack." This occurrence can be modeled by a change in the grain rigidity matrix. It would be very interesting to compare the results of such a study to the detailed experimental crack analyses of Gold.

The ring tensile test can be modeled by the method presented in chapter V, for the purpose of determining the relevant grain threshold stresses which are required to simulate observed strength results. Simulation of creep, stress-strain, and relaxation tests on polycrystalline samples, and the comparison of these simulations to actual test

results can lead to a better understanding of the material properties of the single crystal. The Brazil test can also be modeled using the method presented here, to see if the predicted uniform tensile stress under the load is actually realized in the test sample. Effects of temperature, salinity, load rate, and grain size can be studied in all of these cases.

Ice Sheet Strength

Getting back to the original problem, there are some indications that the mechanisms discussed here have some bearing on the bulk ice behavior in an ice sheet. This author has observed films, taken by the Cold Regions Research and Engineering Laboratory (CRREL), of a cylindrical pile forced against an ice sheet. These tests simulated the forces exerted by an ice sheet on a structural support. It is observed that the application of the load is accompanied by the gradual whitening of a circular region ahead of the pile. This whitening is due to the formation of internal cracks, the same phenomenon studied by Gold. The increased whitening is accompanied by a gradual decrease in the slope of the force-deflection curve.[70] The force dropped off when the white material disintegrated, and it did not pick up until the pile had pushed its way through the disintegrated material to the rim of the circle, where the ice was once again solid. Having done this, the entire process was repeated. The load, therefore, was found to be periodic, and the magnitude and period was a function of the stress state in the ice sheet and the internal craking of the ice. This

periodicity was mentioned in chapter I in connection with ice forces observed on offshore structures.

The prediction of the above behavior using the methods described herein is a feasible research direction. This is not to say that one should model an ice sheet by treating every grain. The methods which have been discussed, however, can be used to describe the bulk properties of a crystal aggregate, properties which can be used in the stress and failure analysis of an ice sheet in contact with a structure.

References [*]

1. Frankenstein, G.E., "Strength of Ice Sheets" in <u>Proceedings of Conference on Ice Pressures Against Structures</u>, Laval University, Quebec, 1966 - National Research Council Technical Memorandum No. 92, 1968.

2. Peyton, H.R., "Ice and Marine Structures - Part III", <u>Ocean Industry</u>, December, 1968.

3. Peyton, H.R., "Sea Ice Forces" in <u>Proceedings of Conference on Ice Pressures Against Structures</u>, Laval Conf. 1968

4. Meyerhoff, G.G., "Bearing Capacity of Floating Ice Sheets," <u>ASCE Journal of the Eng. Mech. Division</u>, Vol. 86, No. EM5, Oct. 1960.

5. Nevel, D.E., "Time Dependent Deflection of a Floating Ice Sheet," CRREL Report RR196, July 1966.

6. Nevel, D.E., "The General Solution of a Wedge on an Elastic Foundation," CRREL Report RR247, Nov. 1968.

7. Dyson, J.L., <u>The World of Ice</u>, Knopf, New York, 1962.

8. Shumskii, P.A., <u>Principles of Structural Glaciology</u>, D. Kraus, trans. Dover Publications, New York, 1964.

9. Butkovich, T.R., "Crushing Strength of Lake Ice," SIPRE Research Paper No. 15, Aug. 1955.

---

[*] The following abbreviations are used:

CRREL - U.S. Army Cold Regions Research and Engineering Lab., Hanover New Hampshire, (formerly SIPRE).

SIPRE - U.S. Army Snow, Ice, and Permafrost Research Establishment

USNCEL - U. S. Navel Civil Engineering Lab., Port Hueneme, California

Ice and Snow - Proceedings of a conference held at MIT Feb. 1962 (W.D. Kingery, ed.), The MIT Press, 1963.

Physics of Snow and Ice - Proceedings of an International Conference on Low Temperature Science, Sapporo, Japan, Aug. 1966,(H. Oura, ed.). Pub. by Institute of Low Temperature Science, Hokkaido Univ., 1967.

Physics of Ice - Proceedings of an International Symposium, Munich, 1968, (N. Riehl, B. Bullemer and H. Engelhardt, editors), Plenum Press, New York, 1969.

10. Butkovich, T.R., "The Ultimate Strength of Ice," SIPRE Research Paper No. 11, Dec. 1954.

11. Frankenstein, G.E., "Strength Data on Lake Ice," SIPRE Technical Report No. 59, December 1959.

12. Frankenstein, G.E., "Strength Data on Lake Ice," SIPRE Technical Report No. 80, Jan. 1961.

13. Weeks, W.F., "Understanding the Variations of the Physical Properties of Sea Ice," from Symposium on Antarctic Oceanology, Santiago, Chile, 1966.

14. Weeks, W.F., and A. Assur, "Fracture of Lake and Sea Ice," CRREL Report RR269, Sept. 1969.

15. Anderson, D.L., and W.F. Weeks, "A Theoretical Analysis of Sea Ice Strength," Transactions, American Geophysical Union, V. 39, No. 4, p. 632, 1958.

16. Assur, A., "Composition of Sea Ice and its Tensile Strength," in Arctic Sea Ice, National Academy of Sciences - National Research Council Publication 598.

17. Weeks, W.F., "Tensile Strength of NaCl Ice," Journal of Glaciology, Vol. 4, p. 25-52, 1962.

18. Voitkovsky, K.F., "The Mechanical Properties of Ice," American Meteorological Society Translation AMS-T-R-391 AD #284777.

19. Savin, G.N., Stress Concentration Around Holes, Pergamon Press, 1961.

20. Peyton, H.R., "Sea Ice Strength," Geophysical Institute, University of Alaska Report UAG R-182, Dec. 1966.

21. Jellinek, H.H.G., "The Influence of Imperfections on the Strength of Ice," Proceedings of the Physical Society of London, Vol. 71, No. 5, p. 797, 1957.

22. Dykins, J.E., "Ice Engineering - Tensile Properties of Sea Ice Grown in a Confined System," USNCEL Technical Report R689, July 1970.

23. South Manchuria Railroad Company, "Study on River Ice: Part II: Dynamic Properties of Ice," August 1941.

24. Mellor, M., and I. Hawkes, "Measurement of Tensile Strength by Diametral Compression of Discs and Annuli," CRREL unpublished technical note. 1971

25. Gold, L.W., "Process of Failure in Ice," Canadian Geotechnical Journal, Vol. 7, p. 405, 1970.

26. Kingery, W.D., and D.N. French, "Stress-Rupture Behavior of Sea Ice," in Ice and Snow, MIT Conference, 1963.

27. Buktovich, T.R., "Strength Studies of Sea Ice," SIPRE Research Report 20, Oct. 1956.

28. Butkovich, T.R., "On the Mechanical Properties of Sea Ice, Thule, Greenland, 1957," SIPRE Research Report 54, Aug. 1959.

29. Dykins, J.E., "Ice Engineering - Material Properties of Saline Ice for a Limited Range of Conditions," USNCEL Technical Report R720, April 1971.

30. Tabata, T., "Studies of the Mechanical Properties of Sea Ice X - The Flexural Strength of Small Sea Ice Beams," in Physics of Snow and Ice, Sapporo Conf.

31. Frankenstein, G.E., "Ring Tensile Strength Studies of Ice," CRREL Tech. Report TR172, Feb. 1969.

32. Paige, R.A., and R.A. Kennedy, "Strength Studies of Sea Ice - Effect of Load Rate on Ring Tensile Strength," USNCEL Tech. Report, R545. 1967

33. Greystone, P., and M.P. Langleben, "Ring Tensile Strength of Sea Ice," in Ice and Snow, MIT Conf.

34. Vinieratos, E.R., and J.E. Dykins, "Ring Tensile Strength and Flexure Strength Correlations of Sea Ice," USNCEL Tech. Report R617. 1969

35. Langleben, M.P., "Some Physical Properties of Sea Ice, II," Canadian Journal of Physics, Vol. 37, pp. 1449 - 1454, 1959.

36. Langleben, M.P., and E.R. Pounder, "Arctic Sea Ice of Various Ages, I. Ultimate Strength," Journal of Glaciology, Vol. 5, p. 93, 1964.

37. Muguruma, J., "Mechanical Properties of Ice Single Crystals," in Physics of Ice, Munich Symp.

38. Brown, J.H., "Elasticity and Strength of Sea Ice," in Ice and Snow , MIT Conf.

39. Ripperger,E.A. and N. Davids, "Critical Stresses in a Circular Ring," Proceedings of the American Society of Civil Engineers, Vol. 12 (1947)

40. Tabata, T., K. Fujino, and M. Aota, "Studies of the Mechanical Properties of Sea Ice XI - The Flexural Strength of Sea Ice in-situ," Physics of Snow and Ice, Sapporo Conf.

41. Nevel, D.E., "The Ring Test, Brazil Test, and the Strength of Sea Ice," CRREL unpublished technical note. 1970

42. Higashi, A., "The Mechanical Properties of Ice Single Crystals," in Physics of Ice, Munich Symp.

43. Griggs, D.T., and N.E. Coles, "Creep of Single Crystals of Ice," SIPRE Report No. 11, Dec. 1954.

44. Readey, D.W., "Plastic Deformation of Single Crystals of Ice," MIT Sc. D. Thesis, 1962.

45. Nakaya, U., "Mechanical Properties of Single Crystals of Ice. Part 1 - Geometry of Deformation," SIPRE Research Report RR28, Oct. 1958.

46. Steinemann, S., "Results of Preliminary Expdriments on the Plasticity of Ice Crystals," Journal of Glaciology, Vol. 2, p. 404, 1954.

47. Kamb, W.B., "The Glide Direction in Ice," Journal of Glaciology, Vol. 3, p. 1097, 1961.

48. Jellinek, H.H.G. and R. Brill, "Viscoelastic Properties of Ice," Journal of Applied Physics, Vol. 27, No. 10, p. 1198, 1956.

49. Butkovich, T.R., and J.K. Landauer, "The Flow Law for Ice," SIPRE Research Report 56, Aug. 1959.

50. Higashi, A., S. Koinuma, and S. Mae, "Plastic Yielding in Ice Single Crystals," Japanese Journal of Applied Physics, Vol. 3, No. 10, p. 610, Oct. 1964.

51. Jones, S.J., and J. W. Glen, "The Mechanical Properties of Single Crystals of Pure Ice," Journal of Glaciology, Vol. 8, No. 54, p. 463, 1969 .

52. Jones, S.J., and J.W. Glen, "The Mechanical Properties of Single Crystals of Ice at Low Temperatures," International Union of Geodesy and Geophysics, General Assembly of Bern, 1967; IUGG Publication No. 79, 1968.

53. Glen, J.W., and M. F. Perutz, "Growth and Deformation of Ice Crystals," Journal of Glaciology, Vol. 2, No. 16, p. 397, 1954.

54. Readey, D.W., and W.D. Kingery, "Plastic Deformation of Single Crystal Ice," Acta Metallurgica, Vol. 12, p. 171, Feb. 1964.

55. Wakahama, G., "On the Plastic Deformation of Single Crystals of Ice," in Physics of Snow and Ice, Sapporo Conf.

56. Johnston, W.G., "Yield Points and Delay Times in Single Crystals," Journal of Applied Physics, Vol. 33, No. 9, p. 2716, 1962.

57. Readings, C.J., and J.T. Bartlett, "Slip in Single Crystals of Ice," Journal of Glaciology, Vol. 7, No. 51, p. 479, 1968.

58. Higashi, A., "Mechanisms of Plastic Deformation in Ice Single Crystals," in Physics of Snow and Ice, Sapporo Conf.

59. Higashi, A., "Mechanical Properties of Ice Single Crystals," in Physics of Ice, Munich Symp.

60. Higashi, A., S. Koinuma, and S. Mae, "Bending Creep of Ice Single Crystals," Japanese Journal of Applied Physics, Vol. 4, No. 8, p. 575, 1965.

61. Lavrov, V.V., "The Temperature Dependence of Ice Viscosity," SIPRE Translation No. 5 from Zhurnal Tekhnicheskoi Fiziki, Vol. 17, No. 9, p. 1027, 1947.

62. Glen, J.W., and S. J. Jones, "The Deformation of Ice Single Crystals at Low Temperatures," in Physics of Snow and Ice, Sapporo Conf.

63. Glen, J.W., "The Rheology of Ice," in Ice and Snow, MIT Conf.

64. Gold, L.W., "Deformation Mechanisms in Ice," ibid.

65. Gold, L.W., "The Dependence of Crack Formation on Crystallographic Orientation for Ice," Canadian Journal of Physics, Vol. 44, p.2757, 1966.

66. Jona, F., and P. Scherrer, "The Elastic Constants of Ice Single Crystals," _Helvetica Physica Acta_, Vol. 25, p. 35, 1952 (in German)

67. Gold, L.W., "The Cracking Activity in Ice During Creep," _Canadian Journal of Physics_, Vol. 38, No. 9, p. 1137, 1960.

68. Gold, L.W., "The Initial Creep of Columnar Grained Ice - Part I. Observed Behavior," _Canadian Journal of Physics_, Vol. 43, p. 1414, 1965.

69. Taylor, G.I., "Plastic Strain in Metals", _Journal of the Institute of Metals_, Vol. 62, p. 307 (1938)

70. Nevel, D.E., Personal communication.

71. Hutchinson, J.W., "Elastic-Plastic Behavior of Polycrystalline Metals and Composites," _Proceedings of the Royal Society of London_. Vol. 319, p. 247, 1970.

72. Maser, K.R., "The Determination of the Strength of Ice Sheets from Small Sample Data," Offshore Technology Conference, Houston, Texas, April, 1971. Preprint Volume.

73. Goetze, C.G., "A Study of Brittle Fracture as Applied to Ice," CRREL unpublished technical note, Nov. 1965

74. Zienkiewicz, O.C., _The Finite Element Method in Structural and Continuum Mechanics_, McGraw-Hill, 1967.

75. Dykins, J.E., "Construction of Sea Ice Platforms", _Ice and Snow_, Proc. of MIT Conf., 1963

Biography

The author was born in New York City on February 19, 1945.
He attended The Cooper Union for the Advancement of Science and
Art between 1962 and 1966, receiving a Bachelor of Civil Engineer-
ing degree in June 1966. He has been a graduate student at M.I.T.
since September, 1966, receiving a Master of Science in Civil
Engineering in September 1967. He has held various part-time
teaching-assistantship and research positions while at M.I.T. He
was employed by the Chevron Oil Field Research Co. during the
summer of 1969, and it was there that he began to study the problem
of ice sheet strength. A paper on the subject of this thesis was
presented by the author at the Offshore Technology Conference,
Houston, Texas, in April 1971, and appears in the preprint volume.

Appendix A

The Interpretation of the Results of Higashi, Koinuma, and Mae[60] in Terms of Eq. (4.14).
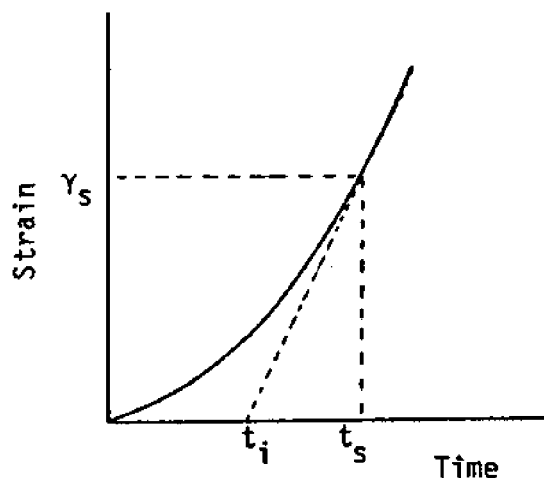
Higashi et al.[60] have reported the steady state strain rate $\dot{\gamma}_s$ and the incubation time t_i to behave according to the following relationships:

$$\dot{\gamma}_s = K_1 \tau^r \exp\ (-Q/RT) \tag{A.1}$$

$$1/t_i = K_2 \tau^r \exp\ (-Q/RT) \tag{A.2}$$

It will be assumed that this constant rate region follows a region describable by Eq. (4.14). Hence these two relationships can be analysed in terms of Eq. (4.21). It will also be assumed that the constant rate portion of figure A.1 occurs at a large enough time so that

$$\gamma_{pm} \approx \gamma_p = [(1-m)k\tau^n t]^{1/1-m} \tag{A.3}$$

This is of the same form as the proposed power law relationships, and hence, for simplicity,

$$q = 1/1-m \qquad (A.4)$$

(A.3) becomes

$$\gamma = \left(\frac{k}{q}\right)^q \tau^{nq} t^q = Ct^q \qquad (A.5)$$

where subscript p has been dropped. $\dot{\gamma}_s$ and t_i are related as follows:

$$\frac{\gamma_s}{t_s - t_i} = \dot{\gamma}_s \qquad (A.6)$$

Using (A.5) for γ_s and $\dot{\gamma}_s$, the following is obtained from (A.6)

$$t_s = \frac{q}{q-1} t_i \qquad (A.7)$$

From (A.1) and (A.2), it is observed that

$$\dot{\gamma}_s = \frac{K_1}{K_2 t_i} \qquad (A.8)$$

Substituting (A.5), (A.7), and (A.8) into (A.6), the following is obtained

$$C = (q-1)^{q-1} \left(\frac{K_1}{K_2}\right) t_i^{-q} \qquad (A.9)$$

Recalling the components of C in Eq. (A.5), and expressing t_i in terms of (A.2), one obtains

$$\left(\frac{k}{q}\right)^q \tau^{nq} = (q-1)^{q-1} \left(\frac{K_1}{K_2}\right) K_2^q \tau^{rq} \exp(-qQ/RT) \qquad (A.10)$$

or, equivalently

$$\frac{k}{q} \tau^n = (q-1)^{q-1/q} \left(\frac{K_1}{K_2}\right)^{1/q} K_2 \tau^r \exp(-Q/RT) \qquad (A.11)$$

Two observations are now apparent. The stress dependence r in Eqs. (A.1) and (A.2) is equivalent to the stress dependence n of Eq. (4.14). Secondly, k is of the form

$$k = k' \exp(-Q/RT) \qquad (A.12)$$

which is equivalent to the temperature dependence found by Readey and Kingery (see Eq. (4.24)).

Appendix B

Derivation of the Force Displacement Relation for the Spring-Dashpot Representation of a Grain.

We begin with the basic flow equation, with $m = 1$.

$$(\dot{\gamma}_T - \dot{\tau}/G) = k\,(\gamma_T + \gamma_0 - \tau/G)\tau^n \tag{B.1}$$

It will be assumed that γ_T and τ represent mean strains and stresses at the section considered. Hence, they can be expressed in terms of the average longitudinal strain and stress, ε and σ, as:

$$\gamma_T = \varepsilon \cdot \sin 2\theta \tag{B.2}$$

$$\tau = \sigma \cdot \left(\frac{\sin 2\theta}{2}\right) \tag{B.3}$$

Since the case of constant strain rate is being considered, ε is represented as vt. For the spring-dashpot model, σ is represented by F/A, and δ represents ε. Noting these substitutions and those of Eqs.(B.2) and (B.3), and changing independent variable from t to δ, Eq. (B.1) yields:

$$v - \frac{v}{2GA}\frac{dF}{d\delta} = k\left(\frac{\sin 2\theta}{2}\right)^n \left(\delta + \frac{\gamma_0}{\sin 2\theta} - \frac{F}{2GA}\right)\left(\frac{F}{A}\right)^n \tag{B.4}$$

Each grain has a different area A_i, and a different orientation θ_i. Equation (B.4) for the spring-dashpot system representing grain i has the form

$$\frac{dF_i}{d\delta} = G_i - \frac{G_i k_i}{v}\left(\delta + \delta_i - \frac{F_i}{G_i}\right)(F_i)^n \tag{B.5}$$

where $\qquad G_i = 2A_i G$

$$\delta_i = \frac{\gamma_o}{\sin 2\theta}$$

$$k_i = (\frac{\sin 2\theta_i}{2A_i})^n \, k$$

This is the relation used in chapter V.

Appendix C

Two-Dimentional Finite Element Analysis of a Polycrystalline Assembly of Elastic-Time Dependent Plastic Grains.

Elastic Analysis

Each grain is composed of square and $45°$ triangular elements. The division of the grain into these elements is part of the computer program. The assembly of these elements into a grain stiffness matrix, K_G, is accomplished by normal finite element techniques. Grain nodes are programmed to be numbered so that all of the boundary nodes come first, and the internal nodes second. Hence, the grain displacement vector, U_G, and the stiffness matrix are partitioned as follows:

$$U_G = \left\{ \begin{array}{c} U_B \\ --- \\ U_I \end{array} \right\} \qquad K_G = \left[\begin{array}{c:c} K_{BB} & K_{BI} \\ \hdashline K_{IB} & K_{BB} \end{array} \right] \qquad (C.1)$$

Applying virtual work to the grain, one obtains

$$\left[\begin{array}{c:c} K_{BB} & K_{BI} \\ \hdashline K_{IB} & K_{II} \end{array} \right] \left\{ \begin{array}{c} U_B \\ ---- \\ U_I \end{array} \right\} = \left\{ \begin{array}{c} P_B \\ ---- \\ 0 \end{array} \right\} \qquad (C.2)$$

where P_B represents the force vector associated with the boundary nodes. Eliminating U_I from Eqs. (C.2), the following stiffness equations is obtained:

$$K_{BB}^c \ U_B = P_B \qquad (C.3)$$

where

$$K_{BB}^c = K_{BB} - K_{BI} \ K_{II}^{-1} \ K_{IB} \qquad (C.4)$$

K_{BB}^{C} is referred to as the condensed stiffness matrix of the grain.
These can then be assembled with other grain condensed stiffness
matrices by usual finite element methods to form the stiffness matrix
of the polycrystal.

Plastic Flow

The total strain of an element is divided into two parts, the
elastic strain vector ε_e and the plastic strain vector ε_p. It is
assumed that at any point in time the total stress is entirely due
to elastic strain. The plastic strain at each time step is treated
as an initial strain, and hence

$$\sigma = D \left(\varepsilon - \varepsilon_p \right) \tag{C.5}$$

where D is the elastic rigidity matrix, σ is the stress vector, and
ε is the total strain vector. According to the finite element method,
the element displacements and strains are expressed as functions of
the element nodal displacements, $U_{E,n}$, as

$$u = N \, U_{E,n} \tag{C.6}$$

$$\varepsilon = B \, U_{E,n} \tag{C.7}$$

where N and B are functions of x and y in a plane problem. The
principle of virtual work states that

$$\int_A \delta \varepsilon^T \cdot \sigma \, dA = \int_s \delta u^T \cdot p \, ds \tag{C.8}$$

where p is the force per unit length applied to the boundary, A is the
element and s is the portion of the element boundary along which forces

are prescribed. Substituting the stress-strain relations (C.5) and the element expansions (C.7), the left-hand side of (C.8) becomes

$$\int_A \delta U_{E,n}^T \ B^T \ D \ (BU_{E,n} - \epsilon_0) \ dA \qquad (C.9)$$

Letting

$$\int_A B^T \ D \ B \ dA = K_E \qquad (C.10)$$

$$\int_A B^T \ D \ \epsilon_p \ dA = P_p \qquad (C.11)$$

(C.9) becomes

$$\delta U_{E,n} \ [K_E \ U_{E,n} - P_p] \qquad (C.12)$$

where K_E is the usual element stiffness matrix and P_p is the load vector due to plasticity.

In assembling Eq. (C.8) for the entire grain, the contributions of the right-hand side cancel along the contiguous element boundaries, leaving a grain boundary force vector P_B. The resulting equation is an altered form of Eq. (C.2) and has the form

$$\begin{bmatrix} K_{BB} & \vdots & K_{BI} \\ \hdashline K_{IB} & \vdots & K_{II} \end{bmatrix} \begin{Bmatrix} U_B \\ \hdashline U_I \end{Bmatrix} = \begin{Bmatrix} P_S \\ \hdashline 0 \end{Bmatrix} + \begin{Bmatrix} P_{Bp} \\ \hdashline P_{Ip} \end{Bmatrix} \qquad (C.13)$$

where P_{Bp} and P_{Ip} comprise the grain load vector due to plasticity which is assembled from the element P_p matrices. Eliminating the internal displacements, Eq. (C.13) becomes

$$K_{BB}^c \ U_B = P_s + P_{Bp}^c \qquad (C.14)$$

where K_{BB}^C is described by Eq. (C.4), and P_{Bp}^C is expressed as

$$P_{Bp}^C = P_{Bp} - K_{BI} \, K_{II}^{-1} \, P_{Ip} \qquad (C.15)$$

and is referred to as the condensed grain boundary load vector due to plasticity.

Eq. (C.14) for each grain can be assembled by usual finite element means to form the stiffness matrix of the polycrystal.

The above analysis is based on a knowledge of ε_p. At $t = 0$, ε_p is computed from the prescribed initial basal strain discussed in chapter IV. It is subsequently updated from the changes in the basal strain as described by the flow rule (4.14).

136

Appendix D

List of Tables and Figures